

Designing Novel Biomaterials for Cornea Replacement

BY

AMELIA L. ZELLANDER
B.A.S., University of Pennsylvania, 2003
M.S., Johns Hopkins University, 2009

THESIS

Submitted as partial fulfillment of the requirements
for the degree of Doctor of Philosophy in Bioengineering
in the Graduate College of the
University of Illinois at Chicago, 2013

Chicago, Illinois

Defense Committee:

Michael Cho, Chair and Advisor
Richard Magin
Ali Djalilian, Ophthalmology and Visual Sciences
Richard Gemeinhart, Pharmaceuticals and Bioengineering
Michael McNallan, Civil and Materials Engineering

Acknowledgements

To my dissertation committee (Michael Cho, Ali Djalilian, Richard Gemeinhart, Richard Magin, and Michael McNallan) thank you for offering guidance and for investing time and resources to help me to complete this project. A special thank you to Michael Cho, my thesis advisor and PI, for allowing me to be creative and for having a contagious positive attitude. During my time at UIC, I received training and mentoring from Shan Sun, a PhD scientist in the Cho lab. To Shan, thank you for your advice and encouragement. To my graduate student friends in the Cho lab, thank you for lending a shoulder to cry on when I felt discouraged, for providing feedback, and for helping to make the journey fun.

I appreciate the contributions of my technical collaborators. Thank you, Mohsen Makhsous of Northwestern University, for giving me access to your mechanical testing equipment. Behrad Milani did all animal surgeries for in vivo testing; thank you, Behrad. I would like to thank technicians who acquired Scanning Electron Microscopy (SEM) images: Chenlin Zhao of the Mechanical Engineering Department at UIC and Kristina Jarosius of the Electron Microscope Service at the Research Resource Center at UIC. To Ryan Ross of Rush University, thank you for obtaining Micro CT scans. Thank you to Ke-Bin Low, of the Research Resource Center at UIC, for generating X-ray Photoelectron Spectroscopy (XPS) data. To Mrignayani Kotecha, thank you for conducting Nuclear Magnetic Resonance (NMR) measures.

To my family and close friends, thank you for believing in me. To Archie, Rena, and Adrian Zellander, thank you for your encouragement and your prayers.

Table of Contents

Acknowledgements.....	ii
Table of Contents.....	iii
1. Introduction.....	1
2. Keratoprosthesis Background.....	3
3. Porous Poly(Ethylene Glycol) Diacrylate.....	10
4. Poly(2-Hydroxyethyl Methacrylate) - Poly(Ethylene Glycol) Diacrylate.....	23
I. Poly(2-Hydroxyethyl Methacrylate) - Poly(Ethylene Glycol) Diacrylate (PHEMA-PEGDA) Based Keratoprosthesis.....	23
II. Using Porogens to Modulate Substrate Topography in Poly(2-Hydroxyethyl Methacrylate) - Poly(Ethylene Glycol) Diacrylate (PHEMA-PEGDA).....	24
III. Evaluating the Potential Utility of a Poly(2-Hydroxyethyl Methacrylate) - Poly(Ethylene Glycol) Diacrylate (PHEMA-PEGDA) Keratoprosthesis.....	45
5. Salt Porogen Scaffold for Keratoprosthesis.....	56
6. Gas Foamed Scaffold for Keratoprosthesis.....	81
7. Summary.....	102
References.....	104
Curriculum Vitae.....	116

1. Introduction

Corneal disease related blindness affects approximately 8 million people worldwide. Donor cornea is commonly used to correct the condition, but various complications and healthcare disparities force some patients to pursue alternative treatment options such as artificial cornea or keratoprosthesis. After 5 years, up to 70% of all corneal grafts remain clear. However, up to 40% of penetrating keratoplasty patients experience immunologic rejection of the corneal graft after a 10 year follow-up period. In addition, insufficient donor cornea supplies limit the treatment options of selected patient populations. [1] [2] [3] This project aims to design synthetic biomaterials to create a keratoprosthesis that permits stable host integration and long term vision restoration. While a number of keratoprosthesis are available on the market, each fails to address one or more of the following vital parameters: host integration, mass transport, tissue epithelialization, or innervation. Inadequate keratoprosthesis design can result in extrusion, necrosis, increased intraocular pressure, or infection. [1] [2]

This project investigated the biocompatibility, structure, transparency, and mechanics of novel polymer scaffolds for cornea replacement devices. Polymeric units used included 2-hydroxyethyl methacrylate (HEMA), methyl methacrylate (MMA), or acrylated poly (ethylene glycol) (PEG) based monomers. The successes and shortcomings of previous corneal replacement devices or keratoprostheses (KPros) guided the biomaterials design. Immune rejection and insufficient host integration are risk factors that can impede the long term survival available corneal replacement agents. [1] [2] This study hypothesizes that the pore structure and aqueous content of a synthetic polymer structure can be designed to induce stable host integration and to permit the transport of life sustaining agents to the ingrown ocular tissue. In addition, this study postulates that the appropriate tissue ingrowth and mass transport can be

achieved in a suturable synthetic structure that is designed to sustain corneal related in vivo forces.

2. Keratoprosthesis Background

Available keratoprosthesis (KPro) designs are composed of natural materials, synthetic materials, or a combination of both. While many keratoprostheses demonstrate a level of utility, all models fail to fully address one or more of the following vital parameters: host integration, mass transport, tissue epithelialization, or innervation. Inadequate keratoprosthesis design can result in extrusion, necrosis, increased intraocular pressure, or infection. [1] [2] [4]

2.1 Boston Keratoprosthesis Type 1

The Boston KPro Type 1 is designed for patients who experienced multiple graft failures. Prospective Boston KPro users have a poor prognosis for primary penetrating keratoplasty. [1] Patients with ocular autoimmune conditions usually do not qualify for use. Prior to 2008, the device consisted of a back plate and an optically transparent stem, both composed poly (methyl methacrylate) (PMMA); a titanium locking ring secures the PMMA components. The most recent Boston KPro Type 1 design includes a titanium back plate with larger holes than the earlier models. [4] A 2011 Todani et. al. study shows that titanium back plates reduce retroprosthetic membrane (RPM) occurrence in Boston KPro. RPM can decrease the optical transparency of the KPro optic or core. RPM forms when cells adhere to the core. Over time the adhered cells can develop and multiply to form the fibrous thin sheet known as RPM. [5] [6] The Todani study includes 78 eyes that developed RPM following implantation of a Type I device. For each subject, RPM was diagnosed at 6 months following surgery. Overall, 13.0% of titanium plate users developed RPM while 41.8% of PMMA plate users developed RPM. [7]

Donor cornea tissue is sandwiched between the stem and the back plate of the Boston KPro. After the device is assembled with donor cornea tissue, the complete implant is sutured via the

donor cornea. The surgical implantation method is the same as the standard method for penetrating keratoplasty (PKP). The optics of the device can be adjusted to match the patient's refractive power. [4] Boston KPro has high retention rates. A 2005 study reports 100% retention of the device during 2 – 12 month follow-up period; a post-operative visual acuity of greater than 6/120 was achieved by 74% of patients. In a 2006 study, graft retention was 95% at an average follow-up of 8.5 months while 57% of patients attained a post-operative visual acuity of 6/60. One year following implantation, visual acuity was 6/60 in 56% and in 6/12 in 23% of users. The most common post-operative complication was retroprosthetic membrane. [4]

2.2 Boston Keratoprosthesis Type 2

The Boston KPro Type 2 is designed for end stage dry eye. The overall design of the Type 2 device is similar to the Type 1 device. Unlike the Type 1 model, the Type 2 model includes an optical portion that protrudes through a permanently closed upper eyelid. The initial device assembly and implantation procedures are identical to the Type 1 model. After the Type 2 model is sutured, it is covered with skin from the eyelid or a mucous membrane graft. [4]

2.3 Osteo-Odonto Keratoprosthesis (OOKP)

The Osteo-Odonto KPro is a full thickness corneal replacement device. It consists of a PMMA optic and a skirt made from autologous tooth. The device has high long term retention rates even in patients with serious ocular diseases including ocular cicatricial pemphigoid (OCP), Stevens-Johnson syndrome (SJS), or graft-vs.-host disease (GVHD). In one study, 100% retention was reported at a mean follow-up 19.1 months with BCVA of $\geq 20/40$ in 73.3% of patients. Another independent study calculated an 85% cumulative probably of retention at 18

years, and a mean BCVA of 20/30 – 20/20 was reported. This data was taken from a group of over 100 patients. An OOKP study with 36 patients resulted in 72% retention at a mean follow-up of 3.9 years. OOKP data taken from a range of follow-up periods was used to compute retention rates and BCVA. Large data sets from specific follow-up time points could permit a more accurate assessment of OOKP retention. The complexity of OOKP surgery, which requires the participation of multiple medical specialists, is a major disadvantage of the device. In addition the availability of a healthy rooted tooth is imperative for successful device construction. Sometimes patients do not have a suitable tooth. In such a case, Tibial Bone Keratoprosthesis (TKPro) may be an option. The surgical procedure is similar to OOKP. [2] [4]

2.4 AlphaCor Keratoprosthesis

The AlphaCor KPro consists of a poly (2-hydroxyethyl methacrylate (PHEMA) optically transparent core and an opaque porous skirt. [1] The device is designed for patients with scarred, vascularized or diseased corneal tissues. It has been used when patients are either not eligible for conventional donor tissue transplants or have had multiple previous graft failures. [1] US Patent 5458819, which describes the AlphaCor KPro, states that 5 – 80 µm pores may be present in a PHEMA sponge created from a monomeric mixture with approximately 45 % weight water. An electron micrograph illustrates the pore structure of the device skirt, [8] but the interconnectivity of the pores maybe be best evaluated based on the extent of cell ingrowth.

In vivo cell ingrowth into porous AlphaCor rims suggested that the device permits host integration, [9] but later studies showed that device retention is strongly related to patient selection and management. A 2002 publication determined that fibroblast ingrowth into the porous skirt facilitates the stabile integration of the device for full thickness keratoplasty. [5] 14

patients with poor prognosis for penetrating keratoplasty and/or uncertain visual acuity outcome were included in the trial. Of the 14 implants, 2 developed optical deposits, 1 caused stromal melting, and 1 resulted in traumatic cataract. Researchers determined that stromal melting and traumatic cataract were only partly related to the device. [10] Optical deposits have been attributed to the patients' heavy smoking habits and certain topical medications. [11]

A 2005 study showed reduced biointegration of AlphaCor when stromal melting occurred. 14 AlphaCor devices were explanted from human subjects. Of the 14 devices, 5 presented medication related calcification in the optic; 3 of the 5 calcified devices also experienced stromal melting. An additional 8 out of the 14 devices were removed due to corneal tissue melting anterior to the device. One of the 14 devices developed retroprosthetic membrane. Neither calcification nor fungal infections were observed in the skirt region of AlphaCor devices. The connection between the skirt and the optic component remained intact. In the absence of stromal melting, devices supported greater collagen deposition and fibroblast invasion. Stromal melting was accompanied by an increase in inflammatory cells around the device skirt. In spite of precondition related side effects, the study indicates that the device may be a reasonable option for selected patient populations. AlphaCor devices permit biointegration in the absence of corneal vascularization and in cases of chemical injury. [8]

A 2006 study presented an attempt to reduce stromal melting in AlphaCor. Retention statistics were reported for on label cases that received medroxyprogesterone (MPG) treatment; MPG may prevent stromal melting. Probability of retention to 6 months, 1 year, and 2 years was 92%, 80%, and 62%, respectively. 64.5% of explanted devices were removed due to stromal melting. Stromal melting refers to any event of stromal thinning or loss, even if the process subsequently stabilized. In the event of AlphaCor complications, reversal to the pre-AlphaCor

state using penetrating keratoplasty (PK) of tissue is possible. Following AlphaCor removal, 78.2% of cases were reversed to PK. On average, preoperative visual acuity allowed patients to recognize hand movements. For some patients, fibrous reclosure restricted visual acuity. Fibrous reclosure of the posterior lamellar opening occurred in 13.0% of implant recipients. Following device implantation, bested corrected visual acuity (BCVA) ranged from light perception to 20/20; mean BCVA was 20/200. This data was taken at a variety of time points following AlphaCor implantation. [11]

2.5 Guangzhou Keratoprosthesis

A group in Guangzhou, China developed a synthetic KPro using poly (2-hydroxyethyl methacrylate) (PHEMA) and poly (methyl methacrylate) (PMMA). [12] The transparent core was made with a 10 : 1 mass ratio of HEMA : MMA. A thin PHEMA-PMMA flange or protrusion surrounded the PHEMA-PMMA core. The flange was perforated with 200 – 300 µm holes; then, a PHEMA sponge was fused to the perforated flange. The PHEMA sponge, with 65 % porosity, had 20 – 60 µm pores. The combined PHEMA sponge and perforated PHEMA-PMMA extension constituted the KPro skirt. The device was tolerated in New Zealand white rabbits for up to 4 months. Vascularization and corneal cell ingrowth was observed in the device skirt. Corneal melting observed in AlphaCor clinical trials suggests that PHEMA sponges like those used in the AlphaCor and Guo et. al. KPros may result in corneal melting in diseased and/or damaged corneal tissues. [8] [13] The Guangzhou KPro is still in development.

2.6 Seoul Type Keratoprosthesis

The Seoul Type KPro includes a PMMA optic and a skirt made of polyurethane, polypropylene, or polytetrafluoroethylene. [1] [14] SEM images indicate that the skirt of the device has pores of

30 µm or greater that appear to be interconnected. Fibroblast ingrowth and collagen deposition were observed on devices that use the polypropylene and polyurethane skirts. Tissue melting occurred in 1 out of 4 devices with the polyurethane skirt. Polyurethane skirts were deemed less desirable due to in vivo degradation. Overall, extrusion was not observed in any of the devices that were inserted in non-diseased rabbit eyes. [15] Similar to AlphaCor, the performance of the Seoul KPro is influenced by patient selection. A study with 9 patients with existing ocular conditions resulted in a 66.7% anatomic retention rate of the device at 68 months. Among the patients in the study, 6 were diagnosed with Stevens–Johnson syndrome (SJS), 2 had chemical burns, and 1 suffered from ocular pemphigoid (OCP). Eventually all devices developed corneal melt leading to full exposure of the skirt. [1] [2] On average, retroprosthetic membrane developed after 16.2 months. [14] Patients maintained a visual acuity of finger counting or higher for an average of 31.6 months. [2]

2.7 Pintucci Keratoprosthesis

The Pintucci KPro consists of a PMMA optic connected to a woven Dacron membrane. [2] In a 1995 study, the Dacron membrane permitted tissue ingrowth in patients with preexisting ocular conditions, but 2 out of 20 devices extruded. 13 out of 20 patients maintained improved visual acuity for more than 2 years. [16] 50% of patients experienced necrosis of the mucous membrane anterior to the device skirt. [4] A 1996 study reported that 60% Pintucci KPro recipients developed mucous membrane pemphigoid (MMP) [2]; MMP is an autoimmune disease that can result in vision loss. [17] The surgical procedure performed influences the incidence of postoperative endophthalmitis or intraocular inflammation. [18] In a study with 31 Indian patients, researchers found no device extrusions at a mean follow-up of 3.2 years. However, only 6.5% of these patients achieved best corrected visual acuity (BCVA) of greater than 20/40. [2]

2.8 Stanford Keratoprosthesis

The Stanford KPro is an experimental core-skirt model keratoprosthesis. Both the central optic and microperforated rim of the device are composed of a poly(ethylene glycol)-poly(acrylic acid) interpenetrating network (PEG/PAA IPN). [1] When collagen type I was connected to the surface of the optic, epithelialization was observed in vivo. [19] The glucose permeability of the PEG (MW 8000)/PAA optic is similar to that of natural cornea. [20] The PEG/PAA optic was implanted under LASIK flaps of rabbit corneas for 14 days. 1 of the 10 implants was extruded. Inconsistencies in the polymer's thickness, raised edges, may have contributed to the extrusion. For LASIK flaps over laying the IPNs, epithelial thinning was observed. In the area of extrusion, researches did not observe fibrosis, inflammation, or neovascularization. Overall, opacification was not observed. [19]

2.9 Natural Polymer Keratoprosthesis

Natural polymer based keratoprostheses demonstrate host integration and epithelialization. McLaughlin et. al. fabricated a cornea construct using carbodiimide cross-linked porcine type I collagen. The implant showed evidence of early stages of remodeling at 4 and 8 weeks post operation. The absence of sodium fluorescein staining indicated that an intact epithelial barrier was restored and remained stable over 12 months. [21] Gonzalez-Andrades et. al. developed a natural polymer substitute for human corneal which consists of cultured keratocytes entrapped in a gel of human fibrin and 0.1% agarose. Data indicates that the air-liquid culture technique succeeded in promoting stratification and differentiation of the epithelial layer. [22] While selected natural polymers demonstrate favorable host integration and biocompatibility, synthetic based tissue engineering scaffolds allows for greater control over mechanical properties, geometry, and biological interaction. [23] [24]

3. Porous Poly(Ethylene Glycol) Diacrylate

3.1 Abstract

This study investigates the effects of polymer chain length on the mechanical properties of gas foamed poly (ethylene glycol) diacrylate (PEGDA). Gas foamed structures were composed of PEGDA MW 700, MW 3400, or MW 10k. Combinations of short (lower MW) and long PEGDA (higher MW) chains created polymer structures with increased strength and stiffness compared to structures composed of a given longer PEGDA chain. Gas foamed PEGDA hydrogels are structurally and mechanically suitable for evaluating cells in 3D culture. SEM images show an interconnected pore structure. Gas foamed PEGDA is also cytocompatible. High cell viability was observed on collagen type I infused polymer structures. Changes in PEGDA chain sizes neither degraded cell viability nor impeded gas foaming. The mechanical tunability of gas foamed porous PEGDA makes it an effective tool for evaluating cellular response to static mechanical properties in 3D.

3.2 Introduction

Efforts to create a mechanically stable porous poly(ethylene glycol) diacrylate (PEGDA) hydrogel were originally intended to culminate in a full thickness cornea replacement device. Various ratios of PEGDA MW 700, 3400, 6k, and 10k were combined in an effort to create a more mechanically stable porous PEGDA scaffold. Different chain length combinations resulted in stiffness values ranging from a weak jelly-like softness to a glass-like hardness, but the structures did not present sufficient strength for full thickness cornea replacement. However, mechanically tunable porous PEGDA could be a useful tool for tissue engineering research.

Tissue engineering constructs made with synthetic polymers allow users to control the mechanical and structural properties of the device. Poly (ethylene glycol) diacrylate (PEGDA) is a synthetic polymer that has been used to investigate the engineering of tissues including bone,

[25] cartilage, [26] [27] and cornea. [28] [29] Previous publications have demonstrated its amenability to chemical, structural, and mechanical modification. [30] [31] [32] [33] In addition, PEGDA is non-toxic [34] and generates minimal immunogenic response. [35] The mechanical tunability of gas foamed PEGDA may give it a range of tissue engineering applications.

Typical PEG hydrogel studies use a singular PEG chain size to adjust the structure's mechanical properties. [33] [36] [37] This study investigated the combination of multiple PEGDA chain sizes to develop gas foamed PEGDA hydrogels with different mechanical properties. Variations in PEGDA molecular weight or solution concentration change the kinetics of polymerization and alter mechanical properties of the gel. [32] [34] [38] [39] Increasing the ratio of PEGDA to water, at the time of polymerization, or decreasing poly (ethylene glycol) (PEG) chain length leads to increased mechanical modulus and decreased mass transport through the gel. [38] Since PEGDA alone is known to resist cell adhesion in vitro, [28] [40] rat tail collagen type I was added to porous PEGDA to permit cell attachment. Throughout this report, the combination of porous PEGDA and rat tail collagen type I is called a hybrid scaffold. This study demonstrates that by simply combining PEGDA chains of given lengths, one can adjust the mechanical properties of porous PEGDA structures that are suitable for tissue engineering.

3.3 Methods

3.3.1 Engineering the Hybrid Scaffold

Porous PEGDA scaffolds were designed based on the protocol published by Keskar et. al. [30] PEGDA MW 10k (Sigma-Aldrich), PEGDA MW 3400 (Glycosan, Salt Lake City, UT), or PEGDA MW 700 (Sigma-Aldrich) were used to create gas foamed PEGDA. To prepare the polymer structures for in vitro evaluation, the structures were immersed in a rat tail collagen type I solution (2 mg/mL) (BD Bioscience). N (3-Dimethylaminopropyl)-N'-ethyl-carbodiimide (EDC)

(5 mM) and N-hydroxysuccinimide (NHS) (5 mM) were used to crosslink the collagen.

Dehydrated porous PEGDA structures absorbed the collagen solution like sponges. After the collagen type I solution absorbed, it was gelled at 37°C. The collagen gel is much weaker than the porous PEGDA structure, [28] so it fails to contribute to the overall mechanical properties of PEGDA and unlikely alters the pore size. The combination of porous PEGDA and collagen type I is referred to as the hybrid scaffold throughout this report.

3.3.2 Tensile Testing of Porous PEGDA

Hydrated porous PEGDA samples were tested in tension using a custom designed 100LM Test Resources mechanical testing machine (Test Resources Inc., Shakopee MN). Three samples of each formulation were tested using a calibrated WF75GS Load Cell (Test Resources Inc.), which is fatigue-rated for 75 g of force (0.735 N) in tension and compression. The scan rate for all tension measures was 50.86 Hz. Samples were cut into rectangular shapes for tensile testing. Average sample dimensions were approximately 4 x 8 mm and 3 mm depth. The tensile strain rate was 0.2 mm/s. Firstly, a strain of 10% was applied for at least 30 cycles to pre-condition the samples. A strain of 200% was applied to measure stress vs. strain to the rupture point. Values taken from the tensile measures included elastic modulus (E), ultimate tensile strength (UTS), and strain at rupture. E is measured in the elastic or linear region of the stress vs. strain plot; $E = \text{stress/strain}$. UTS is the maximum stress response of a material during tensile testing. The strain at rupture is simply the elongation of the sample at the point of rupture; in this study the elongation was reported as a percentage of the original length of the sample.

3.3.3 Structural Evaluation

To observe the pore structure of scaffolds, SEM images of polymers were generated using a S-3000N Variable Pressure SEM (Hitachi). Surface pore areas were measured using SEM

images. Image J applied a threshold to surface pores and measured each pore with the Analyze Particles function. Monoclonal Anti-Collagen Type I antibody at 1: 2000 dilution (Sigma-Aldrich, C2456) was used to stain collagen fibers in the hybrid scaffolds.

3.3.4 Cell Culture and Cell Viability

Two cell types were used to evaluate in vitro cytotoxicity and cell proliferation: primary human corneal fibroblasts (HCFs) passage 11 and human fibroblast cell line (HT1080) passage 7. Cells were cultured in GIBCO MEM alpha media (Invitrogen) with 10% fetal bovine serum (FBS) (Atlanta Biologicals, Lawrenceville, GA) and 1% antibiotic-antimycotic solution (Sigma-Aldrich). A live-dead cell viability assay (Invitrogen) was used to stain live and dead cells in hybrid scaffolds.

3.3.5 DNA Assay

Acellular hybrid scaffolds, approximately 0.5 – 1 mm in thickness and 7 mm in diameter, were placed on a 50 - 60% confluent layer HCFs and incubated for periods of 7, 9, and 13 days. Hybrid scaffolds were rinsed in PBS prior to DNA isolation to ensure that only cells attached to the scaffold were evaluated. TRIzol Reagent (Invitrogen) was used per the product protocol to isolate DNA. DNA pellets were diluted with 250 μ L of TE Buffer, and a fluorescent DNA quantification kit (BioRad 170-2480, Hercules, CA) was used to measure the DNA concentration. For each sample, 80 μ L of the prepared fluorescent DNA solution was added to a well. In all, 6 wells were measured for each DNA pellet; and four DNA pellets were tested (n = 4).

3.3.6 Subcutaneous Implantation in Mice

A four month old female C57BL/6 mouse was anesthetized with intraperitoneal injection of ketamine (100 mg/kg) and xylazine (5 mg/kg). Four acellular and collagen-free PEGDA 10k/700

scaffolds were implanted in the back of the animal and extracted after four weeks. Frozen sections of extracted implants were stained with hematoxylin and eosin (H&E) and anti-CD45 antibody (BD Pharmingen, San Jose, CA).

3.3.7 Statistical Analysis

MATLAB R2012a was employed for all statistical analysis using an alpha value of 0.05. Note that the standard error of a given data set represents the error measure. Standard error is the standard deviation divided by a quantity that is the square root of the number of samples measured. This report references the MATLAB R2012a Product Documentation to discuss the application of MATLAB statistical tests.

3.4 Results

3.4.1 Mechanical and Structural Assessment

Various quantities of PEGDA MW 700, 3400, or 10k were combined to create porous PEGDA scaffolds with different mechanical properties. Monomer combinations resulted in stiffness values ranging from a weak jelly-like softness to a glass-like hardness (Fig. 1).

The grams per milliliter (g/mL) of PEGDA chains used and the equivalent molar concentrations (M) are listed for each polymer sample in Figure 1; and these samples were tested at a strain rate of 0.2 mm/s. Per ANOVA testing, the UTS and *E* of PEGDA 10k/700 are significantly greater than the UTS and *E* for PEGDA 3400. Trends in mechanical data show that the addition of PEGDA 700 to structures increased strength (UTS) and stiffness (*E*). A porous sample composed of PEGDA 10k (0.20 g/mL or 0.02 M) and PEGDA 3400 (0.07 g/mL or 0.02 M) was also tested in tension. However, the force response obtained from the combination was too small and noisy to extract reliable mechanical data. Porous PEGDA 10k (0.20 g/mL or 0.02 M)

was too weak and unstable to test in tension, which had the consistency of jelly or a weak gum-like substance. The specific combination of PEGDA chain lengths determined the mechanical properties of each porous PEGDA substrate.

Combining small quantities of different chain sizes can result in porous PEGDA hydrogels with different mechanical properties (Fig. 1). The addition of PEGDA 10k (0.02 M) to PEGDA 700 (0.21 M) resulted in a structure that was stronger than PEGDA 700 made with a higher concentration of monomer (0.27 M). The combination of PEGDA 3400 (0.05 M) and PEGDA 700 (0.05 M) created a hydrogel that was stiffer than PEGDA 3400 (0.05 M). The mechanical tuning of hydrogels via PEGDA chain size combinations can be advantageous when viscous single size chain solutions inhibit chemical gas foaming. Instead of increasing monomer concentration, thereby increasing solution viscosity, different chain sizes can be combined to alter the mechanical properties of porous PEGDA hydrogels. The PEGDA chain solutions used to make hydrogels (see Fig. 1) were fluid enough to add a high density of pores via chemically initiated gas foaming.

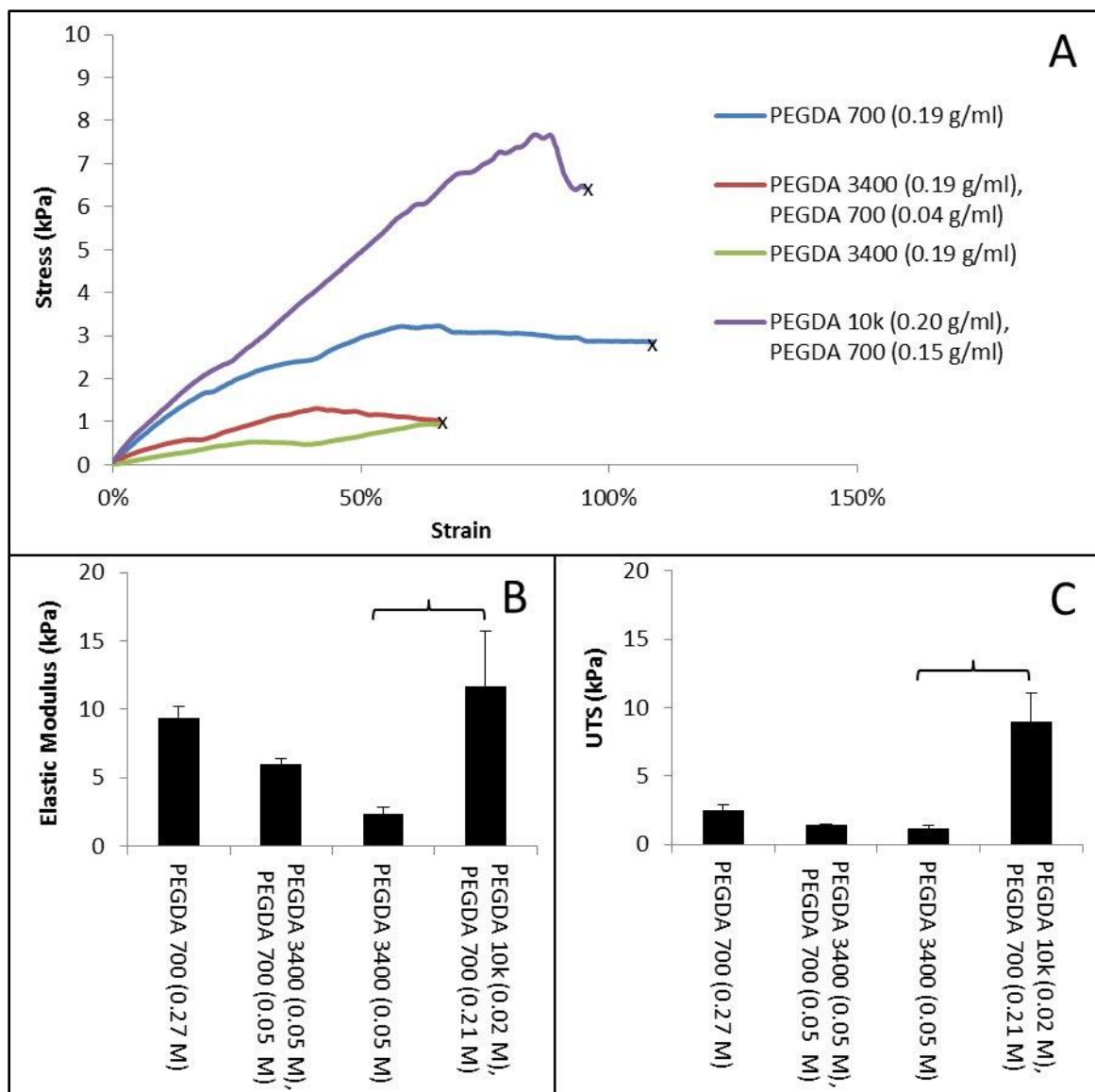


Figure 1. The combination of PEGDA chain lengths or MWs determined the mechanical properties of each substrate. The composition of each sample is listed in g/mL or in its equivalent molar concentration. The substrates' stress response to the point of failure characterized their overall strength and ductility (A); "x" marks the point of rupture for each sample. The combination of PEGDA MW 10k and 700 yielded a significantly stronger (B) and stiffer (C) porous substrate compared to the PEGDA MW 3400 sample. Compared to PEGDA 3400, the stiffness and strength obtained by combining PEGDA MW 700 and PEGDA 3400 is not statistically significant.

Representative SEM images of gas foamed PEGDA 3400 (Fig. 2A) and PEGDA 10k/700 (Fig. 2B) show interconnected pores. Surface pores of PEGDA 3400

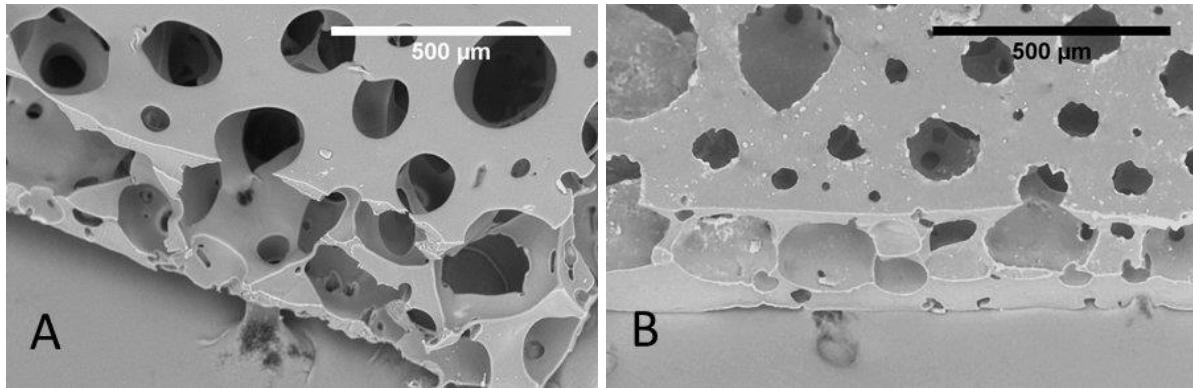


Figure 2. SEM images of PEGDA 3400 (A) and PEGDA 10k/700 (B) show that gas foaming of PEGDA creates an interconnected pore structure in the polymer.

and PEGDA 10k/700 are 65 ± 4 and 46 ± 3 μm in diameter, respectively. The ranges of surface pore diameters are 6 – 317 and 6 – 214 μm for PEGDA 3400 and PEGDA 10k/700, respectively. The pore structure is important because it provides space for cells to grow into the body of the hydrogel structure.

3.4.2 In Vitro Evaluation

The hybrid scaffolds permit cell migration and a high level of cell viability. The collagen type I network in the hybrid scaffold is shown in Figure 3. The collagen type I permits cell adhesion on the structure. At day 4 of cell migration, the majority of HT 1080s, passage 7, were viable in hybrid scaffolds made with PEGDA 3400 and PEGDA 10k/700 (Fig. 4). Calcein-AM stained viable or live cells green. Ethidium homodimer stained dead cells red; it also stains PEGDA at a lesser intensity compared to dead cells. HCF, passage 11, migration into hybrid PEGDA10k/700 scaffolds increased significantly from day 7 to day 13 (Fig. 5) per Kruskal-Wallis testing.

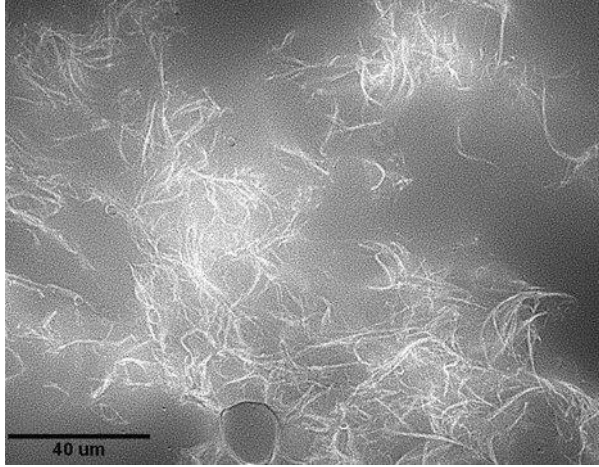


Figure 3. Collagen type I was added to porous PEGDA to aid cell spreading. The fibers displayed were strained with anti-collagen type I antibody.

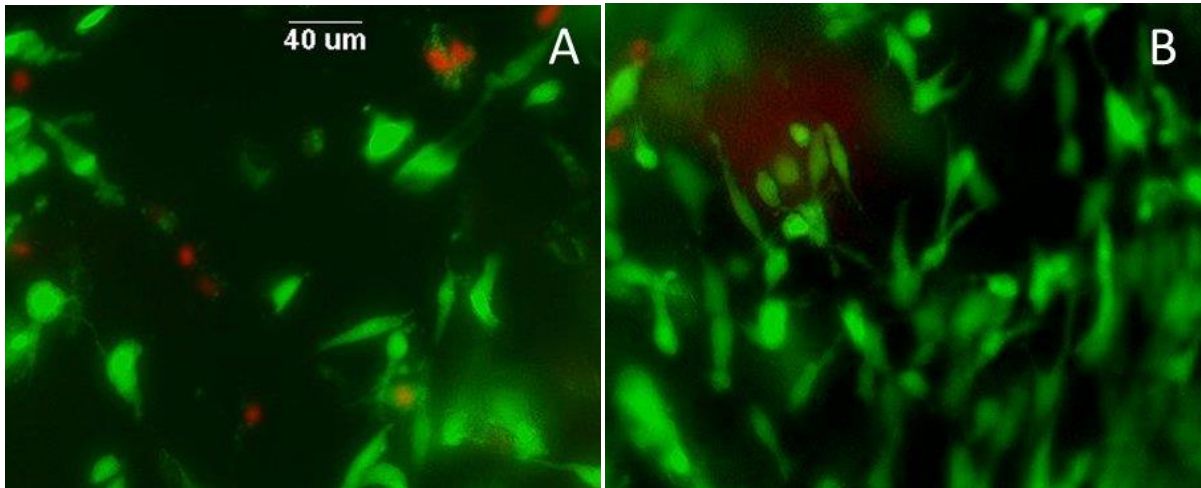


Figure 4. A human fibroblast cell line (HT 1080), passage 7, was used to evaluate the cytotoxicity of porous PEGDA infused with collagen type I. Structures made with PEGDA 3400 (A) and PEGDA 10k/700 (B) were stained to identify live and dead cells; both images were taken at 20X. Cells migrated into the structures over 4 days. Cells showed a high level of viability. Calcein-AM stained live cells green. Ethidium homodimer stained dead cells red; it also stains PEGDA at a lesser intensity compared to dead cells.

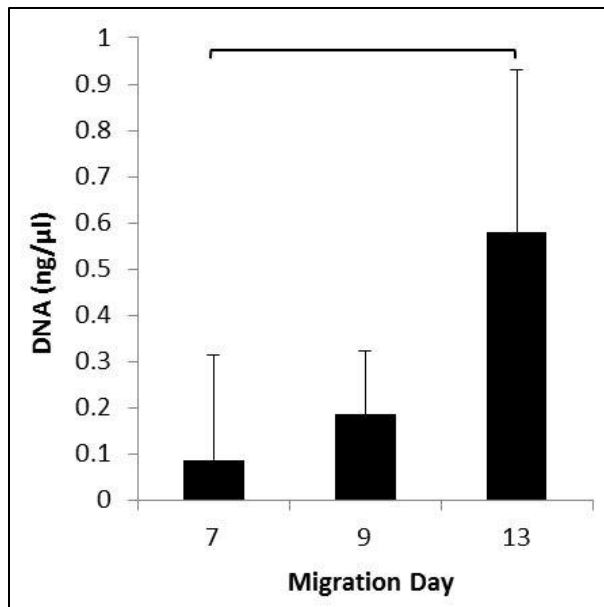


Figure 5. Increased DNA concentrations show that primary human corneal fibroblasts (HCF) migrated into the porous PEGDA 10k/700 coated with collagen type I (n = 4). Per Kruskal Wallis testing, there was a statistically significant increase in cells from day 7 to 13. The horizontal bar notes the statistically significant relationship between the two time points.

3.4.3 Subcutaneous Implants in a Mouse

Cell ingrowth was observed following subcutaneous implantation of a porous PEGDA 10k/700 scaffold into the back of a mouse. Over a period of 4 weeks, cells from the host migrated into the acellular collagen-free implant (Fig. 6A). The PEGDA biomaterial, nuclei of migrated cells, and dermal tissue can be readily be identified in the H&E stained sample, and positive anti-CD 45 staining confirms the presence of leukocytes (Fig. 6B). However, a thin fibrous encapsulation around a segment of the PEGDA suggests that the material is being tolerated by the host. [41]

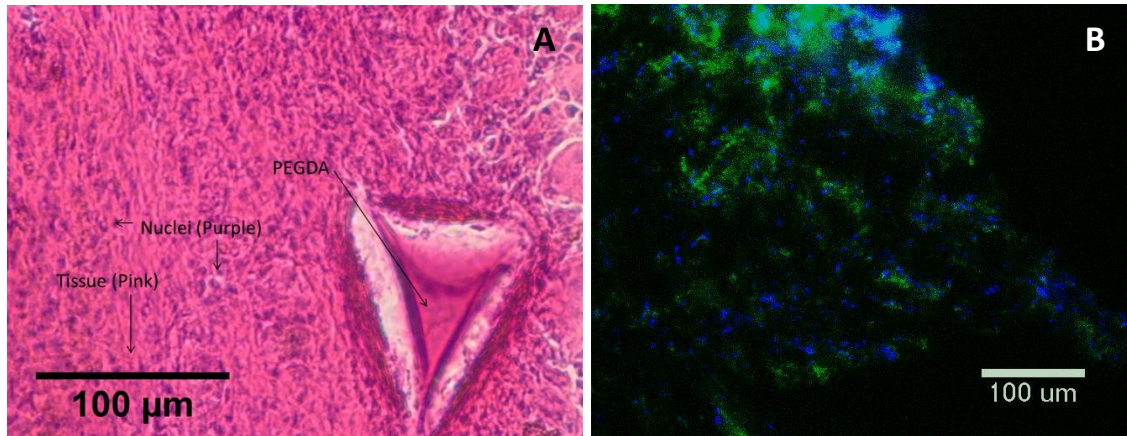


Figure 6. PEGDA 10k/700 remained under the skin of a mouse for 4 weeks. Tissue from the mouse host populated the entire body to the implanted porous PEGDA 10k/700. Following explantation, frozen sections of the sample were stained with H&E (A) and anti - CD 45 (B). Positive CD 45 staining confirms that the implant triggered an immune response. In image B, all nuclei from cells that migrated from the host are labeled with DAPI in blue, and CD 45 staining is labeled with green. Light blue coloring shows overlapping nuclei and CD 45.

3.5 Discussion

This study demonstrates that the mechanical properties of gas foamed PEGDA can be adjusted while preserving cytocompatibility and without sacrificing pore interconnectivity. Previous studies showed that PEGDA and the collagen type I infused into gas foamed PEGDA are cytocompatible. [30] [28] [42] Collagen type I is known to support the growth and development of fibroblasts in vitro and in vivo. [43] [44] [45] Keskar et. al. demonstrated that gas foamed PEGDA supports human mesenchymal stem cell (hMSC) growth for approximately 4 weeks. [30] Zhu et. al. reported smooth muscle cell growth on PEGDA with cell adhesion components. [46] Lin et. al. showed that chondrocytes encapsulated in PEGDA can proliferate for up to 4 weeks. [33] A variety of cell types thrive on PEGDA scaffolds. This suggests that gas foamed PEGDA could potentially serve as a 3D structure for a variety of cell types.

Gas foamed PEGDA structures are designed to mimic the interconnectivity of natural ECM. Interconnected pores in gas foamed PEGDA allow cells to migrate throughout the body of a porous tissue engineering structure. [42] [47] SEM images (Fig. 2) show that the polymer chain

lengths of gas foamed PEGDA can be adjusted while maintaining an interconnected pore structure. A previous study supported this finding that pore morphology remained relatively constant when different chain lengths were used to create gas foamed PEGDA. [37] Given the interconnected pore structure that permits cell ingrowth, the adjustable mechanical properties of gas foamed PEGDA could potentially aid the investigation of cell response to ECM mechanics in 3D. Keskar et. al. showed that the pore structure in gas foamed PEGDA facilitated large scale cell ingrowth in mice; however, tissue ingrowth into non-porous hydrogels was not observed. [42] The preservation of pore interconnectivity following mechanical adjustment is imperative for cell growth throughout the body of the 3D structure.

Adjusting PEGDA chain lengths is an efficient method for modulating the mechanical properties of a gas foamed PEGDA. Other laboratories have reported the effects of polymer chains sizes on the mechanical properties of polymers. [33] [36] Compression testing of blends of PEGDA MW 3400 and PEGDA MW 400 showed that different ratios of PEGDA chain sizes result in different stiffness or elastic modulus values. [34] Myung et. al. used poly (ethylene glycol) (PEG) chains ranging from 3400 to 14000 MW to adjust the mechanical properties of interpenetrating polymer networks composed of PEG and poly (acrylic acid) (PAA). [36] The mechanical properties of a tissue engineering structure can guide cell behavior, and a structure's long term survival depends on the mechanics of in vivo implantation site. [23] [48] [49] [50] [51]

The strength and stiffness of a PEGDA tissue engineering structure can be enhanced by increasing the quantity of a single PEGDA chain type. [34] [38] However, concentrated aqueous PEGDA solutions can be viscous, especially when larger chain lengths are used, and highly viscous solutions can reduce the efficacy of the chemically initiated gas foaming method described in this paper. Monomer solutions used to make hydrogels (see Fig. 1) were fluid

enough to permit gas foaming. Mechanical tuning using combinations of PEGDA chain sizes is an alternative to viscous single size chain solutions that inhibit the chemical gas foaming process. The interconnected pore network introduced by gas foaming is essential for potential 3D cell development in PEGDA.

3.6 Conclusions

The mechanical properties of gas foamed porous PEGDA depend in part on polymer chain length. After testing multiple combinations of PEGDA chain lengths or molecular weights, we determined that the presented polymer fabrication method can be used to produce cytocompatible structures with interconnected pores and a range of mechanical properties. This mechanically tunable porous structure provides a 3D structure for observing the cell's response to substrate mechanics.

4. Poly(2-Hydroxyethyl Methacrylate) - Poly(Ethylene Glycol) Diacrylate

I. Poly(2-Hydroxyethyl Methacrylate) - Poly(Ethylene Glycol) Diacrylate (PHEMA-PEGDA)

Based Keratoprosthesis

Poly(ethylene glycol) diacrylate (PEGDA) was combined with 2-hydroxyethyl methacrylate (HEMA) to create a mechanically stable and structurally relevant core-skirt model keratoprosthesis (KPro). Structures composed of poly(ethylene glycol) (PEG) and poly(2-hydroxyethyl methacrylate) (PHEMA) allow adjustable pore architecture [52] and convenient modifications for cell adhesion [53] [54]. Previous studies report the development of novel PHEMA-PEG based structures that are suitable for tissue engineering. [52] [55] [29] The copolymerization of HEMA and PEGDA units resulted in porous structures with greatly increased stiffness and ductility compared to gas foamed PEGDA hydrogels (Fig. 1). The PHEMA-PEGDA sample displayed in Figure 1 is listed as “PHEMA-PEGDA (W)” in Section II, Table 1 of this chapter. The diversity of surface features and pore sizes that can result by adjusting porogen type and volume may be advantageous for KPro development and the investigation of cell –substrate interaction.

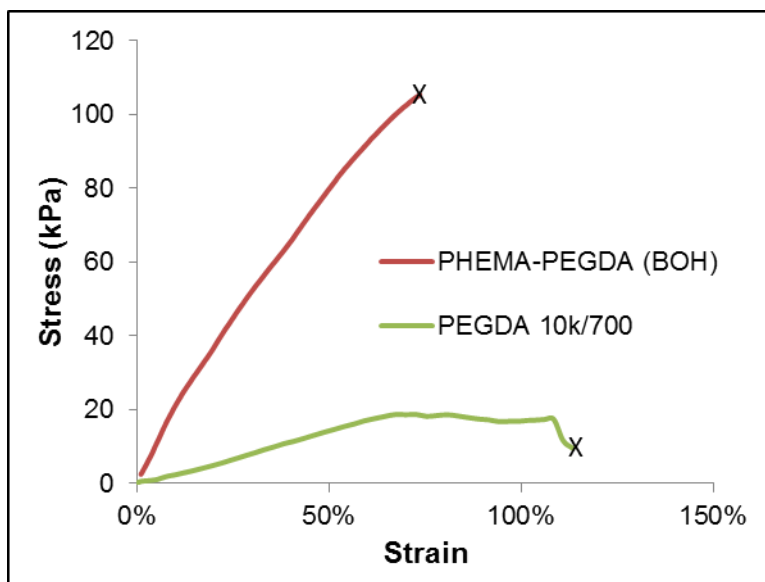


Figure 1. The copolymerization of HEMA and PEGDA resulted in porous structures with greatly increased stiffness and strength compared to PEGDA hydrogels (PEGDA 10k/700). PHEMA-PEGDA (BOH) gels were made using benzyl alcohol. Strain rates for PHEMA-PEGDA (BOH), and PEGDA 10k/700 tensile measures were 5.2 and 3.1 mm/s, respectively. Rectangular samples of each polymer type were tested in tension. “X” marks the point of tensile rupture.

II. Using Porogens to Modulate Substrate Topography in Poly(2-Hydroxyethyl Methacrylate) - Poly(Ethylene Glycol) Diacrylate (PHEMA-PEGDA)

4.1 Abstract

A copolymer composed of poly(2-hydroxyethyl methacrylate) (PHEMA) and poly(ethylene glycol) diacrylate (PEGDA) (PHEMA-PEGDA) is structurally versatile. Its structure can be adjusted using the following porogens: water, sucrose, and benzyl alcohol. A variety of surface architectures and pore morphologies were developed by adjusting porogen volume and type. The porogens appear to be cytocompatible. They add pores without adding cytotoxic impurities to the final polymer structure. Polymers coated with rat tail collagen type I permitted human corneal fibroblast (HCF) migration over 2 weeks. Differences in surface pore sizes appear to influence COL1A2 gene expression. Given known substrate topography and morphology

dependent cell activity, this mechanically stable biomaterial with adjustable pore structure can be used to investigate the influence of pore structure on cell activity.

4.2 Introduction

While cell response to topography has been widely studied, [56] [57] [58] [59] [60] the mechanisms that regulate cell interaction with topography are not clearly understood. [61] Cell – topography interaction can potentially be exploited for tissue engineering. Substrate topography can alter cell alignment and cell development. Reynolds et. al. demonstrated that cell alignment along the axis of micro and nano features is cell type dependent. [59] Multiple cell types displayed alignment in response to linear surface features of different widths and depths. Compared to MDCK canine kidney epithelial and LE2 murine (rat) lung capillary endothelial cells, hTERT immortalized primary human fibroblasts displayed high levels of cell alignment at a wider range of feature dimensions. [59] Patel et. al. used micropegs to show that topographical elements can alter cell adhesion signals. Myoblasts attached to micropegs showed increased RhoA GTPase and myosin heavy chain II (MYH2) expression. [58] Finally, surface roughness appears to regulate phenotype specific protein production in MC3T3 osteoblasts. [60] While previous investigations of cell – topography interaction enlighten our understanding concerning the phenomenon, substrate preparation was largely labor intensive and generally required specialized equipment. Substrates used to evaluate cell – surface interactions are frequently created using casting or lithography. [56] [57] [58] [59] [62] To increase the efficiency of patterned substrate production, an alternative fabrication process may be warranted. This study proposes a fabrication process that utilizes common laboratory equipment and commercially available products to add topographical features to a biomaterial. By reducing substrate fabrication times, the proposed process may also accelerate efforts to better understand and manipulate cell – topography interaction. To this end, we attempted to use phase separation to create a variety of surface features on a PHEMA-PEGDA copolymer.

The patterned PHEMA-PEGDA structures are easy to produce and non – toxic. Furthermore, they are mechanically stable enough to resist fracture during routine handling.

Compared to previously reported poly(2-hydroxyethyl methacrylate) -poly(ethylene glycol) (PHEMA-PEG) structures, [52] our combination of HEMA and PEGDA results in a wide variety of surface features. Since PEG is more hydrophilic than PHEMA, [52] small volumes of PEGDA were used to both preserve phase separation in the copolymer and crosslink HEMA. Greater hydrophilicity introduced by PEGDA can suppress phase separation by increasing the solubility of the copolymer chains, [52] but the selected ratios of HEMA and PEGDA units yield mechanically stable copolymers that are structurally sensitive to solvent or porogen adjustments. Changes in porogen type and volume lead to noticeable changes in surface feature sizes and distributions. PHEMA-PEGDA structures presented in this study may support current efforts to elucidate the mechanisms involved in the cell's response to a substrate's structural features.

4.3 Methods

4.3.1 Making Porous PHEMA-PEGDA

PHEMA-PEGDA copolymers were created for biological testing, mechanical testing, and structural assessment. For biological and mechanical testing, PHEMA-PEGDA structures were made with 7% w/v PEGDA MW 3400 (Glycosan GS710), 2% v/v PEGDA MW 700 (Sigma-Aldrich, 455008), and 38% v/v HEMA (Sigma-Aldrich 128635). Ammonium persulfate (APS) and N,N,N',N'-tetramethylethylenediamine (TEMED) initiated the polymerization. Samples were made using the following porogens: deionized water (W), sucrose (S) 150% w/v, or benzyl alcohol (BOH). Samples W1, S1, and BOH1 in Table 1 are the copolymer formulations that were used in biological and mechanical testing. All copolymers listed in Table 1 were evaluated with scanning electron microscopy (SEM). Additional PHEMA-PEGDA formulations were

created to further explore the relationship between porogens and polymer surface features include samples W2, S2, BOH2, W3, S3, and BOH3 (Table 1). Table 1 outlines the porogen types and volumes that were used. As porogen volumes were increased, monomer and initiator volumes remained unchanged.

Sample	Sample Code	Deionized Water (dH ₂ O)	Sucrose (150% w/v in dH ₂ O)	Benzyl Alcohol	PEGDA 3400 (40% w/v in dH ₂ O)	PEGDA 700	HEMA
PHEMA-PEGDA (W)	W1	52%	--	--	17%	2%	38%
PHEMA-PEGDA (S)	S1	34%	18%	--	17%	2%	38%
PHEMA-PEGDA (BOH)	BOH1	34%	--	18%	17%	2%	38%
PHEMA-PEGDA (W) – 2X	W2	59%	--	--	14%	2%	32%
PHEMA-PEGDA (S) – 2X	S2	29%	31%	--	14%	2%	32%
PHEMA-PEGDA (BOH) – 2X	BOH2	29%	--	31%	14%	2%	32%
PHEMA-PEGDA (W) – 3X	W3	65%	--	--	12%	1%	28%
PHEMA-PEGDA (S) – 3X	S3	25%	40%	--	12%	1%	28%
PHEMA-PEGDA (BOH) – 3X	BOH3	25%	--	40%	12%	1%	28%

Table 1. Porogens used to add pores to PHEMA-PEGDA include water (W), sucrose solution (S), and benzyl alcohol (BOH). Polymers used in biological and mechanical testing include samples W1, S1, and BOH1. In an attempt to adjust the pore structure of PHEMA-PEGDA, added porogen volumes were doubled in samples W2, S2, and BOH2. The doubled volume is in comparison to W1, S2, and BOH. Porogen volumes were tripled in W3, S3, and BOH3.

4.3.2 Adding Collagen to PHEMA-PEGDA

Prior to seeding cells, PHEMA-PEGDA structures were coated with cross-linked rat tail collagen type I (2 mg/mL) (BD Bioscience). Collagen was crosslinked using N(3-Dimethylaminopropyl)-N'-ethyl-carbodiimide (EDC) (5 mM) and N-hydroxysuccinimide (NHS) (5 mM). Dehydrated implants were incubated the collagen gel solution for 2 hours on ice. The collagen was allowed to gel at 37°C for 1 hour.

4.3.3 Cell Culture

In preparation for biological testing, copolymer sheets of samples W1, S1, and BOH1 were cut into disks of approximately 7 mm diameter and 0.5 mm thickness. PHEMA-PEGDA samples were subjected to an extensive washing process. W1 and S2 were rinsed in deionized water and ethanol solutions for 6 days; BOH1 samples were rinsed in the same solutions for 9 days. At the end of the rinsing process, samples were dried in an oven at 37°C. Each sample was UV sterilized prior to biological testing. Cell-free collagen coated PHEMA-PEGDA structures were placed on top of the layer of confluent HCFs. Primary human corneal fibroblasts (HCFs), passage 7, were grown to confluence in a petri dish. Cells were feed every 2 - 3 days with GIBCO MEM alpha (Invitrogen, 12561), supplemented with 10% fetal bovine serum (FBS) (Atlanta Biologicals) and 1% antimicrobial-antimycotic solution (Sigma-Aldrich, A5955).

4.3.4 Cell Survival and Migration

A fluorescent DNA quantification kit (BioRad, 170-2480) was used to assess cell migration onto PHEMA-PEGDA structures. The Hoechst 33258 in the BioRad DNA assay allows double stranded DNA to be quantified in the range of 20 ng to 10 µg. DNA was extracted from the copolymer structures using TRIzol per the manufacture's protocol. Two DNA pellets were tested for each time point. For each sample, 80 µL of the assay solution was added to a well of

a 384 well plate. Six duplicate wells were used to measure each DNA pellet. Fluorescent signals were measured using the Tecan Genios Pro Spectrophotometer.

4.3.5 Collagen Type I Production

Quantitative RT-PCR was used to evaluate collagen type I gene expression. RT-PCR was performed using the AgPath-ID One-Step RT-PCR Kit (Applied Bioscience). Taqman primer and probe sets for human GAPDH and COL1A2 were also obtained from Applied Bioscience. RNA was isolated using TRIzol per the manufacture's protocol. One RNA pellet was tested per time point. Six duplicate wells were measured per RNA pellet.

4.3.6 Testing Porous PHEMA-PEGDA in Tension

PHEMA-PEGDA structures, made per Table 1, were tested in tension using a custom designed Test Resources mechanical testing machine. Three samples of selected formulations (samples W1, S1, and BOH1) were tested using a calibrated WF75GS Load Cell (Test Resources Inc.), which is fatigue-rated for 75 g of force (0.735 N) in tension and compression. Polymer structures were made in dumbbell shaped molds for tension testing. Dumbbell shaped test samples were designed based on ASTM D638 Figure 1 Type IV. Sample dimensions were 95 – 105 x 6.6 – 7.2 x 0.5 – 1.0 mm (height x width x thickness). First, a strain of 2 - 5% was applied for 30 cycles to pre-condition the samples. Next, elastic modulus was calculated using a 2 - 10% strain for 30 cycles. Strain rate was approximately 1 mm/s for all elastic modulus measures. Mid-range cycles, typically 10 - 20, were used to compute the elastic modulus. The scan rate for the force measure was 50.86 Hz. Damping factors were calculated using the phase shifts between the stress over time and strain over time curves. The tangent of the horizontal phase shift corresponds to the energy loss of the copolymer per tension cycle; the value is known as the damping or dissipation factor. [63] Phase shifts were measured using MATLAB.

4.3.7 Structural and Chemical Characterization

Scanning Electron Microscopy (SEM) images were generated using a S-3000N Variable Pressure SEM (Hitachi). Low magnification SEM images were taken of uncoated PHEMA-PEGDA. Prior to high magnification imaging, structures were laser ablated with gold using a Pulsed Laser Deposition System (Excel Instruments). Images were used to evaluate the effects of porogens on surface textures and structures. Surface pore areas and shapes were measured using Image J 1.47c. Images that best represented the overall surface pores were digitally processed and thresholded in preparation for measurement. Each pore area was measured with the Analyze Particles function of ImageJ 1.47c.

The elemental composition of PHEMA-PEGDA structures was evaluated using X-ray photoelectron spectroscopy (XPS). XPS experiments were performed using the Kratos Axis-165 instrument. Samples were irradiated by a monochromatic Al-K α X-ray source (15 kV, 10 mA) at an angle of 30 degrees from the sample surface. Photoelectrons were detected by 8 channeltrons of the concentric hemispherical analyzer over an area of 700 x 300 μm , with a spectrometer take-off angle of zero. The detection was achieved using the constant analyzer energy (CAE) mode. Survey scans were acquired with a pass-energy of 160 eV, 1.0 eV step-size and 100 ms dwell time; while narrow scans were acquired with a pass-energy of 20 eV, 0.1 eV step-size and 200 ms. All scans were performed with the charge-neutralization system running. Charge-referencing was done with the adventitious carbon peak position of 284.8 eV.

Nuclear Magnetic Resonance (NMR) was used to evaluate the stability of the PHEMA-PEGDA gel in aqueous solution. A PHEMA-PEGDA (W) gel, see Table 1, was incubated in PBS for 3 days. Then, NMR measures were taken from both the PBS soaked gel and a solution of HEMA and PEGDA monomers. The ratio of HEMA to PEGDA in the monomer mixture was equal to the ratio of monomers used to create PHEMA-PEGDA gels. All ^{13}C NMR measurements were

acquired using the “zgpg” pulse program at room temperature on a 8.5 T (^1H frequency = 360.13 MHz and ^{13}C frequency, 90.55 MHz) Bruker Avance spectrometer equipped with a QNP probe capable for multinuclear NMR measurements. A capillary filled with D_2O was immersed in NMR tube for locking the deuterium signal. The solid gel samples were immersed in PBS for three days and placed on top of a doty aurum plug (14mm) to keep the samples at the center of rf coil. The 90° pulse width was 13.5 μs for monomer solutions and was used as it is for polymer samples. The relaxation delay in all experiments was set to 2 s. The gel spectra were acquired with 1024 scans (signal accumulations) as compared to only 4 scans for liquid spectra.

4.3.8 Statistical Analysis

MATLAB R2012a was used to conduct all statistical analysis at an alpha level of 0.05. The statistical significance of mechanical data and COL1A2 gene expression were evaluated using ANOVA. Kruskal-Wallis was used to evaluate the statistical significance of copolymer pore measures and cell migration data. All reported error measures are the standard error.

4.4 Results

4.4.1 Testing Porous PHEMA-PEGDA in Tension

The porogen type influenced the elastic modulus and viscoelasticity of PHEMA-PEGDA. PHEMA-PEGDA samples W1, S2, and BOH1 were included in mechanical testing. PHEMA-PEGDA made with water porogen, W1, was significantly stiffer than PHEMA-PEGDA made with benzyl alcohol porogen, BOH1 (Fig. 1A). Damping factors ($\tan(\delta)$) at room temperature show that the porogens had a statistically significant effect on structure viscoelasticity. The damping factor for the sample made with sucrose porogen, S1, is significantly higher than BOH1. Samples W1, S1, and BOH1 were viscoelastic with dominant elastic properties (low energy loss; Fig. 1B). A perfectly elastic material would have a damping factor of 0. [63] [64] The largely elastic PHEMA–PEGDA samples are expected to maintain their mechanical properties

during general laboratory handling. Samples comfortably resist rupture at 25 kPa of force and 20% strain.

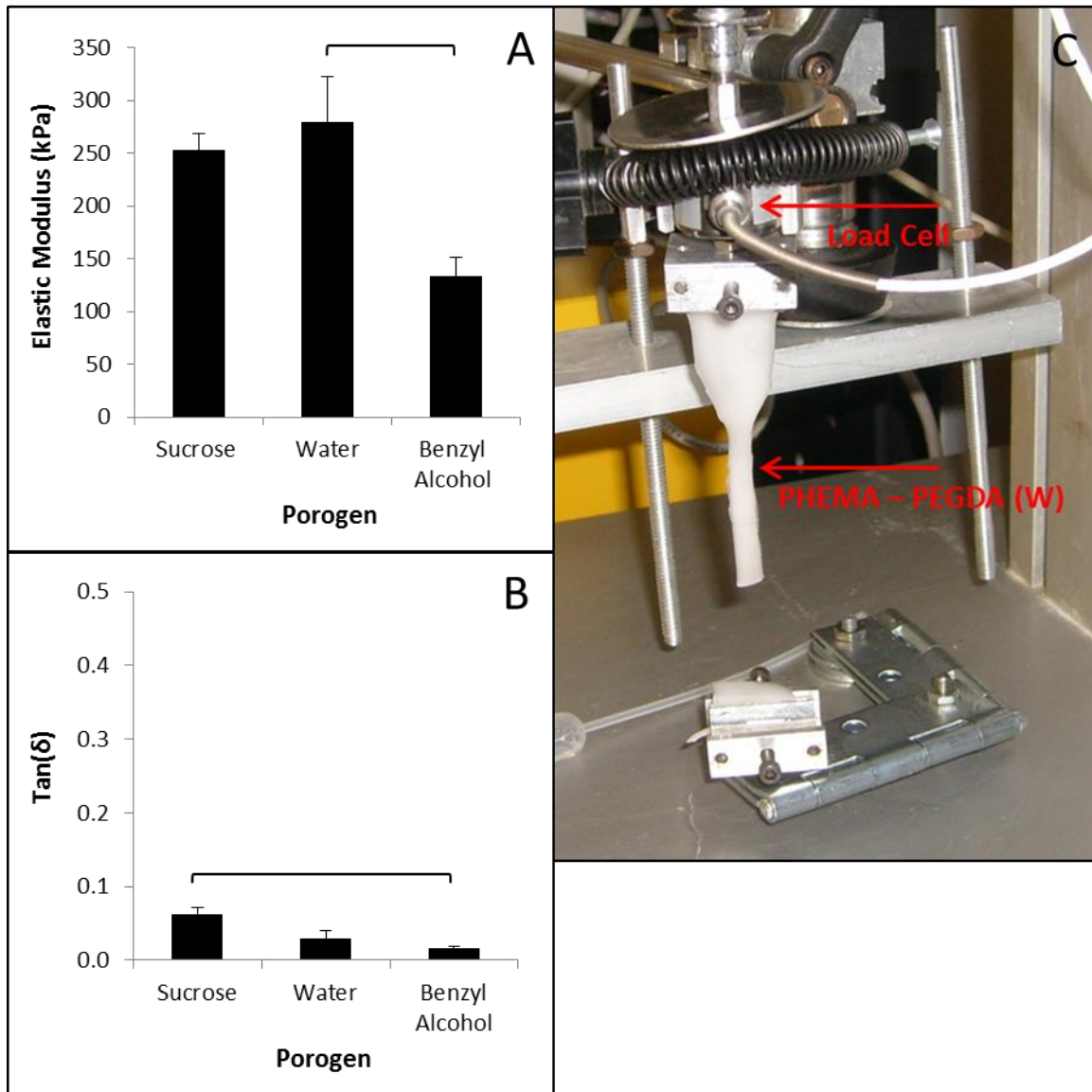


Figure 1. Tensile testing ($n = 3$) showed that the use of a given porogen can significantly alter the mechanical properties of a hydrogel (A). Horizontal bars identify samples with statistically significant relationships. PHEMA-PEGDA made with water porogen was significantly stiffer than samples made with benzyl alcohol porogen. Low damping factors ($\tan(\delta)$) show that the PHEMA-PEGDA samples are viscoelastic with dominant elastic properties (B). PHEMA-PEGDA made with sucrose porogen had a significantly larger damping factor than samples made with benzyl alcohol porogen. Image (C) illustrates the apparatus that was used to test polymers in tension. PHEMA-PEGDA (W) is shown following rupture. The dumbbell shaped sample failed in the narrow mid-section.

4.4.2 Surface Texture of PHEMA-PEGDA

SEM images (Figs. 2 - 3) show that water, sucrose, and benzyl alcohol create a wide variety of surface features on PHEMA-PEGDA. Most PHEMA-PEGDA formulations in Figures 2 – 3 created structures with well-defined surface pores. Three formulations primarily produced 3D projections that cannot be classified as surface pores: PHEMA-PEGDA (W) – 3X (W3), PHEMA-PEGDA (S) – 3X (S3), and PHEMA-PEGDA (BOH) – 3X (BOH3). The aforementioned structures were created by tripling the added porogen volume compared to samples W1, S1, and BOH1. The surfaces of W3, S3, and BOH3 are characterized by wave – like features followed by a few shallow circular surface pores. The surface of sample S3 consists of macrosized bulbous projections and intermittent patches of surface pores. PHEMA-PEGDA copolymers made with tripled porogen volumes exhibit a variety of surface features that are not present in the other PHEMA-PEGDA samples. Only the SEM images of copolymer samples with well-defined surface pores were measured with ImageJ (Fig. 4).

ImageJ was used to measure the pore area of SEM images that best represented the surface pores sizes of PHEMA-PEGDA structures (Fig. 4). Surface pore measures quantified the diversity of pores that the porogens created. The surface pore sizes of PHEMA-PEGDA structures were significantly different from each other. Water created the largest average pore size in PHEMA-PEGDA when the volume of added water was doubled, W2. The increase in water porogen from sample W1 to W2 resulted in an increase in surface pore sizes, but tripling the volume of water porogen resulted in a sharp decline in pore size (W3). Results from sucrose and benzyl alcohol porogens show that surface pore areas were the largest with samples S1 and BOH1. Doubling sucrose and benzyl alcohol volumes reduced average pore areas, S2 and BOH2.

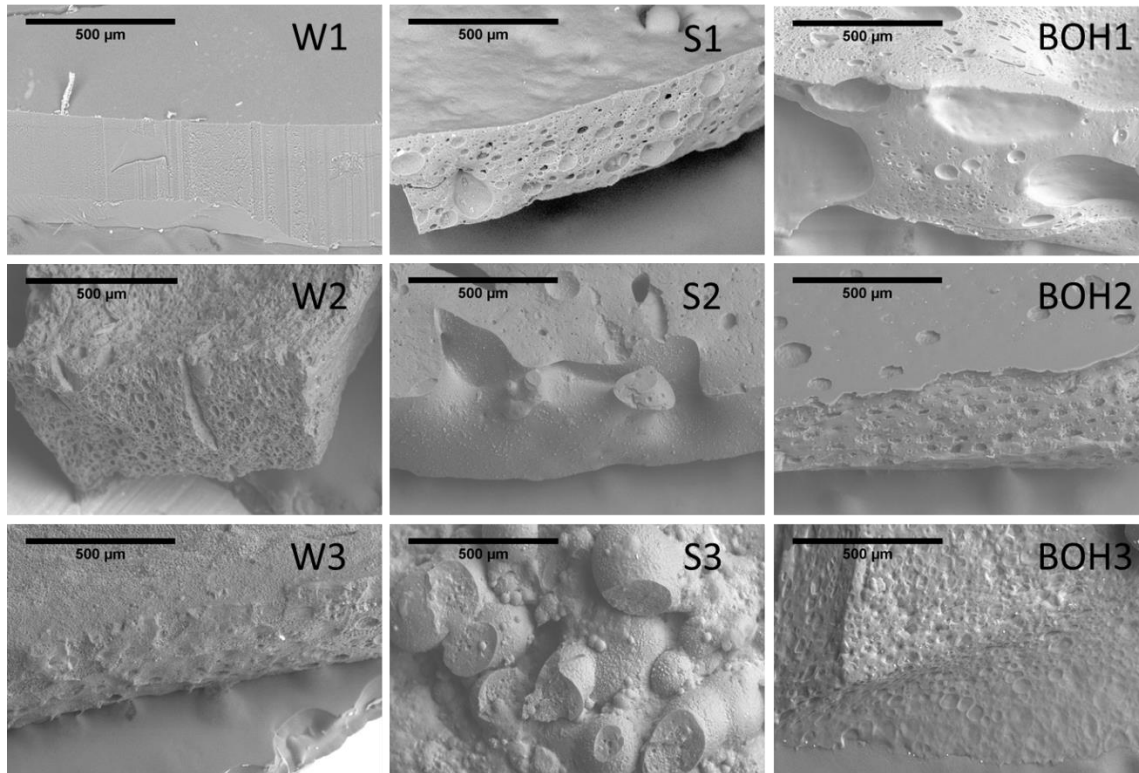


Figure 2. Low magnification SEM images show the effects of porogen volume and type on the surface topography of PHEMA-PEGDA. The image labels correspond to the sample codes in Table 1. Water (1), sucrose (2), and benzyl alcohol (3) were used as porogens. Compared to W1, S2, and BOH1 samples, porogen volumes were doubled for W2, S2, and BOH2. Porogen volumes were tripled for W3, S3, and BOH3.

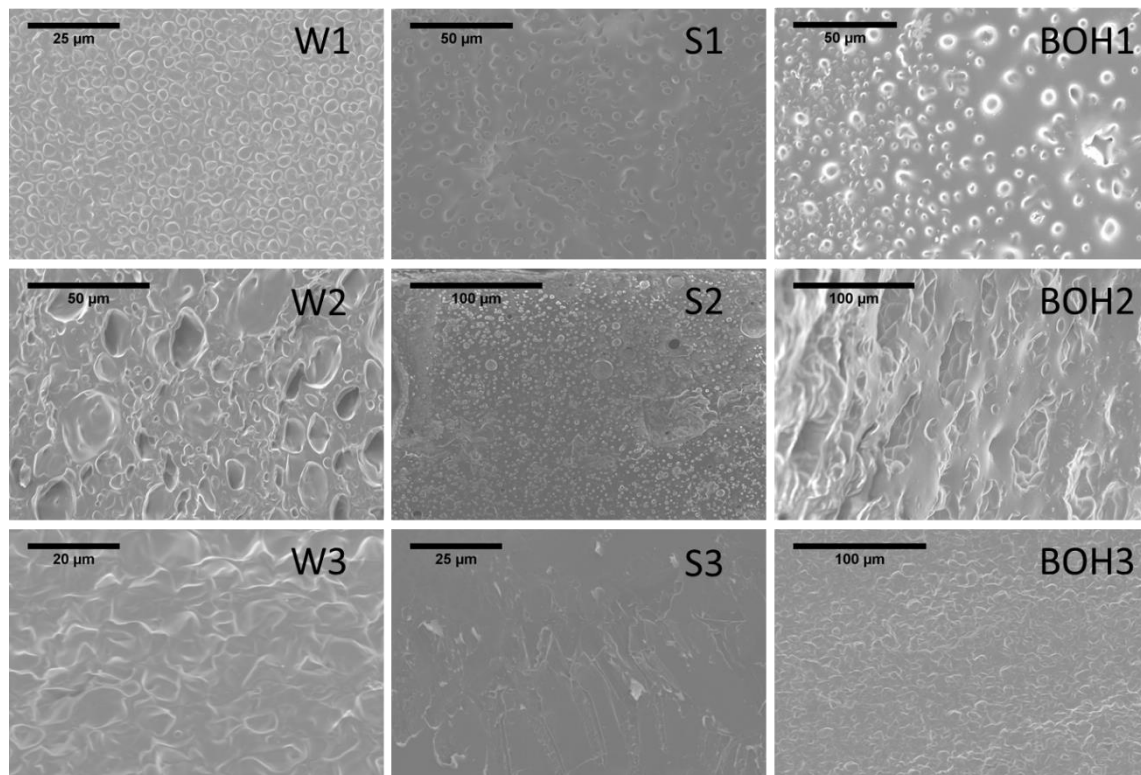


Figure 3. High magnification SEM images show the effects of porogen volume and type on the surface topography of PHEMA-PEGDA. The image labels correspond to the sample codes in Table 1. Water (1), sucrose (2), and benzyl alcohol (3) were used as porogens. Compared to W1, S2, and BOH1 samples, porogen volumes were doubled for W2, S2, and BOH2. Porogen volumes were tripled for W3, S3, and BOH3.

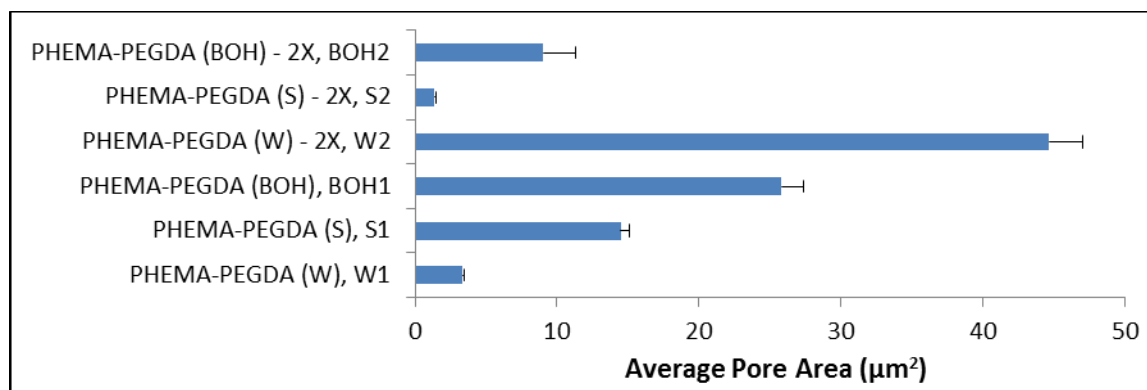


Figure 4. Surface pore areas of PHEMA-PEGDA samples were measured in ImageJ using SEM images. Six of the porogen recipes resulted in measurable pore structures. For each sample, pore areas were significantly different from each other. When the volume of water porogen was doubled, PHEMA-PEGDA (W) – 2X, water created the largest average pore size in PHEMA-PEGDA.

4.4.3 Chemical Assessment of Copolymer

XPS (Table 2) and NMR data showed the elemental composition and aqueous stability, respectively, of PHEMA-PEGDA. XPS data suggests that porogens (water, sucrose, and benzyl alcohol) modified the pore structure of PHEMA-PEGDA without changing the chemical composition of the polymer. XPS was used to evaluate the elemental composition of polymers made with three porogens: water, sucrose, and benzyl alcohol. The carbon (C 1s) to oxygen (O 1s) ratio for resulting structures was 2.2 – 2.3. The C 1s : O 1s ratio for PEGDA was lower, 1.7. The ratio appears to reflect chemical differences between the PHEMA-PEGDA and PEGDA gels.

Element Ratio (C 1s : O 1s)	XPS			
	PHEMA-PEGDA (Each Porogen Type)			PEGDA
	Water	Sucrose	Benzyl Alcohol	
	2.28	2.24	2.31	1.71

Table 2. XPS data suggests that porogens modified the pore structure of PHEMA-PEGDA gels without changing the chemical composition of the polymer. XPS was used to evaluate the elemental composition of polymers made with three porogens: water sucrose, and benzyl alcohol. The carbon (C 1s) to oxygen (O 1s) ratio for resulting structures was ~ 2.2 – 2.3.

Figure 5 shows high resolution ^{13}C NMR spectra at 8.45 T (^1H freq. 360 MHz) for a solution of HEMA and PEGDA (Fig. 5A) and a PHEMA-PEGDA gel soaked in PBS for three days (Fig. 5B). The peak assignments for spectral lines are based on both published literature [65] [66] and general NMR references. [67] [68] The spectra in Figure 5A show that the HEMA and PEGDA units in solution are not chemically connected as all of the peaks can be assigned to individual components. Figure 5B shows the spectra of PHEMA-PEGDA gel following 3 days in PBS. Since the nuclei in gel polymers have stronger dipolar couplings with other nuclei, we did not expect to see any signal from the gel soaked in PBS if the units of gel structure were all linked. However, the middle repeat O-CH₂ group of PEGDA is found to be present at 70 ppm in gel spectra with the line width of approximately 20 Hz (the line width for this spectral line is 6 Hz in liquid spectra), which indicates that PEG units may have leached out of the PHEMA-PEGDA gel following 3 days in PBS (Fig. 5B). It appears that neither HEMA nor PHEMA leached, as none of the peaks from HEMA is present in the PBS soaked gel spectra. The leached PEG units do not appear to impact the cytocompatibility. However, the implications of this for in vivo applications depends on the host's response to PEG units at the given implantation site. For example, PEG units could conceivably present challenges if the leached component obstructed flow in a given tissue.

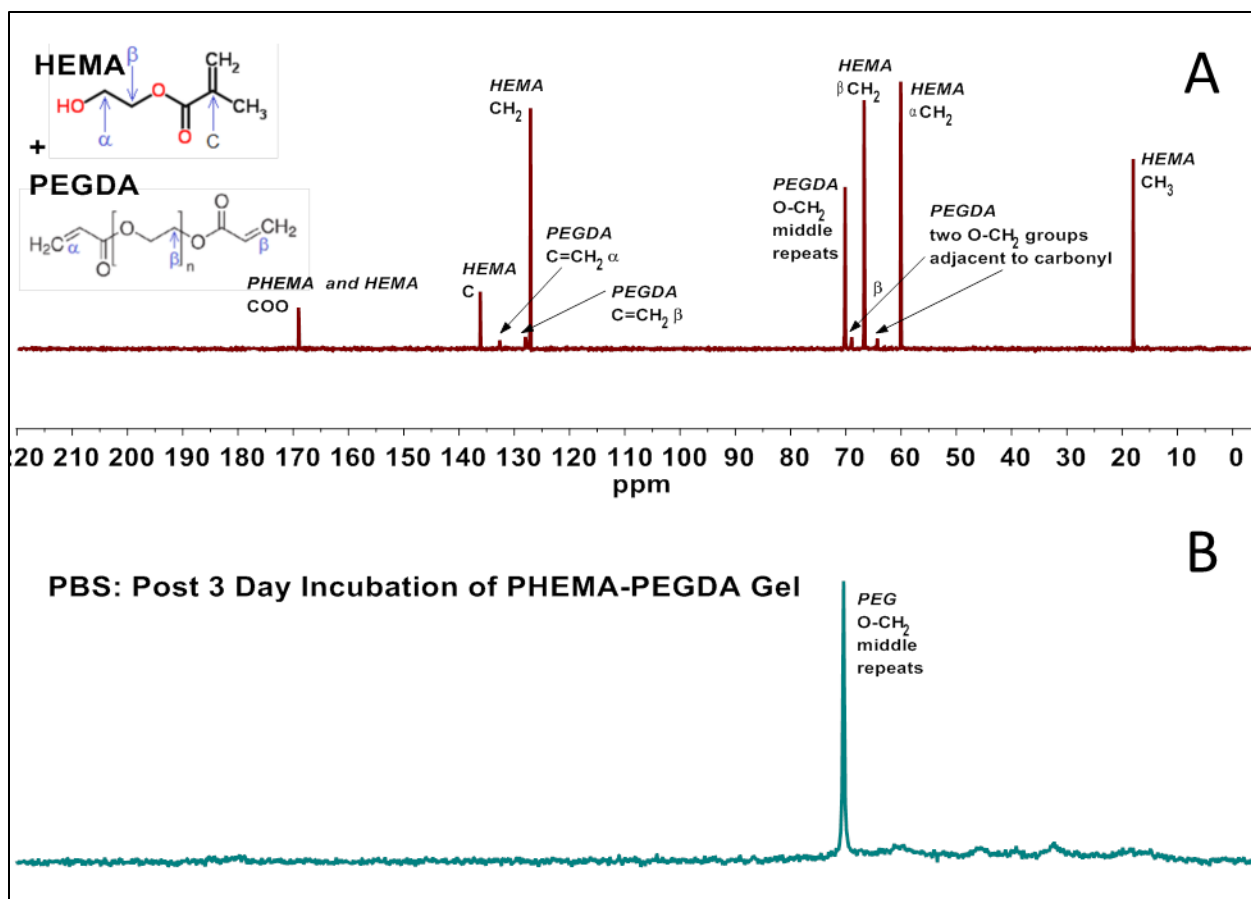


Figure 5. NMR data is shown for PEGDA and HEMA units in solution (A) and for the PHEMA-PEGDA gel in PBS (B). PEG chains may have leached out of the PHEMA-PEGDA gel following 3 days in PBS. The signal for the middle O-CH₂ group of PEGDA (A) and the middle O-CH₂ group of PEG (B) were both be found at approximately 70 ppm. Signals that represent the repeating side groups in PHEMA were not observed in PBS, so it appears that PHEMA did not leach.

4.4.4 Cellular Response to Copolymers

Human Corneal Fibroblasts (HCFs) migrated onto collagen type I coated PHEMA-PEGDA and expressed a type I collagen gene (COL1A2). Figure 6 shows the collagen type I fibers covering PHEMA-PEGDA structures. DNA concentration measures (Fig. 7) show that HCFs migrated onto the PHEMA-PEGDA structures. For PHEMA-PEGDA (S), S1, a significant increase in cells was observed at day 10. Cell migration on PHEMA-PEGDA (BOH) was significantly lower than cell migration measured on substrates made with water (W1) or sucrose (S1). A comparison of W1 and S1 showed that the two structures supported a statistically equivalent amount of cell migration. COL1A2 expression was evaluated to assess HCF activity on the PHEMA-PEGDA structures (Fig. 8). COL1A2 refers to the human gene for pro α 2 type I collagen (α 2(I)); α 2(I) is one of the polypeptide chains that constitutes collagen type I. [69] COL1A2 expression remained constant from days 7 to 13 on W1 and S1 substrates except for a significant drop in COL1A2 expression on S1 at day 10. COL1A2 expression on BOH1 significantly increased from days 7 to 10 and from days 10 to 14.

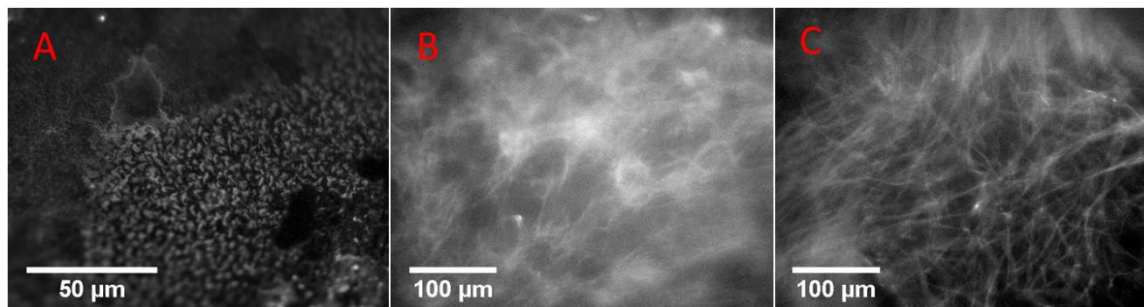


Figure 6. Collagen type I (2 mg/mL) coated PHEMA-PEGDA samples were stained with a collagen type I antibody (Sigma-Aldrich, C2456). Collagen fibers are shown in white. Collagen gelled within the micron sized surface pores of PHEMA-PEGDA (W), image A. Collagen fibers are also apparent in PHEMA-PEGDA (S) and PHEMA-PEGDA (BOH), images B and C respectively.

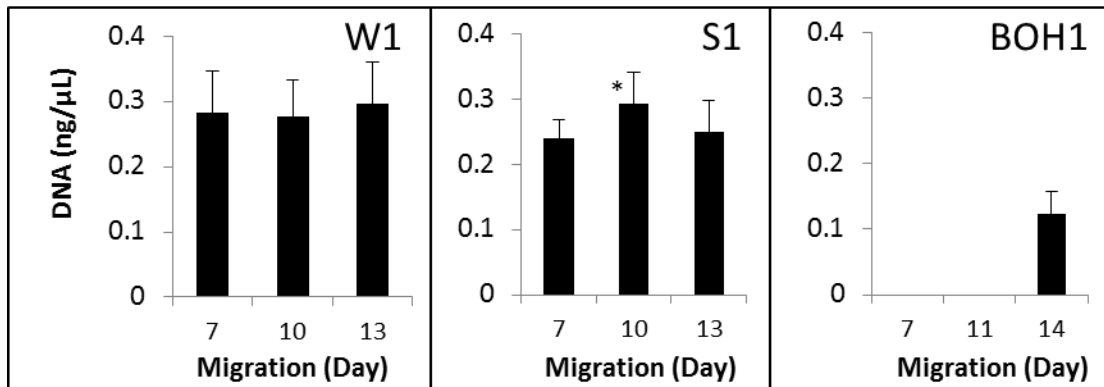


Figure 7. HCFs migrated onto PHEMA-PEGDA substrates, and the presence of the cells was observed for up to 2 weeks (n = 2). The substrates consisted of PHEMA-PEGDA overlaid with cross-linked rat tail collagen type I (2 mg/mL). Water (W1), sucrose (S1), and benzyl alcohol (BOH1) were used to create pores. The asterisk (*) identifies a statistically significant increase in DNA concentration for the sucrose substrate. DNA concentration on the benzyl alcohol substrate is significantly lower than concentrations measured on water and sucrose substrates. A comparison of water and sucrose substrates showed that they support a statistically equivalent amount of cell migration.

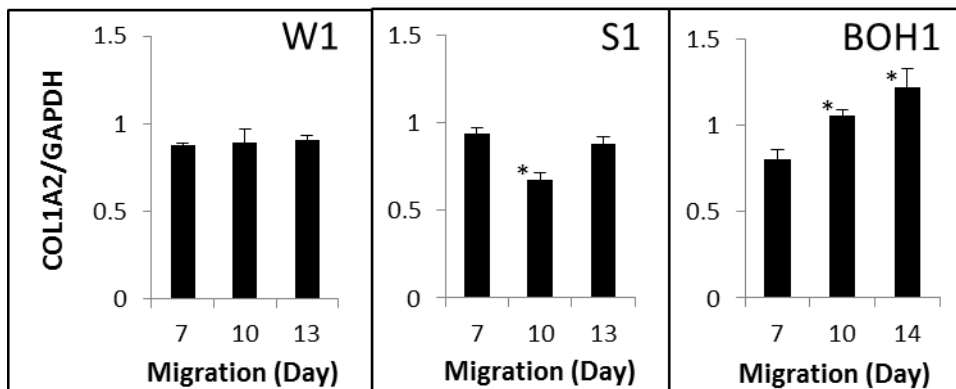


Figure 8. HCF COL1A2 expression was measured on PHEMA-PEGDA substrates. Hydrogel samples were made with water (W1), sucrose (S1), and benzyl alcohol (BOH1) porogens. The asterisk (*) notes a statistically significant increase or decrease in COL1A2 expression for a given substrate. On the sucrose porogen substrate (S1), there was a significant decrease in day 10 COL1A2 expression. On samples made with benzyl alcohol porogen (BOH1), statistically significant increases in COL1A2 expression were observed from day 7 to 10 and from day 10 to 14.

4.5 Discussion

The presented PHEMA-PEGDA formulations (Figs 2 - 4) offer a wider range of surface pore sizes compared to previously published PHEMA and PHEMA-PEG formulations. [52] [55] [70] [71] Horák et. al. created porous PHEMA using sodium chloride (NaCl) and sucrose. Pores made with NaCl were up to 9 μm in diameter, and pores made with sucrose were up to 26 μm in diameter. They demonstrated that PHEMA pore size depends on the type and volume of both crosslinkers and porogens. [71] Dziuble et. al. created PHEMA - poly(ethylene glycol) monomethacrylate (PEGMA). Average pore size for PHEMA-PEGMA was 7 – 16 μm . [70] Baker et. al. created surface pores as large as 50 μm in poly(2-hydroxyethyl methacrylate) - poly(ethylene glycol) methyl ether methacrylate (MeO-PEGMA) using NaCl. [52] PHEMA-PEGDA formulations presented in this study can be adjusted to produce average surface pore areas of from 1.4 ± 0.1 to $44.6 \pm 2.3 \mu\text{m}^2$. The complete range of pore areas for Table 1 structures was $0.8 - 15625.0 \mu\text{m}^2$. However, the surface of a mold can affect the external morphology of the resulting hydrogel. [72] Gel surfaces that were adjacent to the surface of the glass mold had to be removed in order to view the true porosity of the PHEMA-PEGDA structures.

Pore diameters in PHEMA-PEGDA copolymers followed a bell shaped function as solvent fractions increased (Table. 1 and Figs. 2 - 4). Small pores, approximately 2 μm in diameter, were observed in structures made with 52% v/v deionized water. At a mid-range of aqueous solvent content (65% v/v), pore sizes increased, but pore sizes were reduced when aqueous content was increased to 65% v/v. Similar patterns were observed in PHEMA-PEGDA made with sucrose and benzyl alcohol porogens. PHEMA drove the formation of pores in PHEMA-PEGDA. Previous studies show that hydrogels made with low aqueous content HEMA [73] or HEMA-PEGMA [52] solutions result in structures with pores that are impenetrable to cells. Pores in PHEMA-PEGDA formed as polymers fell out of solution during polymerization. The

Gibbs free energy of mixing (ΔG^M) affects the ability of a polymer to remain in solution and the resulting pore structure of a full polymerized hydrogel. When $\Delta G^M < 0$, a homogeneous polymer solution exists. As monomers are converted to polymers in a free radical polymerization, the Gibbs free energy of polymerization (ΔG^P) is negative to make polymerization thermodynamically feasible. $\Delta G^M = G_{12} - (G_1 - G_2)$, where G_{12} is the Gibbs free energy of the solution. G_1 and G_2 are the Gibbs free energy of solution components. Negative ΔG^P is related to the polymer solution and a solution component. Therefore a $-\Delta G^P$ may drive the ΔG^M above 0 and cause polymerizing units to fall out of solution. The pore structures that result from given solvents and additives are also related to ΔG^M . ΔG^M is a function of solvent-polymer interaction. The Flory-Huggins interaction parameter (χ) describes the difference in energy between a pure polymer and a polymer immersed in pure solvent. Since ΔG^M is a function of χ , the resulting voids that form as polymerizing chains fall out of solution are a function of solvent and polymer interaction. [64]

The topographical features of substrates affect both in vitro and in vivo cell activity. Cell membrane alteration caused by surface features may initiate the cell's response to a given topography. [61] Differences in cell activity on the PHEMA-PEGDA structures suggest that they could be used to better understand the mechanisms involved in cell-substrate communication. Compared to PHEMA-PEGDA (W) or (S), PHEMA-PEGDA (BOH) structures slowed and reduced cell migration (Fig. 7). However, COL1A2 expression significantly increased on PHEMA-PEGDA (BOH) from day 7 to 10 and from day 10 to 14 (Fig. 8). Human corneal fibroblast (HCF) expression of COL1A2 was used to evaluate cell activity because COL1A2 is expressed by cornea cells. [74] [75] The majority of HCFs used in this experiment originated from human corneal stroma. Type I collagen is the principal collagen type synthesized by in vitro and in vivo corneal stromal cells. [76] [77] Over time, corneal stromal keratocytes in cell

culture transform to fibroblasts. [78] COL1A2 data shows that pore size may influence COL1A2 expression in HCFs. COL1A2 expression trends observed on PHEMA-PEGDA (BOH) structures differ from expression on PHEMA-PEGDA (S) and PHEMA-PEGDA (W) structures (Fig. 9). Pore sizes on the PHEMA-PEGDA (BOH1) structures were significantly larger than PHEMA-PEGDA (S1) and PHEMA-PEGDA (W1) (Fig. 4). Previous studies identified a relationship between cell activity and substrate pore size. [79] [80] Chondrocytes produced more sulfated glycosaminoglycans (GAGs) on scaffolds with 160,000 μm^2 pores compared to scaffolds with 10,000 μm^2 pores. [79] Vascular cell growth was greater in structures with 38 - 150 μm diameter pores compared to structures with smaller pores (less than 38 μm in diameter). [80]

In addition to pore size, substrate stiffness may also influence cell activity on PHEMA-PEGDA. Ghosh et. al. demonstrated that the migration speed of adult human dermal fibroblasts decreased with increased substrate stiffness, but cell proliferation increased with increased substrate stiffness [50] Compared to the other structures in Figure 1A, PHEMA-PEGDA (BOH) had the lowest stiffness value , and it had the least amount of cells by week 2 (Fig. 7). However, differences in COL1A2 expression trends in PHEMA-PEGDA (W) and (S), which have statistically equivalent stiffness properties, suggest that topography variations alone can alter cell activity. The unique surface topographies produced by PHEMA-PEGDA formulations (Table 1) can potentially be used to investigate the relationship between cell activity and substrate topography.

This study presents a non-toxic and mechanically stable copolymer that can be adjusted to create a variety of surface topographies including pores, waves, and bulbous projections. The versatility of the surface features is achieved by varying porogen types and volumes, and the added porogens do not appear to alter the chemistry of the PHEMA-PEGDA copolymer; further

investigation is needed to confirm this. The level of structural versatility displayed by this unique blend of HEMA and PEGDA monomers has not been observed elsewhere.

4.6 Conclusion

PHEMA-PEGDA structures with a wide range of surface features were developed by adjusting porogen types and volumes. The structures have a variety of surface feature sizes and morphologies that could be used to investigate how topography influences cell activity. Differences in human corneal fibroblast migration and gene expression on different PHEMA-PEGDA topographies indicate that our PHEMA-PEGDA structures can modulate in vitro cell activity. Structures made using this convenient fabrication process could potentially expand our understanding the mechanisms involved in the cell response to topography.

III. Evaluating the Potential Utility of a Poly(2-Hydroxyethyl Methacrylate) - Poly(Ethylene Glycol) Diacrylate (PHEMA-PEGDA) Keratoprosthesis

4.1 Abstract

An artificial keratoprosthesis was created using poly(2-hydroxyethyl methacrylate) (PHEMA) and poly(ethylene glycol) chains. The presented study assesses the in vivo response to porous copolymers composed of PHEMA and poly(ethylene glycol) diacrylate (PEGDA). Given an ultimate tensile strength of 74 ± 4 kPa, the structure appears to be mechanically stable enough to maintain its structural integrity in the ocular environment and possibly during suture-free corneal implantation. Copolymers resisted rupture during subcutaneous implantation and during in vivo incubation. H&E and CD45 staining identified a mild immune response. Tissues migrated into accessible voids in the structures. Further device development to include stably

attached cell adhesion components and physiologically adequate mass transport will likely be required to achieve long-term ocular tissue attachment to the device.

4.2 Introduction

Synthetic polymers that are amenable to biological, structural, and mechanical modifications are ideal for keratoprosthesis design. Poly(ethylene glycol) (PEG) and poly(2-hydroxyethyl methacrylate) (HEMA), widely used cytocompatible polymers, have that flexibility. They can be modified to support cell adhesion. A peptide modified copolymer consisting of HEMA and a low amount of 2-aminoethylmethacrylate (AEMA) permitted increased cell growth as compared to the non-peptide modified copolymer. [81] Studies demonstrated that peptide modifications of PEG permit cell growth on the surface and inside of the hydrogel. [30] [40] Both interpenetrating networks (entangled) and copolymer mixtures of PHEMA and PEG can be manipulated to achieve a range of mechanical properties. Interpenetrating networks of PEGDA and HEMA had greater maximum tensile stress than PEGDA alone, and the hydrogel IPN supported high levels of cell growth and viability in vitro when collagen was coupled to the surface. [82] Porous PHEMA-PEGDA, created in Section I Figure 1, was stronger than gas foamed PEGDA hydrogels, and the chemical properties of PHEMA facilitated the addition of pores using selected porogens (Sec. II, Figs. 2 - 3). The structural and mechanical properties of PHEMA and PEG were exploited to create the presented keratoprosthesis model. The skirt consists of a porous PHEMA-PEGDA, and a transparent PHEMA-PEGTA (poly(ethylene glycol) tetraacrylate) was fused to a center void in the skirt to create the core. This study evaluates the optical clarity, mechanical stability, and in vivo cytocompatibility of the PHEMA and PEG based KPro.

4.3 Methods

4.3.1 Making Porous PHEMA-PEGDA

Porous PHEMA-PEGDA samples were made per Section II, 4.3.1 of this chapter. Copolymers used here in Section III included PHEMA-PEGDA (W), PHEMA-PEGDA (S), PHEMA-PEGDA (BOH), and PHEMA-PEGDA (W) – 2X.

4.3.2 Making the PHEMA-PEGDA KPro

In this core – skirt KPro model, PHEMA-PEGDA (W) – 2X served as the porous skirt while a transparent PHEMA-PEGTA was used to create the core (Fig. 1). A void was created in the porous skirt into which a HEMA and PEGTA gel solution was added. An aqueous gel solution consisting of 70% v/v HEMA, 14 % v/v PEGTA (from a 40% w/v aqueous stock solution), and 4% w/v Irgacure 2959 was UV polymerized (356 nm long wave) for 30 min.

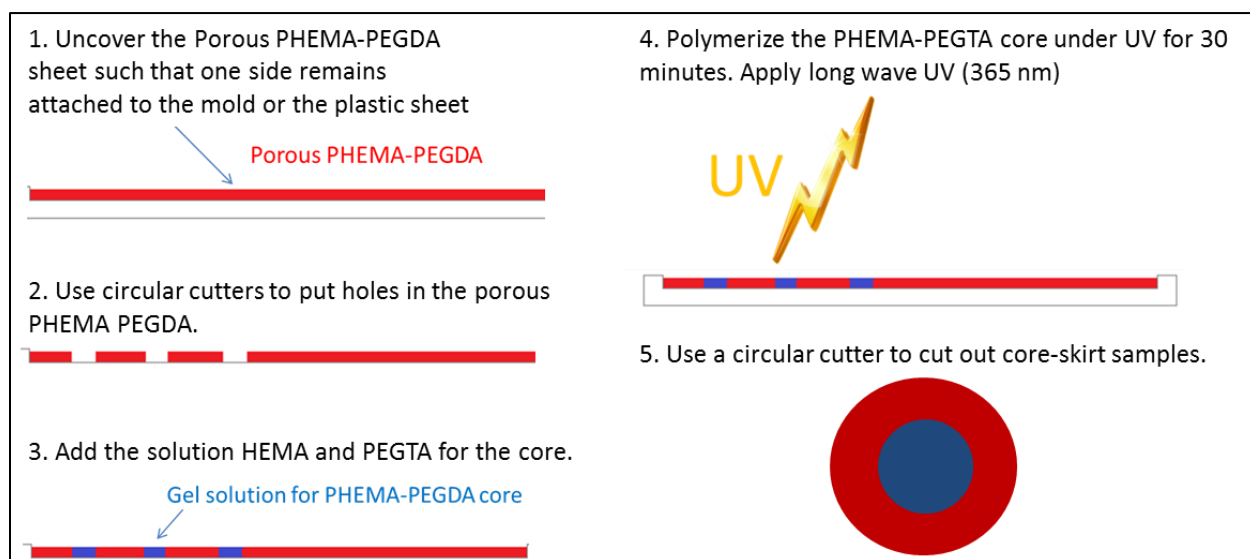


Figure 1. The porous PHEMA-PEGDA and transparent PHEMA-PEGTA were combined to create a core – skirt KPro.

4.3.3 Testing PHEMA-PEGDA KPros in Tension

Four PHEMA-PEGDA KPros (fabricated per Fig. 1) were tested in tension using a calibrated WF75GS Load Cell (Test Resources Inc.), which is fatigue-rated for 75 g of force (0.735 N) in tension and compression. Sample dimensions in the testing apparatus were approximately 5 x

13 mm and 0.6 mm depth. The tensile strain rate was 0.2 mm/s. Firstly, a strain of 10% was applied for at least 30 cycles to pre-condition the samples. A strain of 100% was applied to measure stress vs. strain to the rupture point. Values taken from the tensile measures included elastic modulus (E), ultimate tensile strength (UTS), and strain at rupture.

4.3.4 Visible Light Transmittance through PHEMA-PEGTA

The visible light transmittance of PHEMA-PEGTA samples was measured with a Synergy HT Multi-Mode Microplate Reader (BioTek). Six distinct sample types were evaluated: PHEMA (70%) - PEGTA (7%) – EDGMA, PHEMA (70%) - PEGTA (14%) – EDGMA, PHEMA (40%) - PEGTA (20%) – EDGMA, PHEMA (70%) - PEGTA (7%), PHEMA (70%) - PEGTA (14%), and PHEMA (50%) - PEGTA (20%). Three of the six samples were made with 11 μ M ethylene glycol dimethacrylate (EDGMA, Aldrich 335681). For each sample, 6 structures were measured (n = 6).

4.3.5 Subcutaneous Implantation in Mice

Three 4 month old female C57BL/6 mice were anesthetized with intraperitoneal injection of ketamine (100 mg/kg) and xylazine (5 mg/kg). Three porous copolymers were subcutaneously implanted in the back of an animal: PHEMA-PEGDA (W), PHEMA-PEGDA (S), and PHEMA-PEGDA (BOH). PHEMA-PEGDA (W) and PHEMA-PEGDA (S) were extracted after four weeks. Due to injuries inflicted by neighboring mice, PHEMA-PEGDA (BOH) was extracted from the host after 1 week. Frozen sections of extracted samples were stained with hematoxylin and eosin (H&E), purified rat anti-mouse CD45 (BD Pharmingen 550539), and alizarin red S (Sigma-Aldrich, A5533).

4.4 Results

4.4.1 Mechanical and Optical Properties

Following tensile rupture, the optically transparent PHEMA-PEGTA core remained attached to the PHEMA-PEGDA (W) 2X skirt. PEGTA was used in the core instead of PEGDA because PEGTA provides four acrylate groups for crosslinking. Four crosslinking groups were intended to create a stable bond between the core and skirt; the core fused to the skirt during UV polymerization. Crosslinking can also be increased by increasing PEGTA volumes, but reduced transparency was observed in PHEMA-PEGTA gels made with higher volumes of PEGTA. Copolymers containing up to 14% v/v PEGTA (from a 40% w/v aqueous stock solution) transmitted $\geq 90\%$ of visible light in the 500 – 700 nm range (Fig. 2). Mechanical tensile data showed the strength of the core – skirt connection (Fig. 3). The structures can sustain a maximum of 74 ± 4 kPa of stress (ultimate tensile strength) prior to rupture. The elastic modulus and strain at rupture were 166 ± 26 kPa, and 80 ± 18 % respectively. For 4 out of 4 KPro samples, the core and skirt remained attached following tensile rupture.

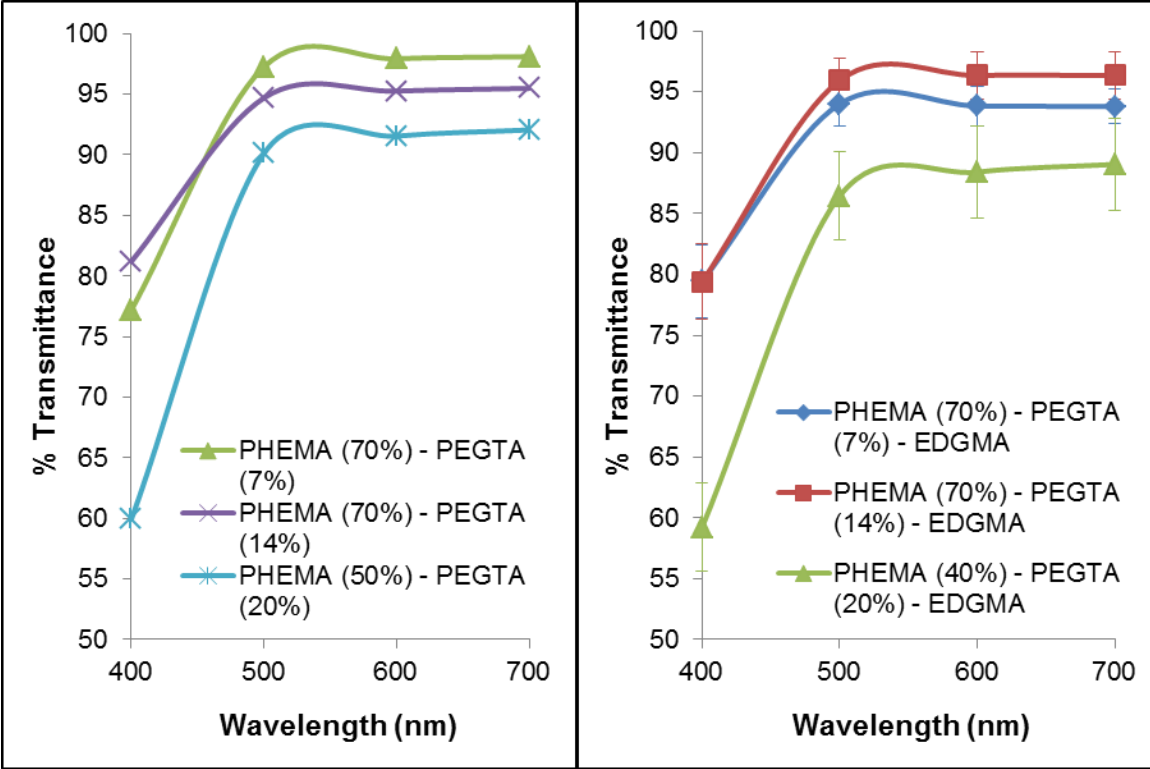


Figure 2. PHEMA-PEGTA copolymers can be designed to transmit greater than 90% of visible light in the 500 – 700 nm range. The addition of EDGMA, a crosslinker, minimally influenced transmittance. However, transmittance decreased with increased PEGTA concentration.

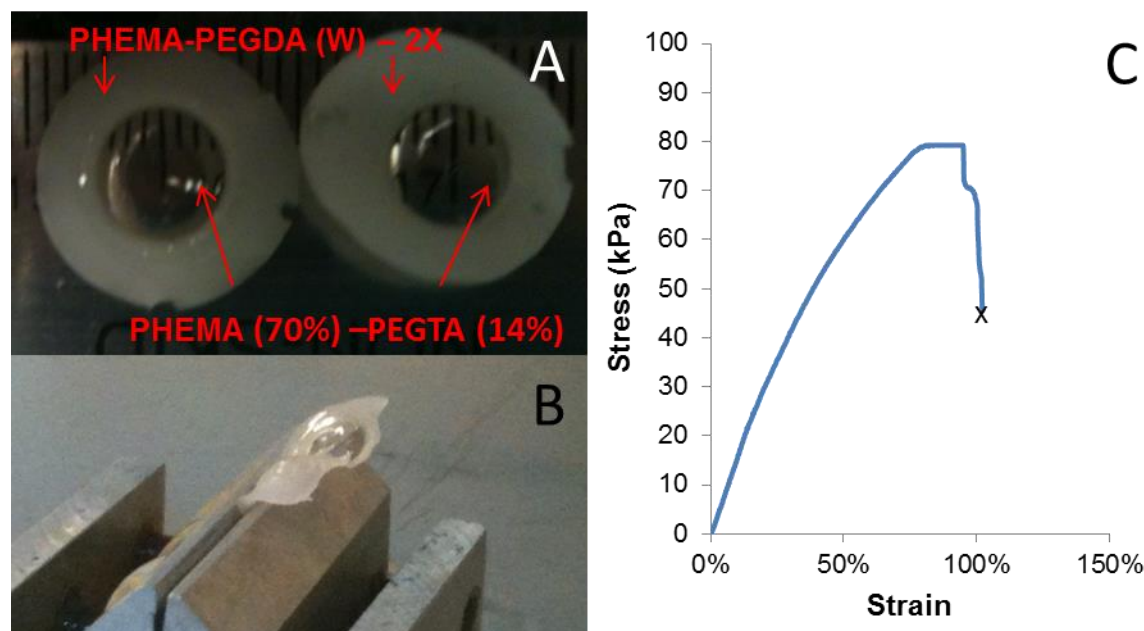


Figure 3. A KPro composed of a porous PHEMA-PEGDA skirt and a transparent PHEMA-PEGTA core was mechanically tested in tension (A). For 4 out of 4 samples that were tested in tension, the core and skirt remained attached following tensile rupture (B). The elastic modulus, ultimate tensile strength, and strain at rupture were 166 ± 26 kPa, 74 ± 4 kPa, and 80 ± 18 % respectively (C).

4.4.2 In Vivo Tissue Ingrowth

Histology results demonstrated that PHEMA-PEGDA structures generate a mild immune response and that tissues can grow into the open porous voids of PHEMA-PEGDA. Positive CD45 staining confirmed the presence of leukocytes surrounding PHEMA-PEGDA (W) (Fig. 4). However, the thin fibrous capsule surrounding PHEMA-PEGDA (W) indicates that the mouse host is tolerating the implant. [41] The 20 μ m thin fibrous layer at week 4 (Fig. 5A) was similar to the cell response observed with medical grade silicone at week 4 in under the skin of a mouse. [35] Following the removal of unreacted residues, we expected that all PHEMA-PEGDA formulations would be equally well tolerated by the host. However, sucrose residue in PHEMA-PEGDA (S) caused a heightened immune response compared to PHEMA-PEGDA (W) at week 4. Under the fibrous capsule surrounding PHEMA-PEGDA (S), foreign body type giant cells developed (Fig. 5B). Cells that migrated into the surface pores of PHEMA-PEGDA (S) appear

to be immune cells, but dermal tissue grew into the deep surface voids of PHEMA-PEGDA (BOH) (Fig. 5C). Compared to the other two polymer samples, the tissue adjacent to PHEMA-PEGDA (BOH) seemed less dense and non-fibrous in nature. PHEMA-PEGDA (BOH) samples were extracted at 1 week due to injury from another animal. All other samples were extracted at 4 weeks. The shorter in vivo incubation time may explain the absence of a fibrous capsulation in PHEMA-PEGDA (BOH). In vivo data from the three PHEMA-PEGDA samples shows that the size of the open pores and the presence of porogen residue can impact cell migration into PHEMA-PEGDA structures.

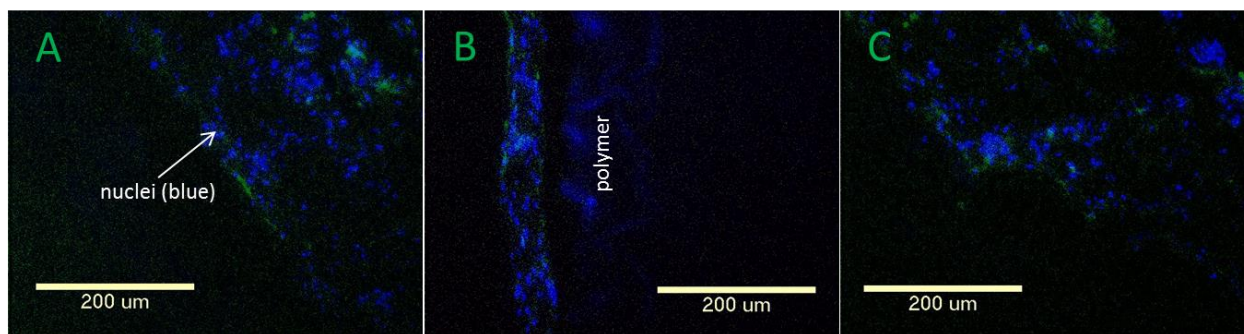


Figure 4. Following a 4 week incubation in mice, PHEMA-PEGDA (W) samples were stained with CD45. Antibodies against CD45 can be used to distinguish leukocytes from non-hematopoietic cells. Positive CD45 staining identified leukocytes adjacent to the polymer scaffold (A-C). Three sections taken from the scaffold show 3 different patterns of leukocyte manifestation. Green represents leukocytes. Blue shows the DAPI stained nuclei of all cells surrounding the copolymer. DAPI also stains the polymer.

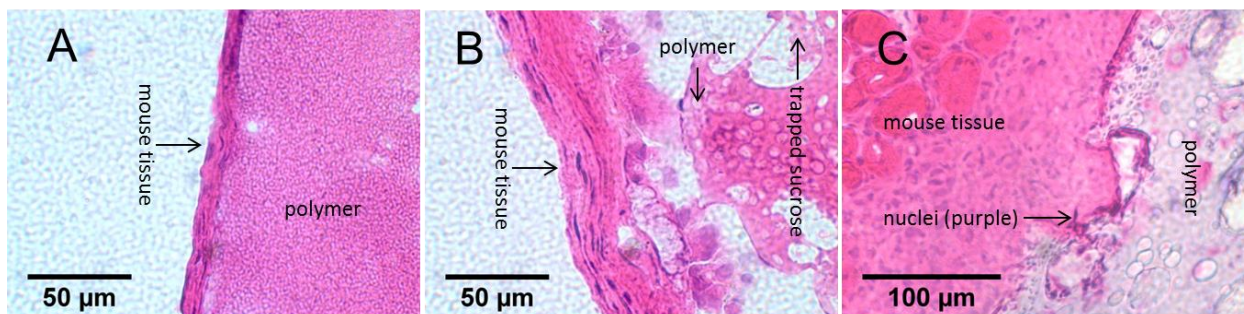


Figure 5. Following subcutaneous implantation in a mouse, porous PHEMA-PEGDA implants were stained with H&E. Porogens used include water (A), sucrose (B), and benzyl alcohol (C). The benzyl alcohol samples were extracted at 1 week due to injury from another animal. All other samples were extracted at 4 weeks.

Images of alizarin stained explants do not confirm calcification in PHEMA-PEGDA structure (Fig. 6). Both Alizarin Red S and H&E staining can detect calcium. Calcium stains orange-red in Alizarin Red S stained samples, and it is blue-black in H&E stained samples [83] [84] [85]. A brownish-orange hue was observed in tissues adjacent to explanted PHEMA-PEGDA (W) and PHEMA-PEGDA (S). However, H&E stained PHEMA-PEGDA samples did not present a blue-black stain.

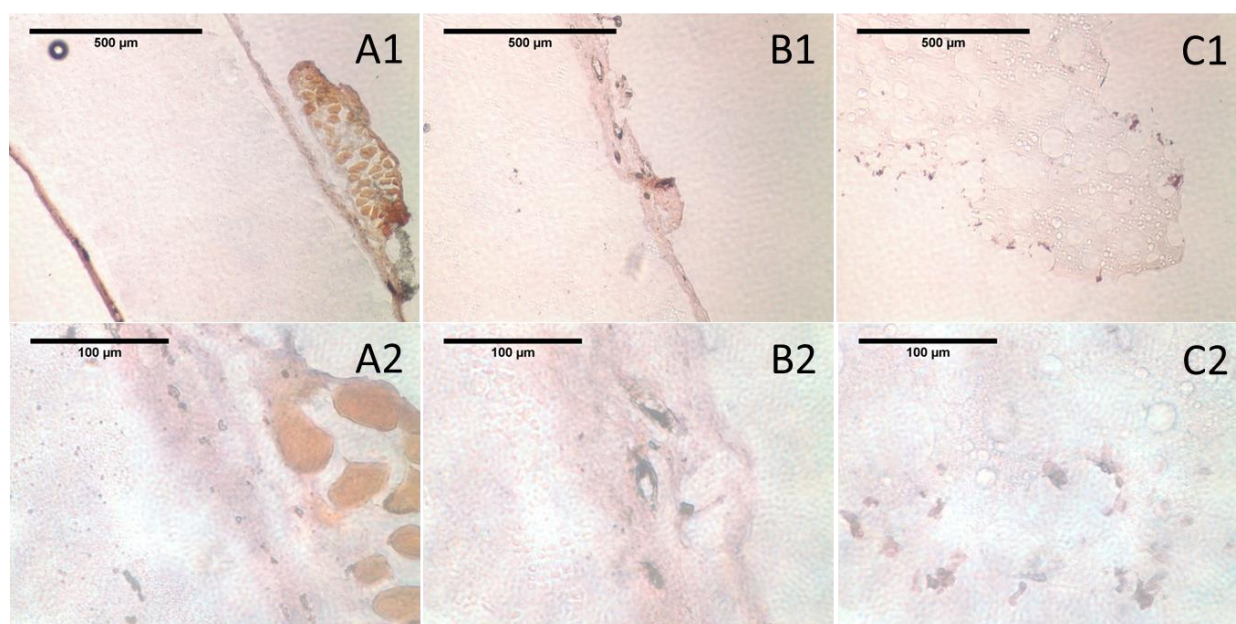


Figure 6. Following subcutaneous incubation in a mouse, porous PHEMA-PEGDA implants were stained with alizarin red S. Water (A), sucrose (B), and benzyl alcohol (C) were used as porogens. The benzyl alcohol samples were extracted at 1 week due to injury from another animal. All other samples were extracted at 4 weeks. Images A1 – C1 were taken at 10X, and A2 – C2 were taken at 40X.

4.5 Discussion

Images from mice show that porous PHEMA-PEGDA may be mechanically stable enough for ocular implantation, but inadequate pore interconnectivity limited tissue ingrowth into the copolymers (Fig. 5). Upon removal, the polymers did not appear to be weakened by the in vivo experience, but few cells migrated into the body of the porous copolymers. Insufficient pore

connectivity, and not pore size, is believed to have blocked widespread cell ingrowth.

Experiments with PHEMA sponges showed that as a minimum 10 – 20 μm diameter pores promote the incorporation of host tissue through cellular invasion and growth. [71] SEM images show that the presented PHEMA-PEGDA (W) – 2X skirts provide much larger surface pores (Sec. II, Fig. 5) for cell ingrowth. While cell colonization throughout the body of the structure is preferred for stable host integration, surface ingrowth could potentially provide a stable host connection given sufficient mass transport via PHEMA-PEGDA and adequate cell adhesion to the polymer structure.

PHEMA-PEGDA is cytocompatible and has low immunogenicity. The thin layer of leukocytes surrounding the copolymers (Figs. 5A - B) and the absence of calcium deposits within the copolymers suggest that the structures may be suitable for long term tissue engineering applications. However, data from longer implantation times would permit a more conclusive assessment. The host response to PHEMA-PEGDA, made with water porogen, was similar to that of mice implanted with medical grade silicone. Medical grade silicone usually presents a well-healed foreign body reaction after 4 weeks. Lynn et. al. report that the layer of inflammatory cells surrounding silicone samples was approximately 20 – 40 μm thin after 4 weeks. [35]

Neither H&E nor Alizarin red S detected calcium deposits on the PHEMA-PEGDA copolymer structure itself. Orange-brown tinted stain was identified in segments of the tissue surrounding copolymers made with water and sucrose porogen. Based on a similar orange-brown tint observed in an alizarin red control for heart valve tissue [86], the orange-brown identified in Figure 6 could represent non-polymer related tissue mineralization. However, previously published experiments with PHEMA indicate that the in vivo response to PHEMA-PEGDA is organism dependent. [87] In vivo calcification of a polymer is influenced by the polymer itself,

the implantation site, and the incubation time. [88] For in vivo polymers, polymer degradation and the adsorption of plasma proteins to the polymer surface can initiate calcification. [89] Given the 85% 18 year retention rate of the Osteo-Odont KPro, a device that contains a skirt made of autologous tooth, [2] calcification in the skirt region is not expected to cause device failure. However, calcification in the optic or core of the KPro can impede optical transparency. [13]

4.6 Conclusion

PHEMA and PEG chains can be combined to create a mechanically stable and cytocompatible core-skirt model KPro. The UTS of the core – skirt model KPro shows that it can maintain its structure under intraocular pressure and blinking, but ophthalmological evaluation revealed that the device cannot be sutured into place like a donor cornea. The device may be suitable for suture-free implantation. Given the hydrophilicity of PHEMA and PEG, [20] [23] [38] [90] surface conjugation of cell adhesion components will likely be required to achieve stable ocular tissue attachment to the device, and the copolymer could potentially be modified to provide sufficient mass transport for ingrown tissues.

5. Salt Porogen Scaffold for Keratoprosthesis

5.1 Abstract

Artificial corneas or keratoprostheses (KPros) are designed to replace diseased or damaged cornea. While many synthetic KPros have been developed, current products are often inappropriate or inadequate for long term use due to ineffective host integration. This study presents an alternative approach of engineering a KPro that comprises a combination of poly (2-hydroxyethyl methacrylate) (PHEMA), poly (methyl methacrylate) (PMMA), and sodium chloride (NaCl) as porogen. Based on the core-skirt model for KPro, the porous outer portion of the KPro (skirt) was designed to promote tissue ingrowth from the host. The skirt was engineered by combining NaCl with HEMA and MMA monomers. The central optic (core) was designed to provide > 85% light transmission in the 500 – 700 nm visible wavelength range. Mechanical tensile data indicated that our KPro (referred to as salt porogen KPro) is mechanically stable enough to maintain its structure in the ocular environment and during implantation. Using human corneal fibroblasts (HCFs), we demonstrate that the cells grew into the pores of the skirt and proliferated, suggesting the biointegration can be achieved. This novel PHEMA-PMMA copolymeric salt porogen KPro may offer a cornea replacement option that offers minimal risk of corneal melting by permitting sufficient tissue ingrowth and mass transport.

5.2 Introduction

The presented KPro engineered with poly (2-hydroxyethyl methacrylate) (PHEMA) and poly (methyl methacrylate) (PMMA) was designed to reduce incidents of tissue necrosis and provide sufficient pore space for ocular tissue ingrowth. Both PHEMA and PMMA are frequently used as biomaterials, and combinations of PHEMA and PMMA have been developed to create nerve guidance channels, [91], dental implants, [92] intraocular lenses, [93] [94] [95], and KPros. [12] [96] The salt porogen KPro appears to be unique to the publicly disclosed PHEMA-PMMA based KPros that the authors identified. Espana et. al. developed a non-penetrated PHEMA-

PMMA KPro that did not permit cell infiltration. [96] Guo et. al. created a PHEMA-PMMA KPro that was tolerated in New Zealand white rabbits for up to 4 months. Their KPro design comprised a transparent PHEMA-PMMA and a porous PHEMA sponge that was fused to the porous PHEMA-PMMA flange that extended from the center transparent PHEMA-PMMA unit. Vascularization and corneal cell ingrowth were observed in the device skirt. [12] Similar to the Guo's KPro, our current study presents a PHEMA-PMMA KPro that incorporates the core-skirt model, [1] [2] [3] in which the core (or central transparent region) is designed to facilitate vision while the porous skirt (outer rim) should permit tissue ingrowth. Unlike Guo's KPro, our KPro design applies an alternate fabrication technique by combining PHEMA and PMMA with sodium chloride (NaCl) to create a porous skirt. The transparent core was made with either PHEMA or PHEMA-PMMA.

Novel KPros comprising PHEMA and PMMA may facilitate biointegration and restore vision. Tissue ingrowth and negligible inflammation were observed in the skirt of a PHEMA-PMMA KPro. [12] A PHEMA- based KPro promoted vision and ocular tissue ingrowth by inducing cell migration into porous PHEMA, but non-porous PHEMA was able to resist cell growth in comparison. [8] [9] Either non-porous PHEMA or PMMA can serve as the KPro core, but cell interaction with the polymers influence their long term clarity. While non- porous PMMA used in KPros also resisted cell growth, the PMMA optics appear to be more susceptible to retroprosthetic membrane than the PHEMA optics. [7] For PHEMA or PHEMA-PMMA, pore structure is a major factor that influences device performance.

Corneal melting observed in clinical trials suggests that PHEMA sponges, like those used in the AlphaCor and Guo et. al. KPros, may not permit sufficient host integration in diseased and/or damaged corneal tissues. [8] [13] We therefore hypothesize that a PHEMA-PMMA skirt with

sufficient mass transport and a pore structure that allows high volumes of tissue ingrowth may potentially reduce incidences of tissue necrosis in KPros and encourage secure host integration. However, additional polymer modifications may be required to facilitate long term device function in diseased or damaged corneal tissues. [11] [14] [16] In this study, we evaluated the corneal replacement potential of a unique copolymeric (PHEMA and PMMA) device. The salt porogen KPro appears to be mechanically, structurally, and biologically suitable for vision restoration and therefore represents a novel biomaterial to serve as an alternate KPro.

5.3 Methods

5.3.1 Making the Salt Porogen KPro

The salt porogen KPro was composed of PHEMA 70 % v/v (core) and porous PHEMA-PMMA (skirt). A concentrated sodium chloride (NaCl) solution was added to MMA and HEMA to create the highly porous PHEMA-PMMA structure that constitutes the KPro skirt. For the porous PHEMA-PMMA skirt (PHEMA-PMMA NaCl), HEMA (Aldrich 525464) and MMA (Aldrich M55909) monomers were combined with chemical initiators in a solvent consisting of a 6:1 ratio of deionized water to dimethylformamide (DMF). The monomer solution included 10 % v/v MMA, 46 % v/v HEMA, 0.02 M pentaerythritol tetraacrylate (Aldrich 408263), 0.074 M NaCl, 0.12 M ammonium persulfate (Sigma), and 0.11 M N,N,N',N'-tetramethylethylenediamine (Acros Organics).

The following steps provide a full description for attaching the core and skirt. First, a cylinder made of PHEMA 70 % v/v was added to the HEMA and MMA monomer solution (Fig. 1A); the core fused to the skirt as the skirt polymerized at 37°C for 20 hours. To create the transparent PHEMA 70% v/v cylinder, an aqueous solution containing 70 % v/v HEMA, 0.1 % v/v ethylene glycol dimethacrylate (EGDMA) (Aldrich 335681), and 1 % w/v Irgacure 2959 (BASF 55047962) was polymerized with UV light (365 nm long wave) for 40 min. To strengthen the bond between

the PHEMA 70 % v/v core and the porous PHEMA-PMMA skirt, a layer of MMA was added to the PHEMA cylinder using UV polymerization. The MMA surface functionalization process was modified from a previously published paper. [32] DMF was used as solvent, but benzyl alcohol and acrylic acid were excluded. Transparent PHEMA-PMMA can also be added to the KPro skirt. A PHEMA 70 % v/v – PMMA 7 % v/v core was added without incorporating the MMA surface functionalization; a void was created in the skirt into which the PHEMA-PMMA core was UV polymerized. Figure 1B illustrates the fabrication method.

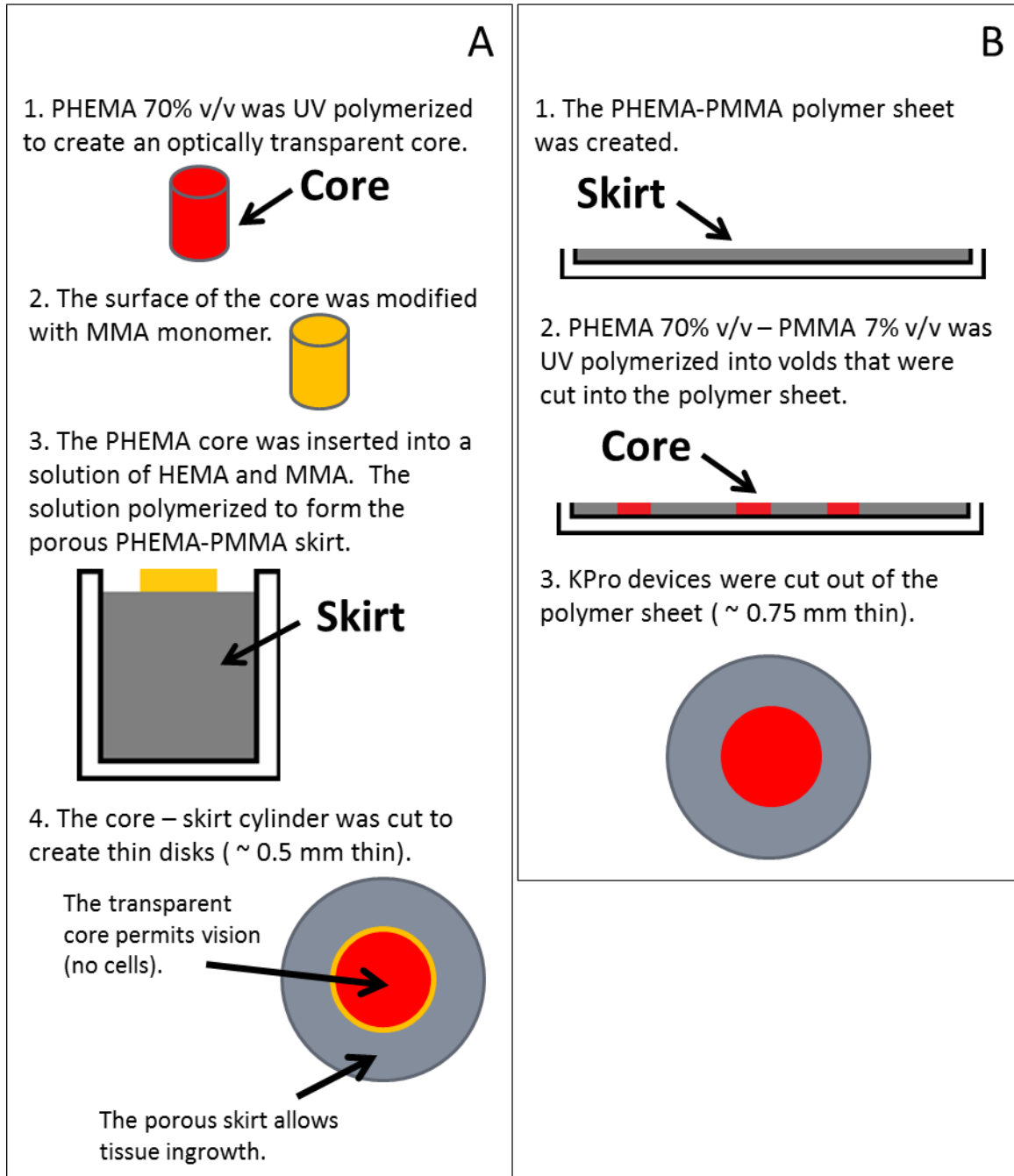


Figure 1. One KPro model was fabricated by inserting a UV polymerized PHEMA cylinder into a solution of HEMA and MMA. The solution polymerized over 20 hours to form the porous PHEMA-PMMA skirt of the KPro (A). The second KPro model was created by polymerizing a PHEMA-PMMA core inside of a void in a thin porous PHEMA-PMMA skirt (B).

5.3.2. Structural, Optical, and Chemical Characterization

To compare the structures of porous PHEMA-PMMA with or without the salt porogen, SEM images of dehydrated polymers were generated using the S-3000N Variable Pressure SEM (Hitachi). Prior to SEM imaging, polymer structures were laser ablated with gold using a Pulsed Laser Deposition System (Excel Instruments). The SEM images were used to evaluate the effects of porogens on the surface pore size using ImageJ 1.47c (NIH). ImageJ was used to digitally process, threshold, and measure SEM images. Alternatively, the pore size was also measured using Scanco model 50 micro CT system. Micro CT images of dehydrated polymers were acquired with an X-ray tube voltage of 45 kV, current of 133 μ A, 0.1 mm aluminum filter, and 1500 ms integration time. Morphological measures were taken using the manufacturer's software. Data were obtained by analyzing three different scaffold regions of equal volume. Each region consisted of 100 image layers of an approximately 0.6 mm² area. The percent change in the pore characteristics following the addition of NaCl to PHEMA-PMMA was calculated. The following equation was applied to the control and experimental (PHEMA-PMMA NaCl) data sets: Percent Change in Pore Structure after Adding NaCl = $100 * [(X_{\text{NaCl}} - X_{\text{control}}) / X_{\text{control}}]$, where X was (1) pore volume, (2) pore diameter, and (3) average separation distance between pores. The optical transmittance of transparent PHEMA and PHEMA-PMMA (n = 8) was measured with a Synergy HT Multi-Mode Microplate Reader (BioTek). Samples were incubated in deionized water for 24 hours prior to optical testing.

Nuclear Magnetic Resonance (NMR) was used to evaluate the stability of porous PHEMA-PMMA gel in aqueous solution. The gel was incubated in PBS for 3 days. Then, NMR measures were taken from both the gel in PBS and a solution of HEMA and MMA monomers. The ratio of HEMA to MMA in the monomer mixture was equal to the ratio of monomers used to create porous PHEMA-PMMA gels per Section 5.3.1. Data was obtained per the NMR methods listed in Chapter 4, Section II, 4.3.7.

5.3.3. Tensile Testing

Hydrated porous PHEMA-PMMA and KPro samples (n = 4) were tested in tension using a custom designed 100LM Test Resources mechanical testing machine (Test Resources Inc., Shakopee MN). Samples were tested at a strain rate of 0.2 mm/s using a calibrated WMC-10 load cell (Test Resources Inc.), which is fatigue-rated for 10 pounds of force in tension and compression. Values taken from the tensile measures included elastic modulus (E), ultimate tensile strength (UTS), and strain at rupture. E is measured in the elastic or linear region of the stress vs. strain plot; $E = \text{stress}/\text{strain}$. UTS is the maximum stress response of a material during tensile testing. The strain at rupture is simply the elongation of the sample at the point of rupture. In this study, the elongation was reported as a percentage of the original length of the sample.

5.3.4. Coating Polymers in Collagen Type I

The PHEMA-PMMA samples made with NaCl porogen were coated with rat tail collagen type I (BD Bioscience) in preparation for in vitro experiments. The collagen type I coating was added to enable cell adhesion and spreading. Samples were immersed in a collagen type I solution (0.2 mg/mL) with 5 mM N-(3-Dimethylaminopropyl)-N'-ethyl-carbodiimide (EDC) and 5 mM N-hydroxysuccinimide (NHS); EDC and NHS were used to crosslink the collagen. After the samples were removed from the solution, collagen gelled at 37 °C after 30 min. A monoclonal antibody against collagen type I (1:2000 dilution, Sigma-Aldrich C2456) was used to stain and visualize the collagen fibers in the scaffold.

5.3.5 In Vitro Assessment

Primary human corneal fibroblasts (HCFs) were cultured in GIBCO MEM alpha media (Invitrogen) with 10% fetal bovine serum (FBS) (Atlanta Biologicals) and 1% antibiotic-

antimycotic solution (Sigma-Aldrich). Cells (6×10^3) were added to the salt porogen PHEMA-PMMA scaffold that was coated with collagen type I. The surface area of each circular polymer disk was approximately 170 mm^2 , and the thickness of samples was approximately $600 \text{ }\mu\text{m}$. A cell viability assay (Invitrogen L3224) was used to stain cells at days 4, 7, and 13. The depth of cell growth was estimated using confocal microscopy and an image processor (ImageJ). To quantify the depth of cell growth into the salt porogen PHEMA-PMMA scaffold, images were recorded at 4 distinct locations on the porous structure. For each time point, 5 depth measures were taken from each image ($n = 20$). The depth of HCF growth was estimated based on the deepest point of cell growth into the structure. Using the side projections, a total of 5 depth measures were taken at approximately $20 \text{ }\mu\text{m}$ intervals from a center vertical line that marked the deepest point of cell growth. An alamarBlue assay (Invitrogen) was used to evaluate the HCF proliferation in the salt porogen scaffold.

5.3.6 In Vivo Testing

A four month old female C57BL/6 mouse was anesthetized with intraperitoneal injection of ketamine (100 mg/kg) and xylazine (5 mg/kg). Four PHEMA-PMMA structures were subcutaneously implanted in the back of the animal. The structures were extracted after 8 days. Frozen sections of extracted samples were stained with hematoxylin and eosin (H&E) and Purified Rat Anti-Mouse CD45 (BD Pharmingen 550539).

5.3.7 Statistical Analysis

MATLAB R2012a was used to perform statistical analysis at an alpha value of 0.05. Data are reported using mean \pm standard error. For all mechanical measures, statistical significance was determined using an independent t – test. ANOVA was used to assess the statistical significance of cell proliferation and cell growth data. Rank Sum testing was used to evaluate the statistical significance of pore measures taken from SEM images.

5.4 Results

5.4.1 Structural and Chemical Characterization

SEM images show that phase separation induced by NaCl created a high density of pores in the PHEMA-PMMA scaffold. When NaCl was excluded from the polymer formulation, the density of macropores was reduced (Fig. 2A). Various concentrations of NaCl were tested to identify a threshold that could induce phase separation. At the NaCl concentrations > 0.36 M, most of the MMA appeared to fall out of the gel solution prior to polymerization. At a much lower concentration (0.074 M), a highly porous PHEMA-PMMA structure was produced (Fig. 2B). However, even with 0.074 M NaCl, vigorous mixing was required for approximately 2 minutes following initiator addition to keep monomers and porogens in solution.

Without the salt porogen, the PHEMA-PMMA skirt demonstrated not only a lower density of macropores but also the average pore size decreased. For example, the pore sizes measured from SEM images show that the average area of pores in the PHEMA-PMMA skirt (0 M NaCl) was about 1-fold or 100% smaller than that observed in the salt porogen PHEMA-PMMA skirt (Fig. 2C). While the SEM images provide the surface pore structure, micro CT images reconstruct and represent the 3D pore structure. We evaluated the effects of salt porogen on 3D pore structure using micro CT. Micro CT data from PHEMA-PMMA without salt (control; Fig. 3A) and with salt (0.074 M NaCl; Fig. 3B) show that the addition of salt porogen increased the pore diameter by about 3-fold or 300%. The 2D pore area was expected to trend with to the 3D pore volume. Both pore area and volume, consistent with that prediction, increased following the addition of salt porogen to PHEMA-PMMA. In addition, the salt porogen decreased the average separation distance between pores by approximately 60%, indicating a higher density

of pores and lending support for improvement in the pore interconnectivity in the copolymeric PHEMA-PMMA skirt.

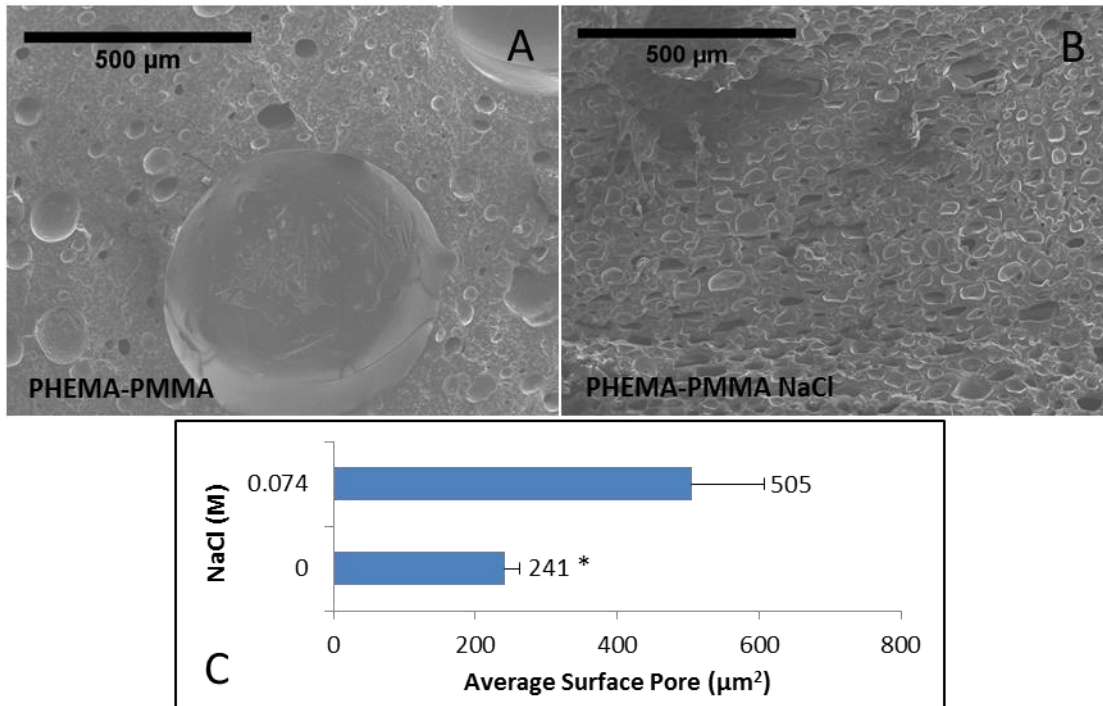


Figure 2. SEM images were taken of dehydrated PHEMA-PMMA made with and without NaCl. PHEMA-PMMA (0 M NaCl) appeared to have a low density of larger pores (A) compared to PHEMA-PMMA made with 0.074 M NaCl (B). Phase separation with NaCl added a higher density of pores to PHEMA-PMMA. Surface pore measures taken from SEM images show that average surface pores in PHEMA-PMMA are significantly smaller than pores in PHEMA-PMMA NaCl (C).

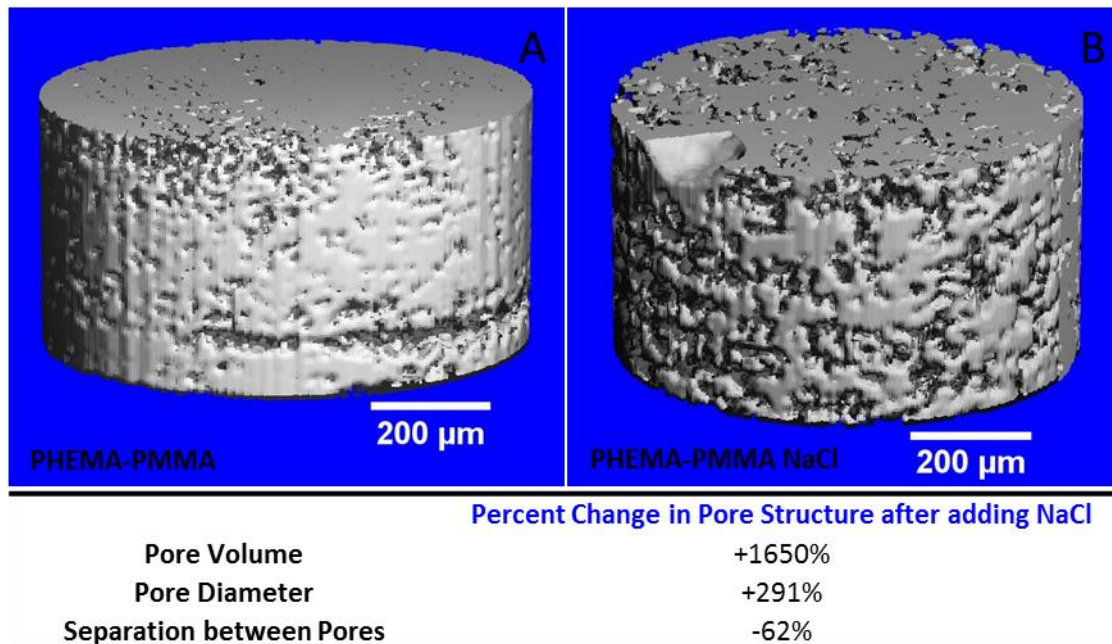


Figure 3. Micro CT scans were used to compare the porosity of PHEMA-PMMA samples made with and without salt (NaCl) porogen. Three distinct sections of each structure were used to compare pore morphology ($n = 3$). PHEMA-PMMA served as the control (A). The addition of NaCl to PHEMA-PMMA, PHEMA-PMMA NaCl (B), resulted in larger pore volumes and diameters compared to the control. The decrease in separation of pores shows that NaCl created a higher density of pores in PHEMA-PMMA. The table below the micro CT images shows the percent change in pore structure in PHEMA-PMMA NaCl compared to the control. “+” denotes an increase compared to the control while “-” denotes a decrease compared to the control.

Figure 4 shows high resolution ^{13}C NMR spectra at 8.45 T (^1H freq. 360 MHz) for a solution of HEMA and MMA (Fig. 4A) and a PHEMA-PMMA NaCl gel soaked in PBS for three days (Fig. 4B). The peak assignments for spectral lines are based on both published literature [66] [97] and general NMR references [67] [68]. The spectra in Figure 4A show that the HEMA and MMA units in solution are not chemically connected as all of the peaks can be assigned to individual components. Figure 4B shows the spectra of the gel in PBS. Most polymeric units of porous PHEMA-PMMA appeared to remain stably linked in PBS. The CH_3 and $^{\alpha}\text{CH}_3$ peaks of MMA are visible in the gel spectra with the line width ~ 483 Hz and ~ 150 Hz, respectively. These peaks have line widths of 2.6 and 1.3 Hz respectively in the liquid samples. Because of high noise level and broad signal in the gel sample, it seems that the signal is coming from the gel and not

from the leaching of MMA in PBS. Figure 4B appears to show that the CH₃ groups from MMA are mobile, but further study with varying temperature and relaxation measurements are needed to confirm this. Overall, the available data suggests that the polymer units of the PHEMA-PMMA gel remain linked in aqueous solution. This is advantageous for in vitro or in vivo applications when the structural stability of the gel is preferred.

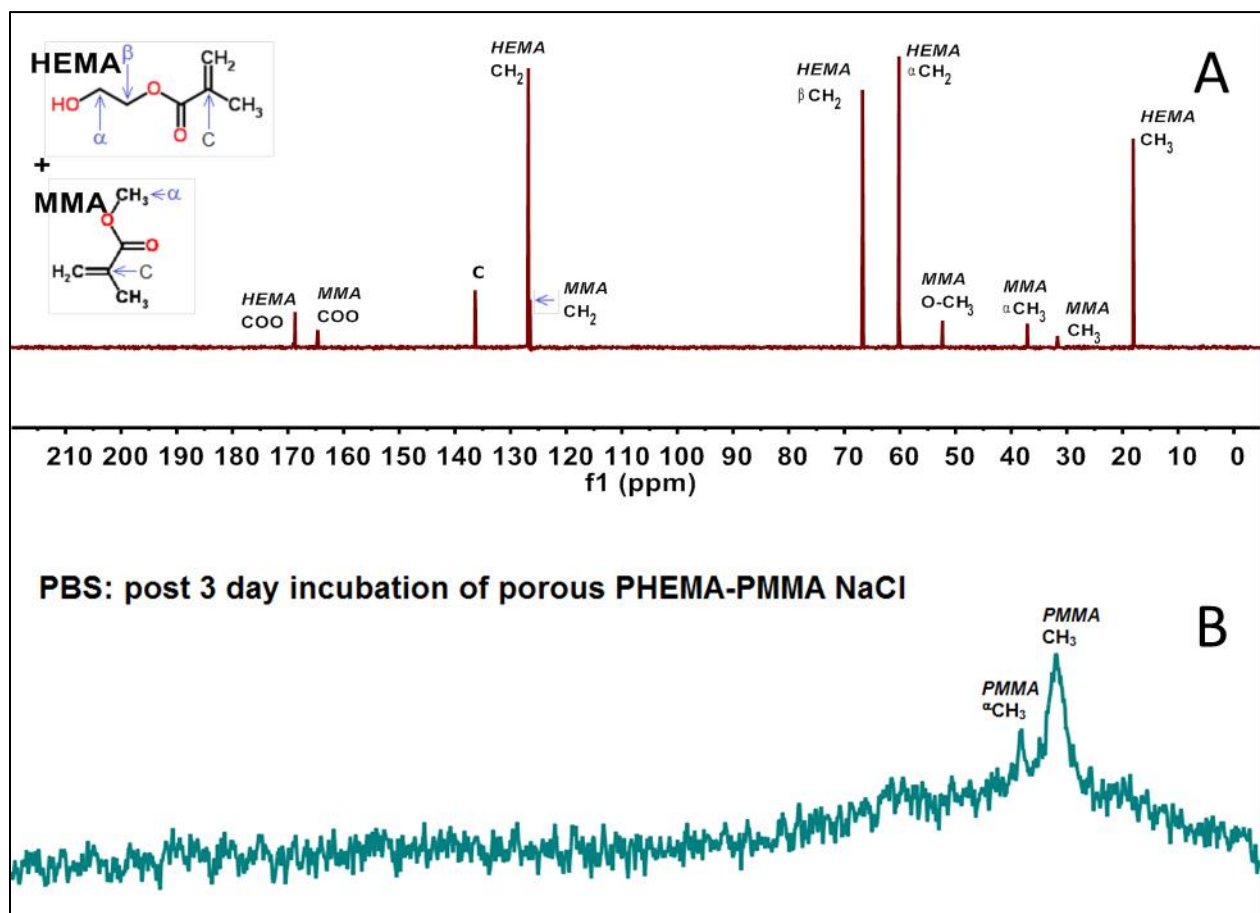


Figure 4. Signals observed in the HEMA and MMA solution (A) were not present in the porous PHEMA-PMMA NaCl gel (B). Most polymeric units of the gel appeared to remain stably linked in PBS. CH₃ groups of MMA appeared to have some mobility in the gel sample.

5.4.2 Tensile Testing

Tensile stresses measured over a range of strain values characterize the mechanical properties of the KPro (Fig. 5). The tensile stress-strain relationship is shown for the KPro that contains the PHEMA 70% v/v core (Fig. 5A - C). The strain value at rupture, $108 \pm 8 \%$ ($n = 4$), indicates that KPros made with the PHEMA core are ductile. For comparison purpose, copolymeric skirts alone without a core were subjected to the mechanical testing. The skirt alone was significantly stiffer than the full KPro. The elastic moduli were 678 ± 72 and 335 ± 87 kPa for the skirt alone and KPro, respectively ($p = 0.02$; Fig. 5B). However, the KPro and the skirt had statistically similar ultimate tensile strengths (UTS); UTS measures were 128 ± 35 and 125 ± 25 kPa for the KPro and skirt, respectively (Fig. 5C). Tensile testing characterized both the mechanical properties of the polymer structures and strength of the core skirt connection in the KPro. A photo taken following the tensile rupture of a KPro illustrated that the PHEMA core and PHEMA-PMMA skirt are fused together (Fig. 5D). In 4 out of 4 samples, the core and skirt remained connected during the application of tensile force and following tensile rupture. As a potential alternative formulation for the KPro core, we constructed a PHEMA 70 % v/v – PMMA 7 % v/v core. Tensile testing data showed that the salt porogen KPro with this alternate core also had a stable attachment to the skirt (Fig. 5E). It appears clear that KPros made with either PHEMA or PHEMA-PMMA cores are mechanically and structurally stable enough as to resist rupture under ocular forces.

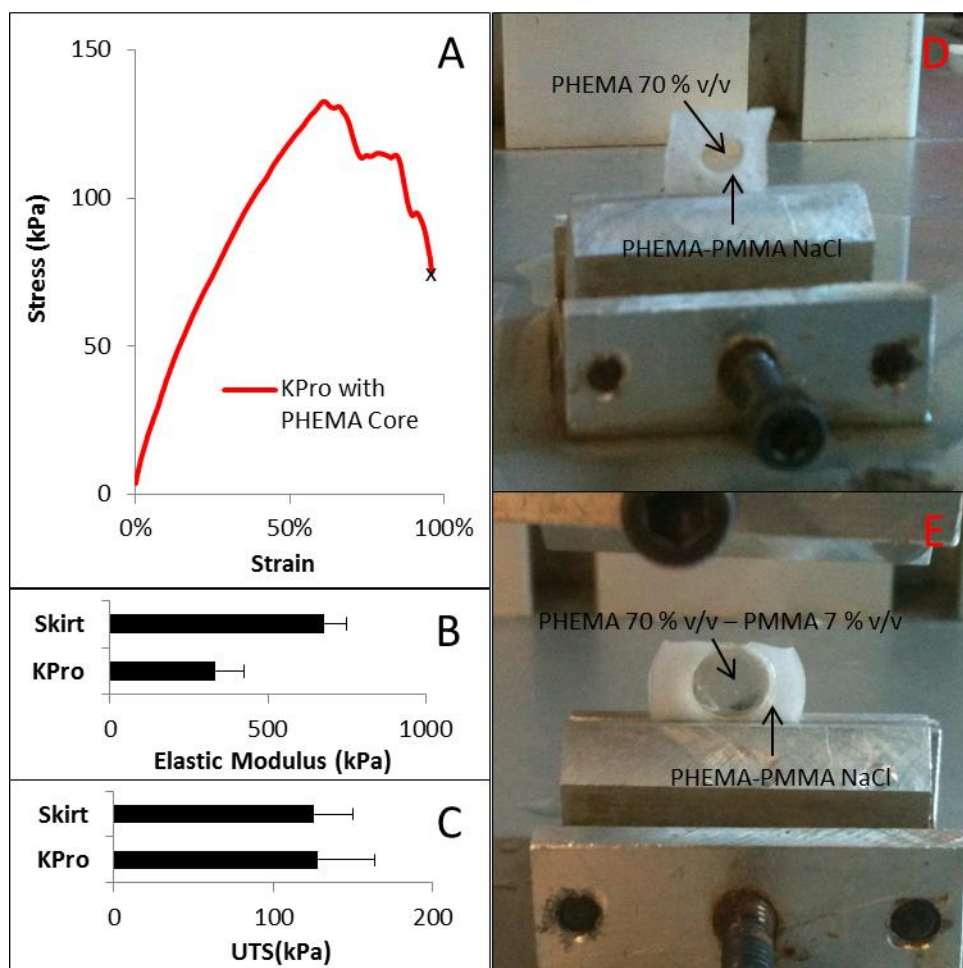


Figure 5. Tensile stresses measured over a range of strain values characterize the mechanical properties of the KPro made with a PHEMA 70 % v/v core (A - C). "X" marks the point of sample rupture under tensile stress (A). The PHEMA-PMMA skirt was significantly stiffer than the KPro (B). The KPro and the skirt of the KPro had a statistically similar UTS (C). A photo taken after KPro rupture illustrates that the PHEMA core and PHEMA-PMMA skirt were fused together (D). In 4 out of 4 samples, the core and skirt remained connected during the application of tensile force and following tensile rupture. The salt porogen KPro can be also be made with a transparent PHEMA 70 % v/v – PMMA 7 % v/v core. Following tensile rupture, the PHEMA-PMMA core remained fused to the skirt in 4 out of 4 samples (E).

5.4.3 Optical Transparency

The optical transparency of the KPro core was evaluated by measuring the transmittance of visible light ($n = 8$). The core of the KPro can be either PHEMA alone or a combination of PHEMA-PMMA. Optical measurements show that both the PHEMA or PHEMA-PMMA cores

can permit approximately 85 % transmittance of visual light in the 500 – 700 nm range (Fig. 6). However, the addition of PMMA > 20 % v/v to PHEMA 70 % v/v reduced the light transmittance to below 80 %. While the most stable fusion of a core to the skirt was observed when the polymer compositions of the core and skirt were similar, higher amounts of PMMA in the core tended to reduce optical transparency.

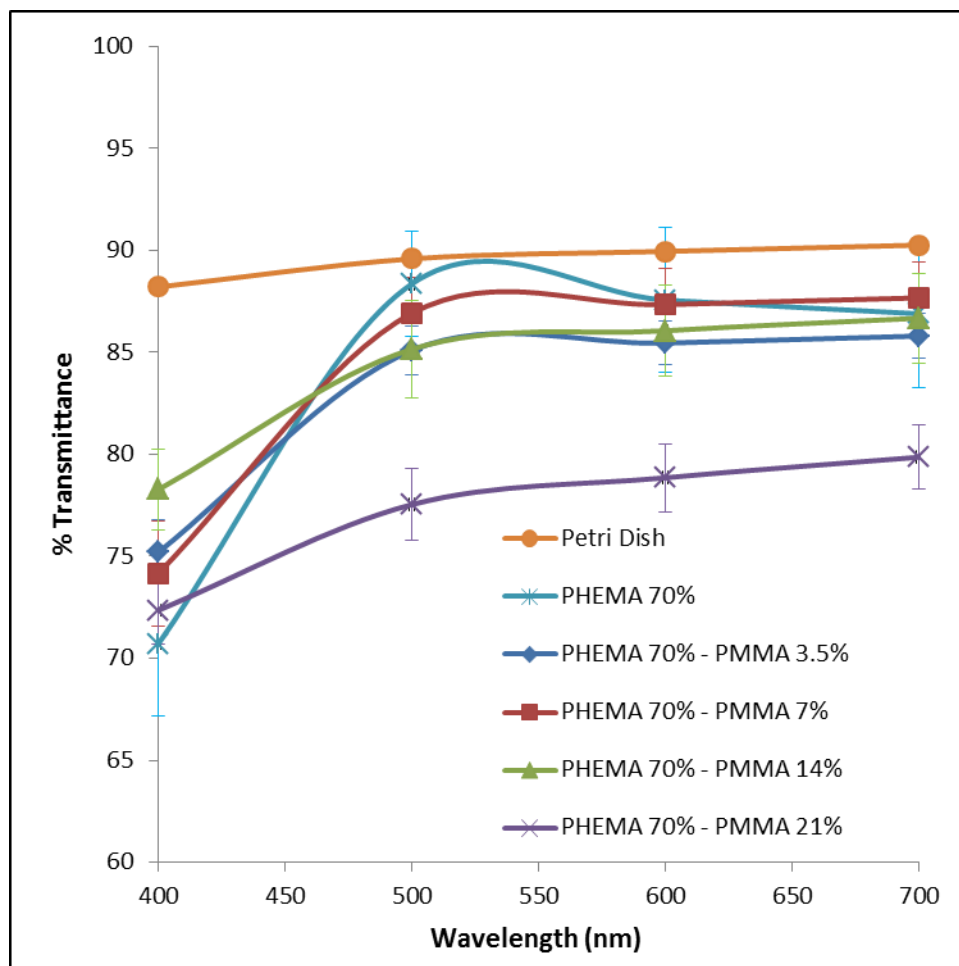


Figure 6. The optically transparent core of the KPro can be made with PHEMA or PHEMA-PMMA ($n = 8$). Both cores can permit approximately 85 % transmittance of visible light in the 500 – 700 nm range. However, the addition of PMMA 21 % v/v to PHEMA 70 % v/v reduced visible light transmittance to below 80 %.

5.4.4 In Vitro Cell Response to KPro

Human corneal fibroblasts (HCFs) proliferated and grew into the pores of the KPro skirt (Fig. 7), but the engineered cores did not permit cell ingrowth, as expected. The absence of micropores rendered the core both transparent and impermeable to cell penetration. However, in vitro cell ingrowth and proliferation in the salt porogen skirt suggests that the porous structure may facilitate in vivo tissue ingrowth. A collagen type I coating that was added to the polymer structure to enable in vitro cell spreading and enhance cell attachment. Cell proliferation measured with an alamarBlue assay showed a statistically significant increase in live cells from day 0 to 8, followed by no additional increase up to day 13 ($n = 3$; Fig. 7A). Next, the depth of cell penetration was quantified using confocal microscopy. As shown in Fig. 7B, the cells were able penetrate into the skirt up to approximately $60 \mu\text{m}$ 8 days following the initial cell seeding, but no additional cell penetration was observed when monitored up to day 13. To enhance cellular imaging, live cells were visualized with calcein AM (green fluorescence). Ethidium homodimer is designed to diffuse into dead cells and fluoresce them in red. While few dead cells were found in the salt porogen PHEMA-PMMA skirt, it was discovered that ethidium homodimer stains the polymer structure and provides images of pores in the skirt. Cell penetration/migration studies were quantitatively determined by reconstructing the side projections of confocal images at different days (Fig. 7C to 7E). The depth of HCF growth was estimated based on the deepest point of cell penetration into the structure. Using 4 reconstructed side projections, a total of 5 depth measures were taken at approximately $20 \mu\text{m}$ intervals from a center vertical line that marked the deepest point of cell growth ($n = 20$). To confirm the presence of collagen in the skirt, antibodies against the collagen type I were applied and fluorescently visualized (Fig. 7F). Representative images of live cells along with the pore structure at days 4 (Fig. 7G), 8 (Fig. 7H), and 13 (Fig 7I) correspond to the cell proliferation data (Fig. 7A). Taken together, in vitro HCF proliferation and growth into the porous skirt provide

good evidence that this uniquely designed salt porogen copolymeric KPro may potentially permit in vivo cell ingrowth.

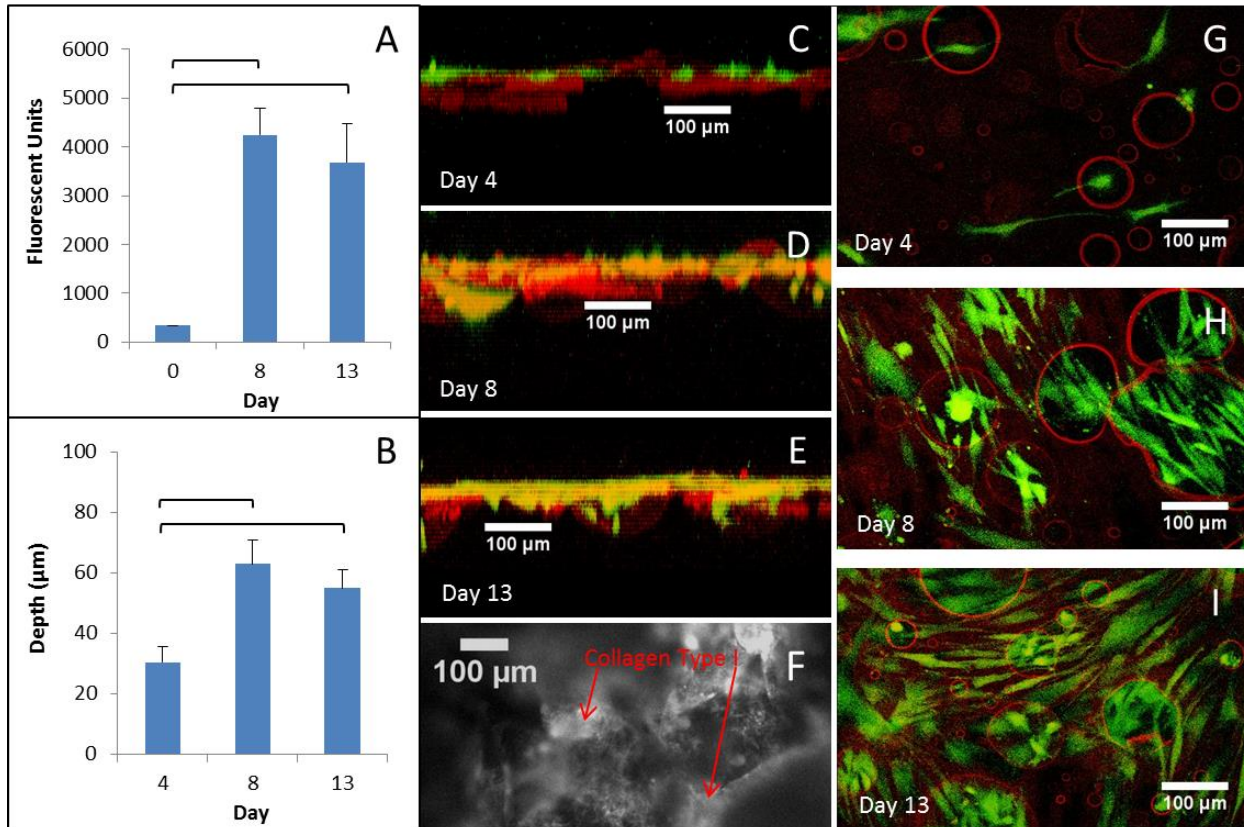


Figure 7. HCF proliferation on PHEMA-PMMA made with NaCl was observed using alamarBlue (A). The fluorescent signal is larger when larger numbers of cells are present; therefore, the fluorescent signal can be used to evaluate cell proliferation. The increase in live cells from day 0 to 8 and day 0 to 13 was statistically significant per ANOVA ($n = 3$). Horizontal bars indicate the statistically significant relationships. The estimated depth of cell growth into the structure significantly increased from day 4 to 8; the depth of growth also increased significantly from day 4 to 13 (B). The depth of HCF growth was estimated based on the deepest point of cell growth into the structure. Using 4 side projections, a total of 5 depth measures were taken at 20 μm intervals from a center vertical line that marked the deepest point of cell growth ($n = 20$). Side projections of HCFs in the porous structure show live cells, in green, at days 4 (C), 8 (D), and 13 (E). Ethidium homodimer, which is designed to stain dead cells red, also stains the polymer structure. The collagen type I coating that was added to the structure is shown in white (F). Representative overhead views of live cell growth at days 4 (G), 8 (H), and 13 (I) correspond to the cell proliferation data measured using alamarBlue.

5.4.5 Subcutaneous Implantation

PHEMA-PMMA structures, made without NaCl, permit some cell ingrowth and generate a mild immune response. Given the implantation site, dermal cells are expected to be the majority cell type. Although interconnected pores are not apparent in PHEMA-PMMA (Fig. 2A), a small amount of cell ingrowth into the body of the structure was observed following 8 days of implantation under the skin of a mouse (Fig. 8). Since cell ingrowth was achieved with this level of porosity, pores produced by saline based phase separation (Fig. 2B) could lead to greater amounts of cell ingrowth. Positive CD 45 staining confirmed the presence of leukocytes surrounding the PHEMA-PMMA implant (Fig. 9). However, leukocytes are expected at this stage due to the acute immune response. [98]

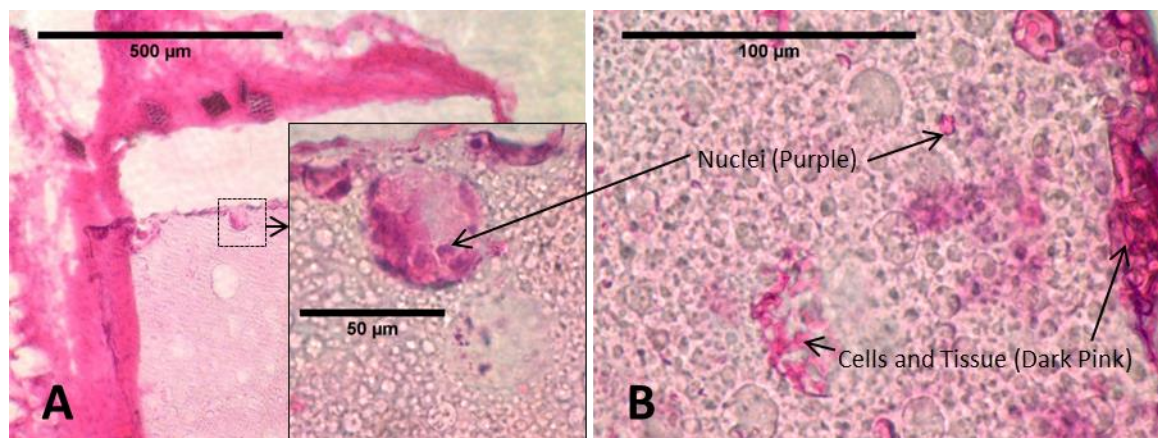


Figure 8. Although interconnected pores are not apparent in the SEM image of dehydrated PHEMA-PMMA, a small amount of cell ingrowth into the body of the structure was observed following 8 days of implantation under the skin of a mouse (A, B). This suggests that the addition pores produced with salt could lead to greater amounts of cell ingrowth.

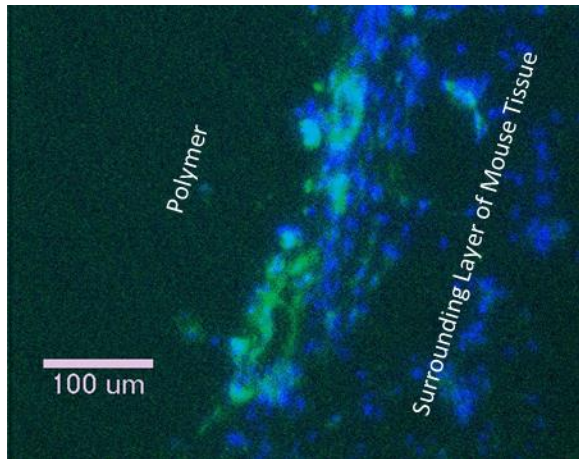


Figure 9. The presence of leukocytes confirms that the implant generated an immune response in the mouse host. Nuclei are labeled with DAPI in blue, and CD45 staining is labeled with green. Light blue coloring shows overlapping nuclei and CD45. Positive CD45 staining identifies the presence of leukocytes.

5.5 Discussion

PHEMA and PMMA were successfully combined to create a core-skirt model KPro that resists adverse events, including rupture or core-skirt separation, while permitting vision and cell ingrowth into the KPro skirt. Salt porogen was utilized to engineer a porous skirt that enabled cell penetration while creating a mechanically and structurally secure connection between the core and the skirt. Several imaging modalities as well as in vitro cell studies were performed to characterize this novel KPro. A comparison of the SEM data (Fig. 2) with the micro CT data (Fig. 3) shows that the micro CT scans underestimate the pore sizes. Dehydrated polymers were scanned in air to enhance the micro CT image signal, but low x-ray attenuation of the polymer samples reduced the image signal. [99] In addition to poor signal-to-noise ratio which is believed to be the main contributor to the underestimation of pore size, the sphere fitting method that was applied to analyze micro CT images might have underestimated the pore size as well. However, previous studies with polymers and micro CT suggest that the resulting micro CT data provides a reliable comparison of the two pore structures due to the equivalent micro CT scanning parameters and thresholding techniques. [100] [101] We adhered to the same

micro CT scanning parameters for each of the two porous PHEMA-PMMA samples (Fig. 3), and the micro CT comparison reported in Figure 3 is consistent with the results obtained from the SEM image analysis in Figure 2.

The mass transport of nutrients through the porous polymer structure is imperative for the vitality of ingrown tissue. A relationship between mass transport and aqueous fluid uptake has been established for hydrogels. [20] [102] After rehydrating salt porogen PHEMA-PMMA in PBS, its thickness increased by 15 %. The maximum PBS uptake of the skirt was measured using the weight of samples at dehydration and the weight following complete hydration in PBS. Following hydration, the weight of salt porogen PHEMA-PMMA increased by 67 %. The equilibrium water content of salt porogen PHEMA-PMMA may enhance the transport of water soluble nutrients.

PHEMA and PMMA were combined to create a suturable and flexible KPro. Mechanical tensile data (Fig. 5) indicated that the KPro can comfortably maintain its structure in the ocular environment while permitting cell ingrowth. PMMA, which has been used in hard contact lenses, [103] gives the copolymer its strength, while PHEMA provides the copolymer its ductility. Lou et. al. showed that PHEMA sponges are mechanically soft and ductile. [104] MMA and HEMA monomers can be adjusted to tailor the mechanical properties of a PHEMA-PMMA copolymer. [70] [91] In our study, KPro models were designed to sustain blinking forces and intraocular pressure because eyelid movement and intraocular pressure are major forces that the corneal implant is expected to encounter. The natural tear film can minimize shear forces between the eyelid and the PHEMA optic of the KPro during blinking. [105] [106] PHEMA is used in contact lenses because of its favorable tear film wettability. [103] Reports concerning the ocular response to PHEMA and PMMA [2] [96] and mechanical data (Fig. 5) suggest that

the novel KPro may sustain intraocular pressure and resist mechanical rupture. For example, average intraocular pressure is only up to 2 - 4 kPa, [107] [108] which falls well below the UTS of the KPro (Fig. 5C). High elastic modulus (Fig. 4B) and UTS indicate that the device should resist rupture during and following implantation. Similar to other KPro models, [2] [5] the presented artificial cornea does not perfectly match the mechanical properties of natural human cornea. [109] [110] [111] However, results from previously published KPro designs indicate that corneal tissues can integrate structures (e.g., biointegration) that possess a range of mechanical properties. [2] [9] [16] [15]

The degree of pore interconnectivity and aqueous swelling in the KPro is expected to influence mass transport and host integration. Since the KPro core is small, it is expected to make an insignificant contribution to gas and nutrient exchange. Studies with contact lenses suggest that the low water content of the PHEMA 70% v/v core will yield low oxygen permeability. [95] However, a KPro with effective host integration into the skirt can achieve long term stability in the absence of physiologically equivalent mass transport in the core. [1] [2] [4] Depending on its pore interconnectivity, a combination of tissue ingrowth and mass transport in the skirt may be required for the long term retention of the KPro. Based on ocular tissue ingrowth into synthetic porous structures, we predict that tissue ingrowth into a highly interconnected porous structure could provide sufficient mass transport via the network of tissue, but a less interconnected pore structure would limit the tissue network in the skirt. [9] [15] [112] Therefore, a less interconnected skirt structure would rely more on gas and nutrient exchange via the polymer structure of the skirt. Bulk aqueous regions created by pores can aid the transport of water soluble agents that are imperative for the maintenance of ingrown tissues, [102] and increasing the water content of a hydrogel can increase the diffusion coefficient of a water soluble through a hydrogel. [20] Following hydration with PBS, the weight of salt porogen PHEMA-PMMA increased by 67 %. Given the cell penetration into the skirt, the pore structure together with the

aqueous swelling capacity may enable the long term vitality of integrated tissue. Since the diffusion coefficient may vary as a function of the distance of travel, [98] minimizing the thickness of the KPro skirt could enhance mass transport. While structural (Figs. 2 and 3) and in vitro (Fig. 7) assessments of the KPro suggest that pore structure and bulk aqueous content could potentially promote stable host integration, pre-clinical ocular implantation can provide a more complete assessment of the in vivo performance of the device.

The ocular response to non-porous PHEMA (i.e., core) indicates that the KPro model developed and reported in this manuscript may resist cell growth into its non-porous core, thereby preserving an unobstructed path for vision. Studies with the AlphaCor KPro showed reduced cell growth on the non-porous PHEMA core compared to the porous PHEMA skirt. [2] [8] [13] If the KPro optics remain relatively free of cell growth, light transmittance in the visible wavelength range through PHEMA and selected PHEMA-PMMA cores (Fig. 6) could approximate that of natural cornea. Approximately 90 to 95 % transmittance of visible light, 400 - 550 nm wavelength, was observed for rabbit cornea, [113] and up to 85 % transmittance in human cornea. [114] Limiting uncontrolled cell growth on the KPro optic or core aids the proper function of the KPro as uncontrolled cell growth can opacify the optic. For example, retroprosthetic membrane is a cell-mediated opacification of the KPro optic. PMMA cores or optics have been used in several KPro models, [2] but our KPro model uses a PHEMA or PHEMA-PMMA optic because fewer incidents of retroprosthetic membrane were reported for PHEMA optics. [8] [9] [7] Increased retroprosthetic membrane in PMMA could be attributed to its greater hydrophobicity compared to PHEMA. Surface hydrophobicity favors protein adsorption which aids cell attachment in vivo. [29] [98] [115] [116] However, calcification reported in PHEMA optics could potentially offset the benefits of reduced retroprosthetic membrane. [8] If a combination of PHEMA and PMMA demonstrates more resistance to

calcification compared to PHEMA, the PHEMA-PMMA core could prove to be a better long term choice.

Calcification is a potential in vivo complication for PHEMA based KPros. [117] For in vivo polymers, polymer degradation and the adsorption of plasma proteins to the polymer surface can initiate calcification. [89] The calcification in the KPros optic or core can potentially be reduced by the addition of PMMA and the reduction surface flaws in the optic. In vivo calcification of a polymer is influenced by the polymer itself, the implantation site, and the incubation time. [88] PMMA may be less susceptible to calcification than PHEMA. After 30 days of intramuscular implantation, an energy-dispersive x-ray spectroscopy (EDS) histogram did not detect calcium or phosphorous containing deposits on PMMA. The PMMA sample was non-porous, and it had surface irregularities. [88] On the other hand, surface flaws can impact calcification in PHEMA. Both surface flaws and pore size influence calcium deposition in PHEMA. [117] Surface flaws enhance the nucleation and growth of calcium crystals. Pore size affects Ca^{2+} diffusion and is therefore a factor that influences calcium deposition. [117] Bone formation has been observed in microporous, approximately 20 μm in diameter, PHEMA structures following 4 weeks of implantation into the fat tissue of a pig. [118] In PHEMA sponges with nanosized pores, bulk calcification may result from the diffusion of Ca^{2+} into the body of the sponge. [119] Copolymerization of PHEMA with ethyl methacrylate (EMA), N-vinylpyrrolidone (NVP), or styrene (St) did not eliminate calcification in a Zainuddin et. al. study. PHEMA copolymers including P(HEMA-co-EMA), P(HEMA-co-NVP), and P(HEMA-co-St)) experienced calcification at 1 to 9 weeks in simulated body fluid. [119] However, the influence of the ratio of monomers in the copolymer was not examined. Further testing is required to determine if the PHEMA : PMMA ratios used in the presented KPros can minimize in vivo calcification in the KPro optic..

Biofilm formation is another major threat to the KPro optic and overall device retention. Rhamnolipids are instrumental in biofilm formation on KPros. They are surface active glycolipids that are produced by a variety of bacterial species, including *Pseudomonas aeruginosa*. Lipopolysaccharide excretion induced by rhamnolipids creates a more hydrophobic polymer surface thereby increasing the adhesion of proteins, and rhamnolipids help to optimize bacterial migration which is essential for biofilm development. [120] Biofilm formation on synthetic implants can result in infection. [121] It predisposes a KPro user to infection because biofilm favors microbe growth and compromises the efficacy of the immune response. The synthetic core component of the PHEMA-PMMA based KPro, which will experience long term exposure to the environment, is expected to be most susceptible to biofilm formation. Biofilm formation has been reported on a variety of hydrogel based contact lens, including the HEMA based polymacon lens. [122] [123] Surface conjugation of an antibacterial agent reduced biofilm formation on the PMMA based Boston KPro. [124] The addition of a cytocompatible antimicrobial coating may inhibit biofilm formation on PHEMA-PMMA based KPros, thereby enhancing the longevity of the devices.

The addition of a corneal epithelial layer to the KPro can potentially reduce biofilm formation and infection. A number of groups have proposed epithelialization methods for synthetic polymer gels. [115] [19] [29] This can be accomplished using ECM proteins or peptides. [1] Carbonyldiimidazole (CDI) treatment can be used to covalently attach collagen type I to the PHEMA-PMMA. [54] Since collagen type I constitutes approximately 70% of the dry weight of corneal stroma, the collagen type I coating may sufficiently mimic the natural environment of corneal cells. Alternatively, aminosilane coupling followed by the addition of SAND (a photo-reactive crosslinker) may enable collagen type I crosslinking to PHEMA-PMMA. [125] The surface of the KPro can also be modified with peptides. Peptide modification of biomaterials is a widely used technique. [126] Aucoin et. al. demonstrated greater adhesion of corneal

epithelial cells when the polydimethyl siloxane (PDMS) surface was modified with a combination of YIGSR and PDSGR as compared to single peptide modification. [127] Acrylated YIGSR and PDSGR could be covalently attached to a PHEMA-PMMA gel via UV polymerization. [32] An alternative method involves surface conjugation via tresyl chloride chemistry [127]. Previous studies with peptides suggest that a range of peptide concentrations can be employed to achieve cell adhesion. [46] [128] [129] [40] [81] Researchers continue to investigate methods to create a stable epithelial layer over a KPro optic that permits physiologically relevant mass transport. The PHEMA and PHEMA-PMMA based optics presented here require modification in order to permit physiologically appropriate mass transport, but methods to enable cell growth are known.

5.6 Conclusion

The salt porogen KPro design includes a highly porous PHEMA-PMMA structure to permit cell ingrowth, and the central transparent core can consist of PHEMA or a PHEMA-PMMA copolymer. Mechanical data indicates that the device can sustain ocular forces and maintain its structure during surgical handling such as suturing onto the patient's eye. The PHEMA alone or PHEMA-PMMA cores, both capable of being fused to the skirt, permit physiologically relevant optical transparency. Structural and in vitro biointegration data suggest that the KPro skirt can potentially facilitate cell ingrowth in vivo. This novel salt porogen PHEMA-PMMA KPro may offer a cornea replacement option that minimizes incidents of corneal melting by enhancing stable tissue integration and mass transport.

6. Gas Foamed Scaffold for Keratoprosthesis

6.1 Abstract

Artificial corneas or keratoprotheses (KPros) are intended to replace diseased or damaged cornea in the event that vision cannot be restored using donor cornea tissue. A new class of artificial cornea comprising a combination of poly (2-hydroxyethyl methacrylate) (PHEMA) and poly (methyl methacrylate) (PMMA) was developed which was fabricated using a gas foaming technique. Referred to as the gas-foamed KPro, it was designed to permit clear vision and secure host biointegration to facilitate long-term stability of the device. In vitro assessments show cell growth into the body of the porous edge or skirt of the gas-foamed KPro. The optically transparent center (i.e., core) of the device demonstrates 85 – 90 % of light transmittance in the 500 – 700 nm wavelength range. Mechanical tensile data indicates that the gas-foamed KPro is mechanically stable enough to maintain its structure in the ocular environment and also during implantation. The gas-foamed KPro may provide an alternate option for cornea replacement that minimizes post implantation tissue melting, thereby achieving long-term stability in the ocular environment.

6.2 Introduction

An inadequate keratoprosthesis design can result in extrusion, necrosis, increased intraocular pressure, or infection. [1] [2] [4] Conversely, a well-designed artificial cornea would comprise mechanically stable and non-toxic materials to facilitate long term biointegration with the host. This report presents a novel synthetic KPro for full thickness keratoplasty. The KPro is composed of poly (2-hydroxyethyl methacrylate) (PHEMA) and poly (methyl methacrylate) (PHEMA-PMMA). This study demonstrates that the newly engineered PHEMA-PMMA KPro, referred to as the gas-foamed KPro, is biocompatible, optically transparent, and mechanically strong enough to maintain its structure in the ocular environment.

Typical KPro designs follow a core-skirt model in which an optically transparent core permits vision while a porous skirt allows for tissue ingrowth. [1] [2] [4] This is a challenging engineering task because uncontrolled cell growth and debris adsorption on the core should be discouraged to maintain its optical clarity, while the opaque porous skirt (e.g., outer rim of the KPro) is designed to promote tissue ingrowth. When implanted, biointegration achieved through tissue ingrowth into the device is imperative for long term retention in the patient's eye. A technique known as gas foaming may benefit KPro designs because the gas foaming of hydrogels is known for generating interconnected pores during polymerization. [42] KPro skirts that permit biointegration may then be created by at least two methodologies. First, an interconnected pore structure can be introduced to a synthetic polymer that has ocular compatibility. [2] [4] Second, natural polymers, such as collagen or decellularized animal tissue, can be used as KPro skirts. [21] [130] Synthetic polymers, PHEMA and PMMA, allowed us to create a mechanically stable KPro that may benefit patients who are immunologically sensitive to donor cornea or foreign biological material. Synthetic tissue engineering scaffolds also permit a high level of control over mechanical properties, geometry, and biological interaction. [23] [24] Both the ocular compatibility and pore interconnectivity of KPro skirts appear to be major determinants of long term KPro stability.

Clinical outcomes for other core-skirt KPros such as AlphaCor, Seoul Type, and Pintucci indicate that device performance depends on both device design and patient selection. The aforementioned KPros include a core made of either PHEMA or PMMA. Both transparent PHEMA and PMMA cores can permit vision. However, long term vision restoration depends on KPro retention in the host, and the skirt's ability to promote tissue ingrowth influences device retention. [1] [2] The AlphaCor KPro, a PHEMA-based device which consists of a center optic surrounded by a porous rim or skirt, [1] appeared to enhance cell ingrowth following implantation into rabbit cornea. [9] An electron micrograph illustrated the pore structure of the

skirt into which cells migrated. However, a 2005 clinical trial composed of patients with preexisting ocular conditions reported that 8 out of the 14 AlphaCor devices were removed due to corneal tissue melting anterior to the device. [8] Tissue melting could result from inadequate host integration or excessive inflammation. [13] Similar to AlphaCor, the performance of the Seoul Type was influenced by patient selection. The device includes a PMMA optic and a skirt made of polyurethane, polypropylene, or polytetrafluoroethylene. [1] [14] SEM images indicate that the skirt of the device has pores of 30 μm or greater that appear to be interconnected. In preclinical trials, fibroblast ingrowth and collagen deposition were observed on devices that use the polypropylene and polyurethane skirts [15], but in clinical trials with patients with preexisting ocular conditions, anatomic retention at 68 months was 67 %. Eventually all devices developed corneal melt leading to full exposure of the skirt. [1] [2] Increased tissue melting in the Seoul Type KPro compared to AlphaCor suggests that the PHEMA skirt is better tolerated in the cornea than polymers used in the Seoul Type KPro. Like the Seoul Type and AlphaCor KPros, Pintucci triggered complications including corneal melting. Its dacron membrane permitted tissue ingrowth in patients with preexisting ocular conditions, but 2 out of 20 devices extruded. 13 out of 20 patients maintained improved visual acuity for more than 2 years. [16] Necrosis of the mucous membrane anterior to the device skirt was reported for 50% of patients. [4] A 1996 study reported that 60% Pintucci KPro recipients developed mucous membrane pemphigoid, [2] which is an autoimmune disease that can result in vision loss. [17] Clinical data from synthetic KPros show that both materials selection and device design are imperative for long term host retention.

The use of gas foamed PHEMA-PMMA represents a novel approach to create a mechanically and structurally effective artificial cornea that could potentially promote long term host integration. The biomaterial selection was inspired by the long-term clinical performance of PMMA in the Boston KPro, [4] rabbit corneal epithelial cell proliferation on PHEMA-PMMA, [131]

and the in vivo response to PHEMA-PMMA copolymers in the ocular lens. [94] Since a previous in vivo study indicated that pore interconnectivity in a gas foamed structure facilitates tissue ingrowth throughout the body of the structure, [42] pores were introduced to PHEMA-PMMA using a gas foaming technique. This study presents a structural and material design that may permit stable host integration while maintaining a healthy immune response.

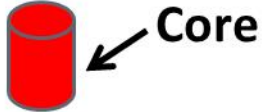
6.3 Methods

6.3.1 Engineering the Gas-Foamed KPro

The KPro was fabricated by foaming a PHEMA-PMMA copolymer around a UV polymerized PHEMA cylinder (Fig. 1A). Briefly, to create a transparent PHEMA 70% v/v cylinder that serves as the core, an aqueous solution containing 70 % v/v HEMA (Aldrich 477028), 0.1 % v/v ethylene glycol dimethacrylate (EGDMA) (Aldrich 335681), and 1 % w/v Irgacure 2959 (BASF 55047962) was polymerized with UV light (365 nm long wave) for 40 min. For the porous PHEMA-PMMA skirt, HEMA and MMA (Aldrich M55909) monomers were combined with chemical initiators in a solvent consisting of a 1.5 to 1 ratio of deionized water to dimethylformamide (DMF). The monomer solution included 19 % v/v MMA, 37 % v/v HEMA, 0.014 % w/v (g/mL) pentaerythritol tetraacrylate (Aldrich 408263), 0.012 % w/v Pluronic PF-127 (Anatrace), 0.027 % w/v ammonium persulfate (Sigma), and 0.013 % v/v N,N,N',N'-Tetramethylethylenediamine (Acros Organics). The monomer solution was added to a Chemrus disposable filter funnel. Then, nitrogen gas was pushed through the filter funnel at approximately 10 kPa for 5.5 min to add pores to PHEMA-PMMA. Prior to introducing nitrogen to PHEMA-PMMA, a transparent PHEMA cylinder with a surface modification was added to the filter funnel. To strengthen the bond between the PHEMA core and the porous PHEMA-PMMA skirt, a layer of MMA was added to the PHEMA cylinder using UV polymerization. The MMA surface functionalization process was a modification of a method published by Lee et. al. [32] and uses DMF as the solvent in the monomer solution; unlike the Lee. et. al. protocol, benzyl

alcohol and acrylic acid were excluded from the monomer solution. After porous PHEMA-PMMA was added to the transparent PHEMA, the product was cured in 37°C oven for 20 hours. Prior to cutting the large Gas KPro cylinders into ~ 0.5 mm disks with a microtome, the cylinders were rinsed in aqueous ethanol solutions in two different concentrations (10% and 20%) and finally hydrated in deionized water. An image of the completed gas-foamed KPro shows a transparent core connected to a porous skirt (Fig. 1B).

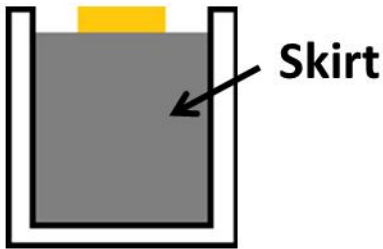
1. PHEMA 70% v/v was UV polymerized to create an optically transparent core.



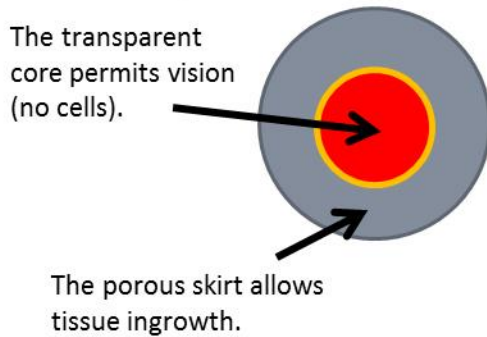
2. The surface of the core was modified with MMA monomer.



3. PHEMA-PMMA copolymer (HEMA : MMA = 1 : 2) was foamed around the core using nitrogen gas. It was polymerized at 37°C for 20 hours.



4. The core – skirt cylinder was cut to create thin disks (~ 0.5 mm thin).



A

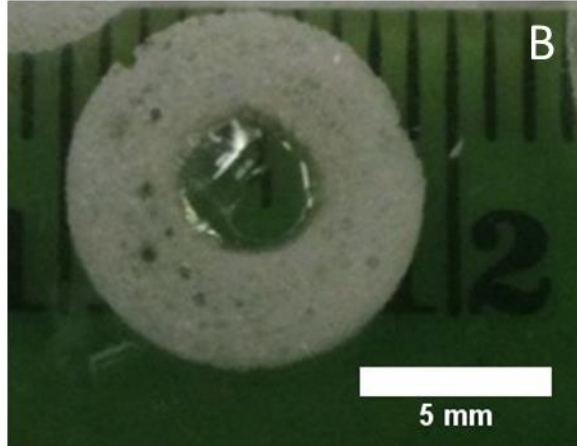


Figure 1. The KPro was fabricated by foaming a PHEMA-PMMA copolymer around a UV polymerized PHEMA cylinder (A). The transparent core is easy to distinguish from the white porous skirt (B).

6.3.2 Structural and Optical Characterization

To observe the pore structure of gas foamed and non-gas foamed PHEMA-PMMA, SEM images of the polymers were generated using a S-3000N Variable Pressure SEM (Hitachi). Pore size was measured using the Scanco model 50 micro CT system. Micro CT data was acquired with an X-ray tube voltage of 45 kV, current of 133 μ A, 0.1 mm aluminum filter, and 1500 ms integration time. Pore size measures were taken using the software included in the Scanco micro CT system; data was obtained by analyzing three scaffold regions of equal volume.

The optical transmittance of transparent PHEMA 70% v/v ($n = 8$) was measured with a Synergy HT Multi-Mode Microplate Reader (BioTek). Transmittance was measured for three sample groups ($n = 8$): PHEMA 70% v/v, PHEMA 70% v/v subjected to cell culture conditions, and PHEMA 70% v/v seeded with primary human corneal fibroblasts (HCFs). PHEMA 70% v/v samples were seeded with 1500 HCFs per well in a 96 well plate. After 7 days of cell growth, transmittance was measured. The control samples were non-cell seeded polymers that were subjected to the 7 day cell culture process. Polymer samples were covered in fresh PBS during measurements; therefore, absorbance values for wells that contained PBS were subtracted from the polymer samples' absorbance values.

6.3.3 Tensile Testing

Hydrated porous PHEMA-PMMA and gas-foamed KPro samples ($n = 4$) were tested in tension using a custom designed 100LM Test Resources mechanical testing machine (Test Resources Inc., Shakopee MN). Average sample dimensions were approximately 7.0 x 6.0 mm and 3.6 mm depth for porous PHEMA-PMMA. In the tensile testing clamps, the average dimensions of the disk shaped Gas KPros were 5.6 x 14.2 mm and 1.3 mm depth. Samples were tested at a strain rate of 0.2 mm/s using a calibrated WMC-10 load cell (Test Resources Inc.), which is

fatigue-rated for 10 pounds of force in tension and compression. Values taken from the tensile measures included elastic modulus (E), ultimate tensile strength (UTS), and strain at rupture. E is measured in the elastic or linear region of the stress vs. strain plot; $E = \text{stress/strain}$. UTS is the maximum stress response of a material during tensile testing. The strain at rupture is simply the elongation of the sample at the point of rupture. In this study, the elongation was reported as a percentage of the original length of the sample.

6.3.4 Coating Gas-Foamed KPros in Collagen Type I

The gas-foamed KPros were coated with rat tail collagen type I (BD Bioscience) in preparation for in vitro testing. Samples were immersed in a rat tail collagen type I solution (2 mg/mL) with 5 mM N-(3-Dimethylaminopropyl)-N'-ethyl-carbodiimide (EDC) and 5 mM N-hydroxysuccinimide (NHS); EDC and NHS were used to crosslink the collagen. After the samples were removed from the solution, collagen type I gelled at 37 °C for 30 min. Monoclonal anti-collagen type I antibody at 1:2000 dilution (Sigma-Aldrich C2456) was used to stain and visualize collagen fibers.

6.3.5 In Vitro Assessment

Primary human corneal fibroblasts (HCFs), passages 8 and 11, were cultured in GIBCO MEM alpha media (Invitrogen) with 10% fetal bovine serum (FBS) (Atlanta Biologicals) and 1% antibiotic-antimycotic solution (Sigma-Aldrich). 10000 HCFs were added to the surface of gas-foamed KPros coated with collagen type I, and to the surface of non-gas foamed PHEMA-PMMA. A live-dead cell viability assay (Invitrogen) was used to stain cells at days 4 and 7. The depth of cell growth was estimated using confocal microscopy and Metamorph Software (Molecular Devices). Ethidium homodimer which stains dead cells also made the polymer surface visible. To quantify the depth of cell growth, cell populations were imaged at 2 distinct locations on the porous structure. For each time point, 5 depth measures were taken from each

image (n = 10). The depth of HCF growth was estimated based on the deepest point of cell growth into the structure. Using the side projections, a total of 5 depth measures were taken at ~ 20 μm intervals from a center vertical line that marked the deepest point of cell growth. Where cells were spaced apart greater than 20 μm on non-porous, non-collagen coated PHEMA-PMMA, measure intervals were increased to measure the near cell or group of cells. The depth measures were taken from a defined polymer edge to the lowest extension of the cell. An alamarBlue assay (Invitrogen) was used to evaluate cell seeding efficiency in porous PHEMA-PMMA with and without collagen coating. A calibration curve was created to convert fluorescent signals from the alamarBlue assay to cells per unit volume. To evaluate cell seeding efficiency on the KPro skirt, ~ 33,000 HCFs were added to the surface of porous PHEMA-PMMA or collagen-coated porous PHEMA-PMMA. Polymer structures were cut to cover the cell culture well (1.9 cm^2 area). Cell quantities measured at day 9 using alamarBlue showed the efficiency of cell seeding on porous PHEMA-PMMA. Two structures of each porous PHEMA-PMMA type, with and without collagen, were measured three times.

6.3.6 Statistical Analysis

MATLAB R2012a was used to conduct two sample t-tests at an alpha value of 0.05. Data are reported using mean \pm standard error.

6.4 Results

6.4.1. In Vitro Cell Response to KPro

Biocompatibility of the gas-foamed KPro was first established before we pursued other characterization such as pore structures, mechanical and optical properties of the scaffold. After seeding human corneal fibroblasts on the surface of collagen-coated KPros, cell growth was monitored at days 4 and 7 in the porous KPro skirt (Figs. 2A and 2B). Live cells, stained green by calcein AM fluorophore, exhibited the typical long spindle-like morphology that would

be expected of cells seeded in a 3D scaffold. [43] [132] The majority of cells (> 90 %) were found to be viable. The fluorophore ethidium homodimer synthesized to stain dead cells showed very few non-viable cells; rounded cell morphology and strong red fluorescence signal would be expected from dead cells. We also noticed that ethidium homodimer stained the polymer structure; fluorescence images show the pores created by the gas-foaming technique. The collagen coating should enhance cell retention in the porous skirt of the KPro, since collagen is an extracellular matrix protein that provides binding sites for integrins for cell adhesion. [133] In order to validate this, the same number of cells was seeded in the PHEMA-PMMA scaffolds with or without collagen coating. Following 9 days after initial cell seeding, virtually no cells were detectable when collagen coating was not applied. In contrast, when coated with collagen, cells were found to be attached to the scaffold (Fig. 2C). Disk shaped porous PHEMA-PMMA samples, with and without collagen, were seeded with 174 cells/mm^3 to evaluate the cell seeding efficiency. Cells were not detected on the collagen-free porous PHEMA-PMMA because virtually all of the seeded cells fell through the pores of the structure. Approximately 16 cells/mm^3 were found on collagen coated porous PHEMA-PMMA at day 9. We believe that the entrapped collagen network permitted greater cell retention. The collagen network increased cell retention by enhancing cell adhesion and filling some voids in the polymer structure.

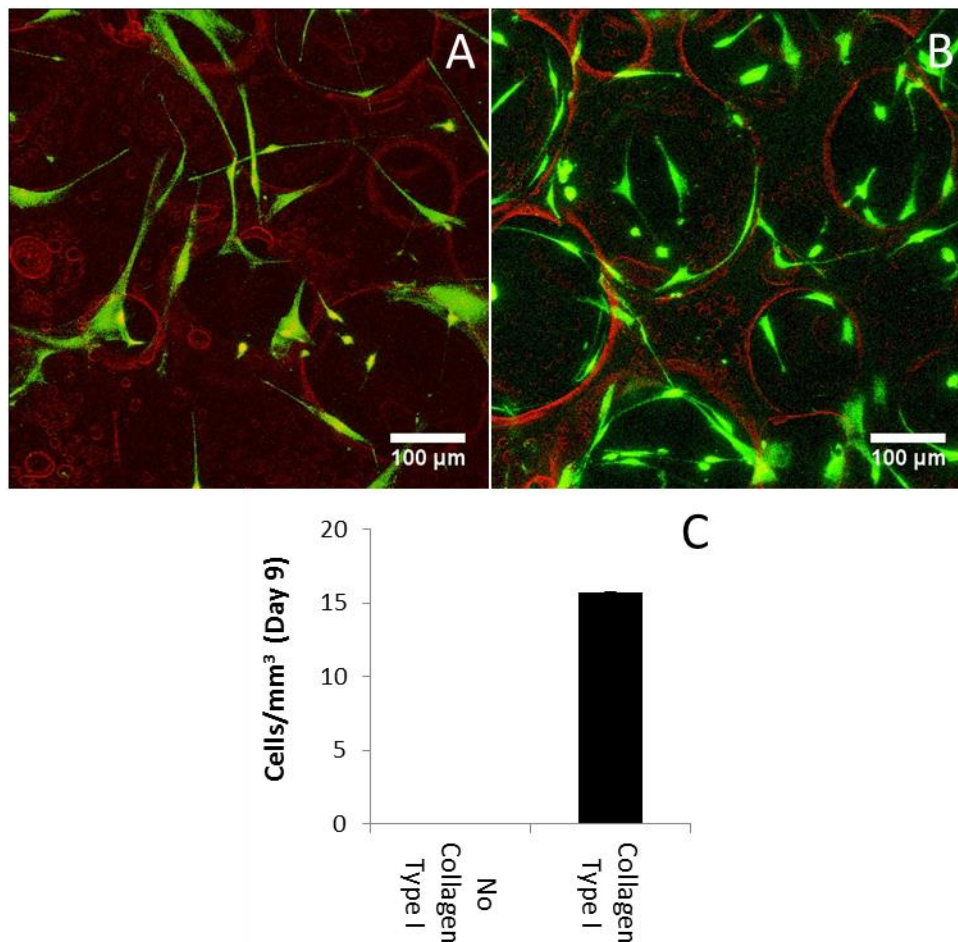


Figure 2. At days 4 (A) and 7 (B), cell viability staining shows live HCFs on porous PHEMA-PMMA. Calcein-AM stained live cells in green. Ethidium homodimer, which is designed to stain dead cells, also stains the polymer structure. Coating the polymer with collagen type I aided in vitro cell retention in the structure (C). At day 9 following HCF seeding, cells were not detected on the porous PHEMA-PMMA that was not coated with collagen type I, n = 6.

Confocal microscopy was therefore used to assess the depth of cell growth into the collagen-coated porous scaffolds. Side projections of live HCFs show that the depth of HCF growth into the skirt, porous PHEMA-PMMA, increased from day 4 (Fig. 3A) to day 7 (Fig. 3B). The average depth of cell growth was estimated by measurements taken from fluorescent images (Fig. 3C). At day 4, the average depth of cell penetration was $57 \pm 5 \mu\text{m}$, whereas at day 7 the depth increased significantly and doubled to $102 \pm 9 \mu\text{m}$ ($p < 0.001$). This demonstrates that viable HCFs can penetrate into the body of the collagen-coated porous scaffold. Positive

immunofluorescent staining for collagen type I confirmed that a collagen network may have been established throughout the porous skirt (Fig. 3D). Non-gas foamed PHEMA-PMMA, without collagen coating, permitted shallow depths of HCF growth at days 4 (Fig. 3E) and 7 (Fig. 3F). Not only less viable cells were recorded in this scaffold, but also average depths of cell penetration remained unchanged from $35 \pm 4 \mu\text{m}$ at day 4 to $38 \pm 3 \mu\text{m}$ at day 7, suggesting no cell penetration into the collagen-free, non-gas foamed PHEMA-PMMA (Fig. 3G).

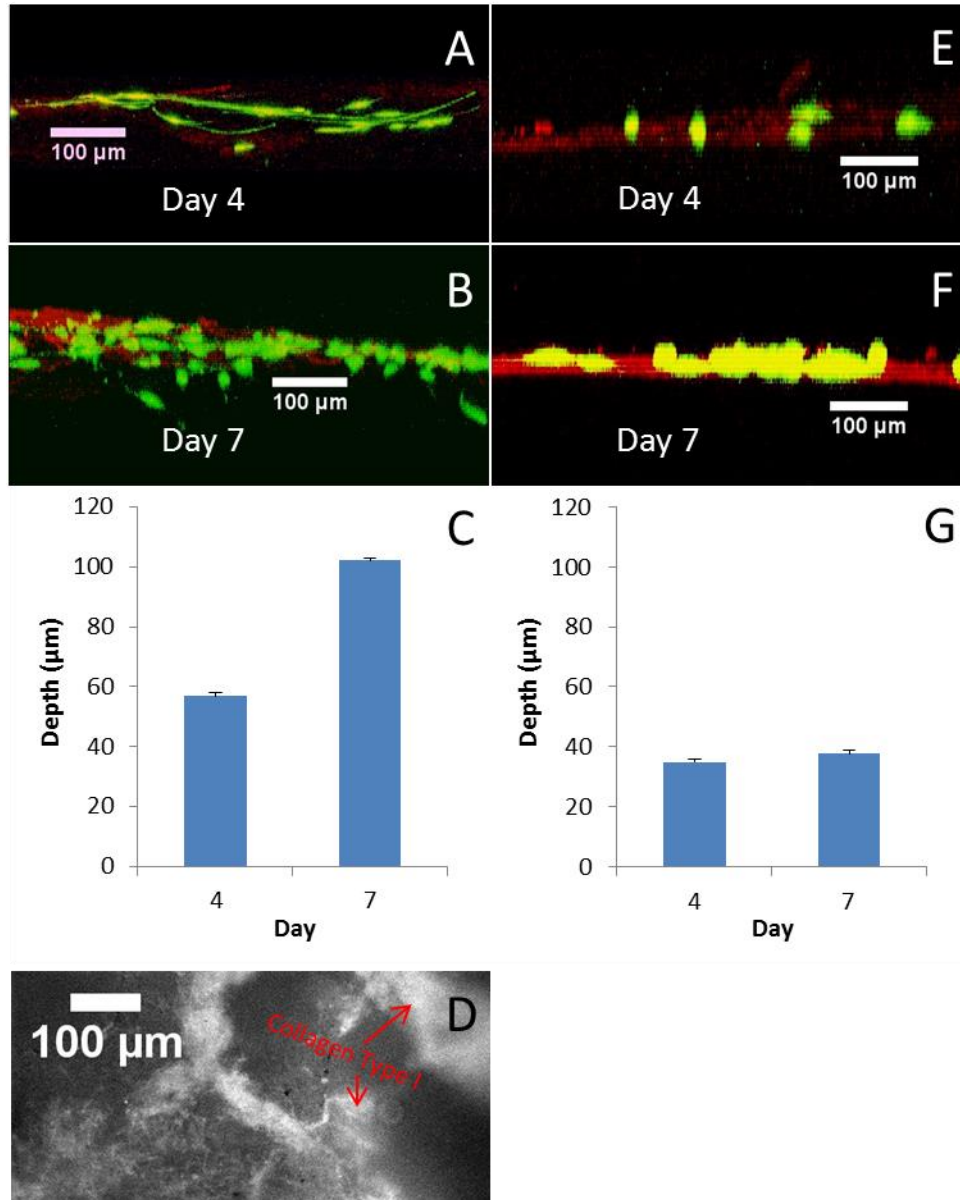


Figure 3. Side projections of live HCFs, in green, show HCF growth inside of porous PHEMA-PMMA at days 4 (A) and 7 (B). Ethidium homodimer, which is designed to stain dead cells red, also stains the polymer structure. The depth of HCF growth into porous PHEMA-PMMA increased significantly ($p < 0.001$) from day 4 to 7 (C). The presence of the collagen type I coating on PHEMA-HEMA was verified using anti-collagen type I antibodies. The collagen fibers are shown in white (D). Non gas foamed PHEMA-PMMA, without a collagen coating, permitted shallow depths of HCF growth at days 4 (E) and 7 (F). The depth of HCF growth remained constant from day 4 to 7 on the collagen-free, non-porous polymer (G).

6.4.2 Structural and Optical Characterization

Motivated by encouraging results regarding cell viability and growth, the physical properties of the gas-foamed KPro were characterized next. The pore structure in the skirt and optical transparency of the core are expected to regulate the functionality of the gas-foamed KPro. First, SEM and micro CT images show that gas foaming with nitrogen created a high density of interconnected pores to the PHEMA-PMMA skirt (Figs. 4A and 4C), which was designed to encourage large scale cell ingrowth. During the gas foaming process, monomers polymerized to form an interconnected or open pore structure around nitrogen gas bubbles as the bubbles moved through the monomer solution. Without gas foaming however, PHEMA-PMMA has a mostly closed pore structure and no pore interconnectivity was noticeable (Fig. 4B). Closed pore structures are not expected to promote tissue ingrowth throughout the body of a polymer. For the gas-foamed polymer, referred to as porous PHEMA-PMMA, average pore size was $70 \pm 8 \mu\text{m}$ in diameter, and the range was from $10 \mu\text{m}$ to $> 1000 \mu\text{m}$ in diameter. MicroCT data showed that approximately $68 \pm 1 \%$ of the porous scaffold was occupied by pores. Furthermore, optical transmittance data shows that the PHEMA (70% v/v) core of the KPro transmits most visible light (Fig. 5A). In the wavelength range from 500 to 700 nm, $> 85\%$ transmittance was achieved, while the transmittance was as low as 70 % below 500 nm. The PHEMA 70 % v/v core used in the gas-foamed KPro appears to be optically transparent enough to permit vision. In the wavelength range between 650 to 700 nm, the addition of HCFs to PHEMA 70% v/v core (PHEMA 70% v/v + HCFs; Fig. 5B) had a negligible effect on transmittance compared to the control (PHEMA 70% v/v without cells). Phenol red in the cell culture media used as a pH indicator caused a significant loss in the light transmittance.

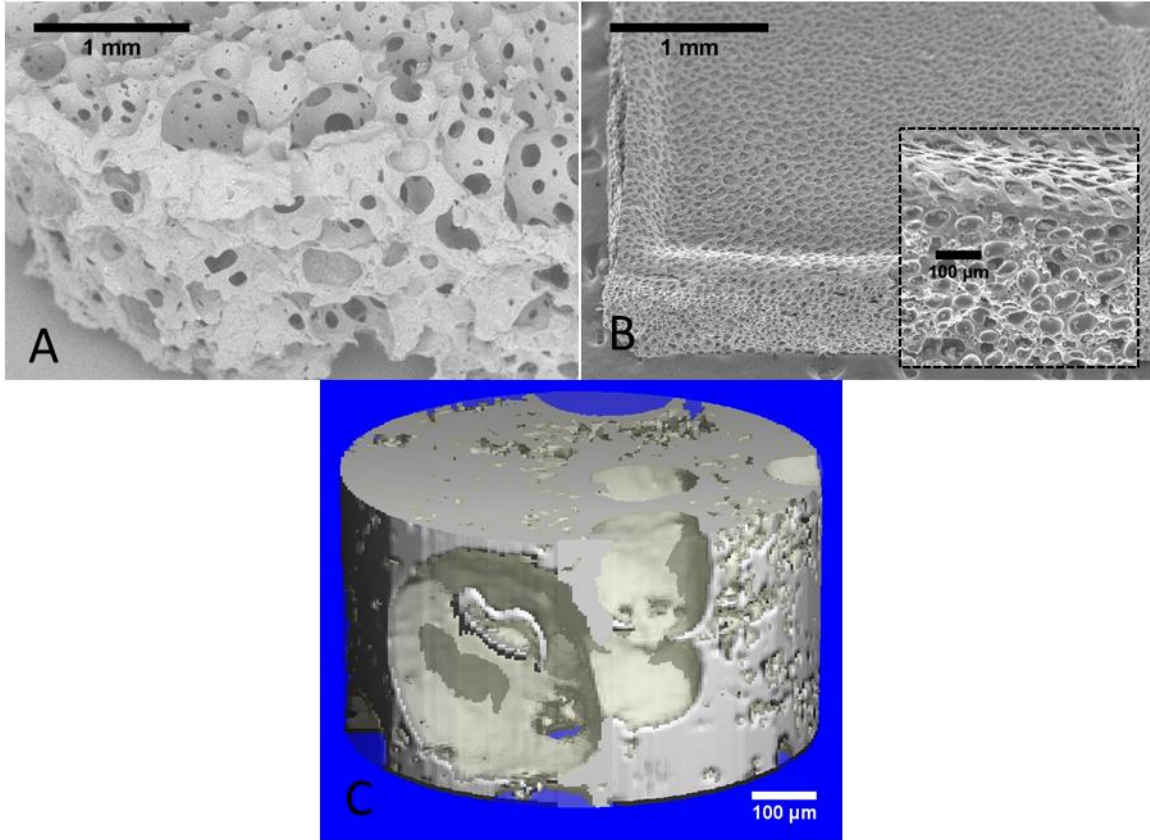


Figure 4. SEM (A, B) and micro CT (C) images show that gas foaming with nitrogen added a high density of interconnected or open pores to PHEMA-PMMA. The gas foamed PHEMA-PMMA (A), known as porous PHEMA-PMMA throughout this report, constitutes the KPro skirt. Without gas foaming (B), PHEMA-PMMA has a predominately closed pore structure; the box inside of image B is a zoomed in view of the pores of the non-gas foamed polymer.

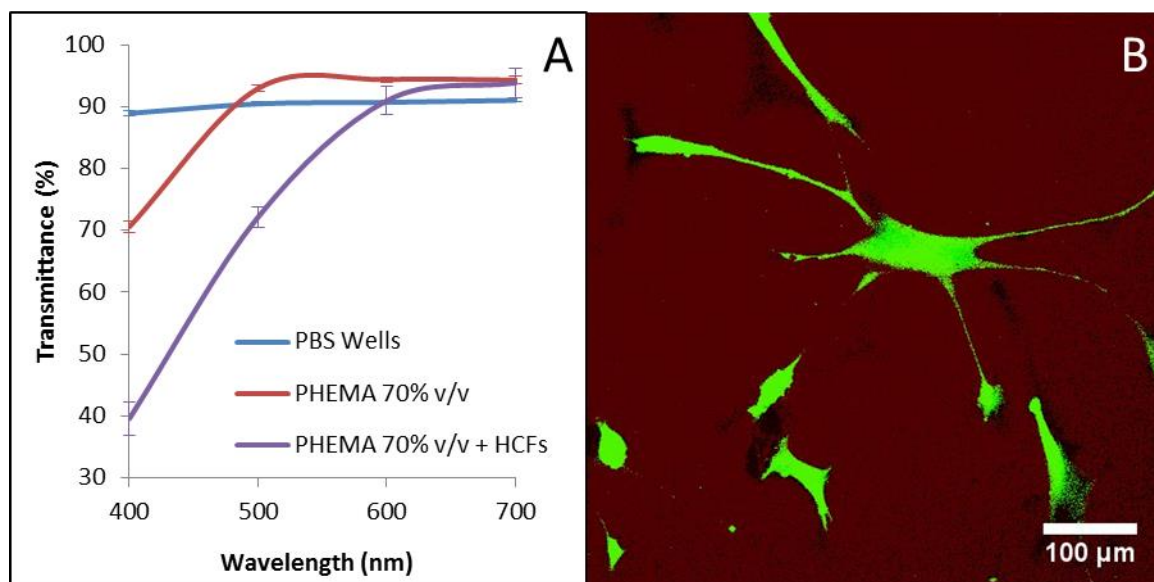


Figure 5. Transparent PHEMA 70% v/v provided 85 – 90% transmittance of visible light in the 500 – 700 nm range (A). Polymer samples were covered in PBS during measurements; therefore, transmittance data for polymers was normalized using data from wells filled with PBS. At 650 – 700 nm, the addition of HCFs to the polymer (PHEMA 70% v/v + HCFs) had a negligible effect on transmittance compared to the control (PHEMA 70% v/v). The phenol red in the cell culture medium, which was added to detect pH, reduce transmittance in “PHEMA 70% v/v + HCFs” in the 400 – 600 nm range. A representative image of HCFs on PHEMA 70% v/v shows sparse cell growth; the polymer was not coated with collagen or any cell adhesion component (B). Live cells are green. Ethidium homodimer, which is designed to stain dead cells red, also stains the polymer structure.

6.4.3 Mechanical Characterization

Mechanical properties of the skirt alone and gas-foamed KPro were quantified. The KPro device and the skirt alone were found to have statistically equivalent elastic modulus (E) ($p = 0.61$) and ultimate tensile strength (UTS) ($p = 0.90$) values (Figs. 6A – 6B). However, strain at rupture for the KPro device was significantly greater than the porous skirt ($p = 0.01$) (Fig. 6C). Due to the elimination of an outlier strain to rupture value, the sample size was $n = 3$ for KPro data in Figure 6C; $n = 4$ for the other data sets in Figures 6A – 6C. For the KPro, E , UTS, and strain at rupture were 3557 ± 536 kPa, 273 ± 31 kPa, and 139 ± 18 %, respectively. For the porous skirt alone, E , UTS, and strain at rupture were 4082 ± 808 kPa, 263 ± 66 kPa, and 64 ± 9 %, respectively. The stress response of gas-foamed KPros and porous skirts was recorded

until the samples ruptured (Fig. 6D). The materials displayed both hardness and strength. Prior to applying tensile force, the core was securely attached to the edge of the skirt. The partial attachment of the core to the skirt following device rupture showed that the gas-foamed KPro can maintain its structure under stresses that exceed the forces expected in the ocular environment (Fig. 7A). Following the tensile rupture of the skirt, the zigzag fracture pattern at the midsection of the sample resembled that of the KPro (Fig. 7B). Taken together, the novel artificial cornea composed of copolymers was deemed biologically and mechanically suitable for corneal implantation.

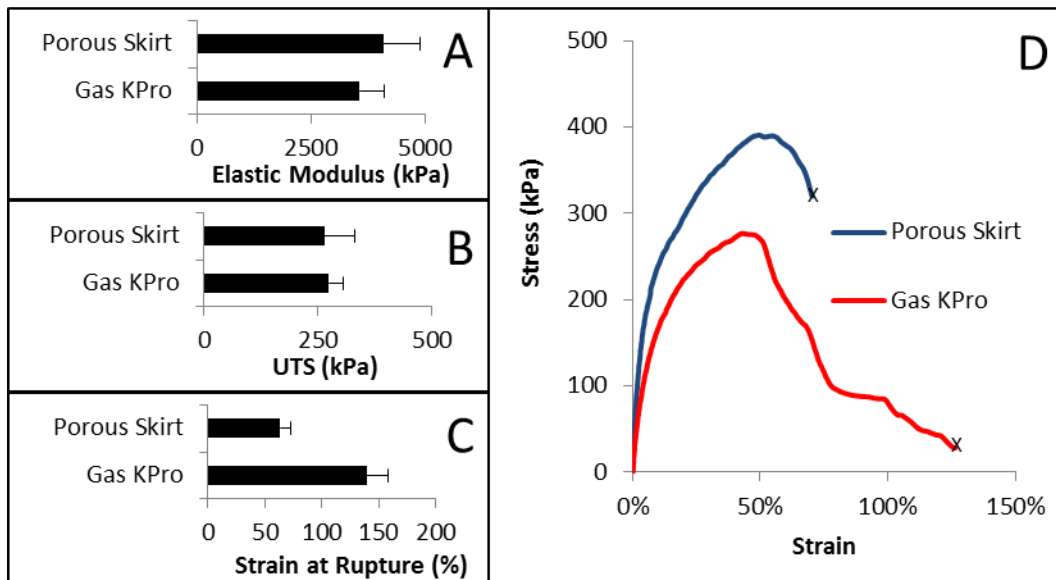


Figure 6. The KPro device and the skirt alone were found to have statistically equivalent elastic modulus (E) ($p = 0.61$) and ultimate tensile strength (UTS) ($p = 0.90$) values (A - B). However, strain at rupture for the KPro device was significantly greater than the porous skirt ($p = 0.01$) (C). Due to the elimination of an outlier strain to rupture value, the sample size was $n = 3$ for KPro data in "C". For all other data sets, $n = 4$. The stress response of the KPros and porous skirts were measured until the samples ruptured. "X" marks the point of rupture for the samples (D).

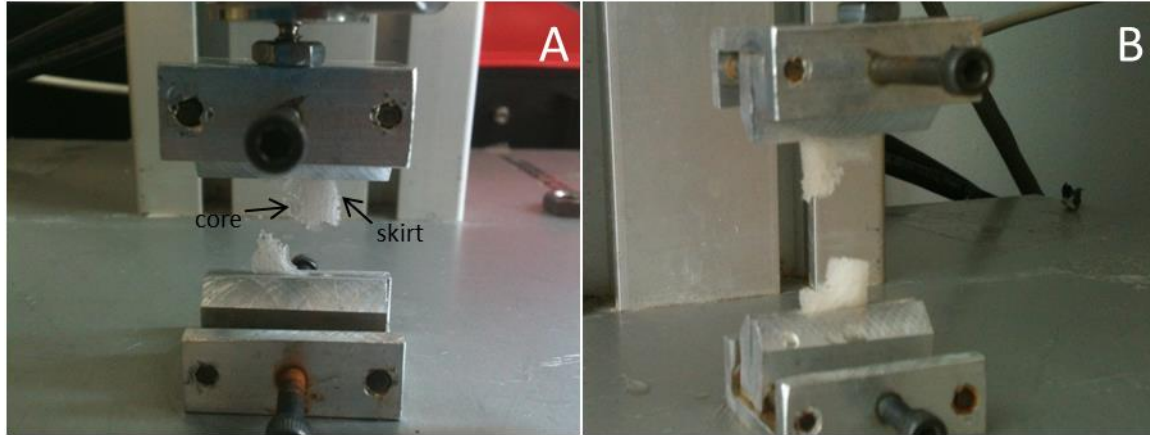


Figure 7. The partial attachment of the core and the skirt following device rupture illustrate the strength of the core-skirt connection in the Gas-Foamed KPro (A). Like the KPro, the rectangular sample of the skirt (B), porous PHEMA-PMMA, had a zigzag fracture pattern at the midsection of the sample.

6.5 Discussion

The gas-foamed KPro was designed to resist adverse events including rupture or core-skirt separation, while permitting vision and ocular tissue ingrowth into the KPro skirt. Visible light transmittance through the KPro core (see Fig. 5) approximates that of natural cornea, 90 to 95 % in the 400 to 550 nm wavelength range. [113] Transmittance (> 90%) through the PHEMA 70 % v/v core at the wavelength range > 500 nm is consistent with similar measurements reported by Gulsen et. al for transparent PHEMA. [73] Since the commercially available AlphaCor KPro includes a PHEMA core made with a high fraction of HEMA, 70 – 90 % by weight concentration in water, [134] it is expected to demonstrate similar transmittance. In addition, visual acuity following AlphaCor implantation demonstrates that a transparent PHEMA core can restore vision in patients who cannot receive donor cornea. Following device implantation, best corrected visual acuity (BCVA) ranged from light perception to 20/20; results were taken at a variety of time points following AlphaCor implantation. [11] Clinical studies with transparent PHEMA suggest that it can be used as the core to restore vision in a core-skirt model KPro.

Mechanical tensile data indicates that the KPro can comfortably maintain its structure in the ocular environment (Fig. 6). Intraocular pressure and eyelid movement are major forces that any corneal implant encounters. Average intraocular pressure is only up to 2- 4 kPa, [107] [108] which falls well below the UTS of the gas-foamed KPro. High elastic modulus and UTS values for the gas-foamed KPro suggest that the device can resist rupture during implantation. Similar to other KPro models, [2] [5] our gas-foamed KPro does not perfectly match the mechanical properties of natural human cornea. [109] [110] [111] However, results from previously published KPro designs indicate that corneal tissues can integrate structures that possess a range of mechanical properties. [2] [9] [15] [16] Functionally, the natural tear film is expected to minimize shear forces between the eyelid and the PHEMA optic of the KPro. It is worth noting that PHEMA is used in contact lenses because of its favorable tear film wettability. [103] In addition, the AlphaCor KPro which contains a PHEMA core or optic was FDA approved for patients with a satisfactory tear film. [2]

Following KPro implantation, ocular tissues that can potentially grow into the porous skirt of the gas-foamed KPro are expected facilitate nutrient and gas exchange. The size of the optic, ~ 3.5 mm in diameter, will likely limit the effects of its non-physiological gas and nutrient exchange. Studies with contact lenses suggest that the low water content of the PHEMA 70% v/v optic, 24 ± 1 %, will yield low oxygen permeability. [95] Experiments with poly (ethylene glycol) diacrylate – poly (acrylic acid) (PEGDA-PAA) hydrogels showed that nutrient exchange, particularly glucose flux, increased with the increased water content of the polymer structure. [20] The ocular tissues surrounding the small PHEMA optic, including those integrated into the KPro, are expected to compensate for the limited mass transport of the optic. Given the volume and interconnectivity of pores in the skirt, the development of functional tissue in the skirt is anticipated in vivo. Studies with gas foamed PEGDA show that the gas foaming processes creates an interconnected pore structure that facilitates large scale in vivo tissue ingrowth. [42]

Cornea receives its oxygen and nutrients from the tear field and aqueous humor, respectively. [28] If vascularization occurs, mass transport in the skirt would likely resemble that of vascularized ocular tissue. Clinical data from the Boston KPro shows that a device with highly effective host integration in the skirt can achieve long term stability in the absence of physiologically equivalent mass transport in the core. [4]

The in vivo response to other KPros containing PHEMA or PMMA indicates that the gas-foamed KPro can potentially allow ocular tissue ingrowth while permitting vision. Cell migration, a prerequisite to tissue development, favors non-toxic and cell adhesive surfaces. Cell growth and viability data show that the gas-foamed KPro is non-toxic (Figs. 2 and 3). The addition of collagen was required to facilitate in vitro cell growth on porous or gas foamed PHEMA-PMMA. However, in vivo studies indicate that a porous PHEMA material can allow cell ingrowth without the addition of cell adhesion molecules. For example, ocular cells migrated into porous PHEMA in the AlphaCor KPro. [9] However, minimal cell growth was observed on the non-porous PHEMA optic of AlphaCor. [8] This highlights an advantage of using non-porous, transparent PHEMA as the KPro core. Limiting uncontrolled cell growth on the optic aids the proper function of the KPro, as uncontrolled cell growth can opacify the optic. While low levels of in vitro HCF growth do not impact visible light transmittance (Fig. 5), large scale cell growth that covers the optic could reduce vision. Rather than PMMA optics that have been used in several KPro models, [2] a PHEMA optic we have chosen for the gas-foamed KPro may potentially reduce the incident of retroprosthetic membrane (i.e., cell mediated opacification of the KPro optic). Higher incidents of retroprosthetic membrane have been reported with PMMA optics compared to PHEMA optics, [7] [8] [9] attributing this unwanted effect, [7] to its greater hydrophobicity compared to PHEMA. Surface hydrophobicity favors protein adsorption which aids cell attachment in vivo. [98] Ocular tissue ingrowth observed in porous PHEMA [13] suggests that a porous PHEMA-PMMA, having greater hydrophobicity, would also permit ocular tissue ingrowth.

Based on the expected cell response to the polymers and the device structure, the gas-foamed KPro can potentially promote tissue ingrowth into the skirt and maintain an optically transparent core by deterring cell adhesion to the core.

The same gas foamed polymer that is expected to permit a large volume of tissue ingrowth can potentially permit aqueous humor leakage following implantation. The surgical implantation strategy can be designed to minimize fluid loss as ocular tissues colonize gas foamed PHEMA-PMMA. Potential surgical implantation schemes include the stromal pocket method used with AlphaCor [10], or as with the Osteo-Odonto KPro, surgeons could cover the implant with oral mucosa from the cheek until stable host integration is achieved. [135]

6.6 Conclusion

We engineered a novel artificial cornea that is composed of PHEMA and PMMA, referred to as the gas-foamed KPro. Experimental results demonstrate that the KPro may be biologically, mechanically, and structurally compatible for full thickness corneal replacement. Mechanical data indicates that the device can maintain its structure in the ocular environment and resist rupture during implantation. The KPro core, which is securely attached to the skirt, is optically transparent. Given the device's structure and known ocular compatibility of the polymers, the gas-foamed KPro may offer a cornea replacement option that generates fewer incidents of corneal melting and therefore achieve long-term stability in the ocular environment.

7. Summary

Synthetic corneal replacement or keratoprosthesis provides an alternative treatment to patients for whom donor cornea is incompatible or inaccessible. This study presented synthetic based corneal substitutes that facilitate cell ingrowth into a porous skirt while permitting vision through an optically transparent unit. The addition of cell adhesion components to PEGDA, PHEMA-PEGDA, and PHEMA-PMMA structures was critical for assessing in vitro cell ingrowth and cell activity. Although cells colonized available polymer voids in vivo, the stable conjugation of cell adhesion components to the polymer skirt is imperative for host integration in the intended patient population. Keratoprosthesis recipients often have preexisting ocular diseases, ocular tissue injury, or a history of corneal graft failure. The diseased or damaged ocular tissue is more reluctant to integrate a synthetic structure compared to healthy eye tissue. Preclinical studies with rabbits have shown that an interconnected porous biomaterial, such as gas foamed polymer, can permit 3D tissue ingrowth and thereby stable host integration. However, results are less favorable in diseased ocular tissues. Compared to synthetic KPros, KPro models that combine synthetic and cell adhesion components (i.e. natural ECM components or peptides) show greater long term success in the target populations for KPro use.

KPro models presented in this study can be combined with cell adhesion components to encourage more stable host integration in the target user population. Specifically, the PHEMA-PMMA based KPros are mechanically stable enough to be sutured, amenable to surface modification, and structurally appropriate for vision and tissue ingrowth. The goal is to use the Salt Porogen and Gas Foamed KPros, both PHEMA-PMMA based, as full thickness corneal replacement devices. Approximately 70% of the skirt of the Gas Foamed KPro provides an interconnected void space for tissue ingrowth. The skirt of the Salt Porogen KPro does not provide an interconnected void space for cell ingrowth, but the surface voids together with

appropriate mass transport via the skirt could potentially facilitate host integration. A cell adhesive KPro skirt with a high density of cell permeable surface pores and physiologically relevant mass transport could potentially facilitate the stable integration of a KPro into ocular tissue. Biological, structural, and mechanical evaluations indicate that the presented PHEMA-PMMA based KPros may be effective alternatives to currently available full thickness corneal replacement therapies.

References

- 1 Griffith M, Fagerholm P, Liu W, McLaughlin CR, Li F. Essentials in Ophthalmology: Cornea and External Eye Disease . Springer; 2005. p. 37-53.
- 2 Jun JJ, Siracuse-Lee DE, Daly MK, Dohlman CH. Chapter 10: Keratoprosthesis. In: Krieglstein GK, Weinreb RN, editors. Cornea and External Eye Disease: Essentials in Ophthalmology. 2012. p. 137-144.
- 3 Ghaffariyeh A, Honarpisheh N, Karkhaneh A, Abudi R, Moroz ZI, Peyman A, Faramarzi A, Abasov F. Fyodorov–Zuev Keratoprosthesis Implantation: Long-Term Results in Patients with Multiple Failed Corneal Grafts. Graefes Arch Clin Exp Ophthalmol. 2011;249:93-101.
- 4 Gomaa A, Comyn O, Liu C. Keratoprostheses in Clinical Practice – a Review. Clinical and Experimental Ophthalmology. 2010;38:211-224.
- 5 Sheardown H, Griffith M. Principles of Regenerative Medicine. Academic Press; 2008. p. 1060-1071.
- 6 Hicks CR, Fitton JH, Chirila TV, Crawford GJ, Constable IJ. Keratoprostheses: Advancing Toward a True Artificial Cornea. Surv Ophthalmol. 1997;42:175-189.
- 7 Todani A, Ciolino JB, Ament JD, Colby KA, Pineda R, Belin MW, Aquavella JV, Chodosh J, Dohlman CH. Titanium Back Plate for a PMMA Keratoprosthesis: Clinical Outcomes. Graefes Arch Clin Exp Ophthalmol. 2011;249:1515–1518.
- 8 Hicks CR, Werner L, Vijayasekaran S, Mamalis N, Apple DJ. Histology of AlphaCor Skirts Evaluation of Biointegration. Cornea. 2005;24:933-940.
- 9 Vijayasekaran S, Fitton JH, Hicks CR, Chirila TV, Crawford GJ, Constable IJ. Cell Viability and Inflammatory Response in Hydrogel Sponges Implanted in the Rabbit Cornea. Biomaterials. 1998;19:2255-2267.
- 10 Crawford GJ, Hicks CR, Lou X, Vijayasekaran S, Tan D, Mulholland B, Chirila TV, Constable IJ. The Chirila Keratoprosthesis: Phase I Human Clinical Trial. Ophthalmology. 2002;109:883–889.
- 11 Hicks CR, Crawford GJ, Dart JKG, Grabner G, Holland EJ, Stulting RD, Tan DT, Bulsara M. AlphaCor Clinical Outcomes. Cornea. 2006;25:1034-1042.
- 12 Guo P, Chen JQ, Tan BH, Wang ZC, Liu ZG, Yuan J, Gu JJ, Huang H. Implantation of Modified Polyhydroxyethyl Methacrylate-Polymethyl Methacrylate Keratoprostheses in Rabbit and Monkey Corneas. Zhonghua Yan Ke Za Zhi. 2007;43:602-607.

- 13 Hicks C, Crawford G, Chirila T, Wiffen S, Vijayasekaran S, Lou X, Fitton J, Maley M, Clayton A, Dalton P, et al. Development and Clinical Assessment of an Artificial Cornea. *Prog Retin Eye Res.* 2000;19:149-170.
- 14 Kim MK, Lee SM, Lee JL, Chung TY, Kim YH, Wee WR, Lee JH. Long-Term Outcome in Ocular Intractable Surface Disease with Seoul-Type Keratoprosthesis. *Cornea.* 2007;26:546–551.
- 15 Kim MK, Lee JL, Wee WR, Lee JH. Comparative Experiments for in Vivo Fibroplasia and Biological Stability of Four Porous Polymers Intended for Use in the Seoul-Type Keratoprosthesis. *Br J Ophthalmol.* 2002;86:809–814.
- 16 Pintucci S, Pintucci F, Cecconi M, Caiazza S. New Dacron Tissue colonisable Keratoprosthesis: Clinical Experience. *Br J Ophthalmol.* 1995;79:825–829.
- 17 Chan LS. Ocular and Oral Mucous Membrane Pemphigoid (Cicatricial Pemphigoid). *Clin Dermatol.* 2012;30:34-37.
- 18 Kresloff MS, Castellarin AA, Zarbin MA. Endophthalmitis. *Surv Ophthalmol.* 1998;43:193-224.
- 19 Myung D, Farooqui N, Zheng LL, Koh W, Gupta S, Bakri A, Noolandi J, Cochran JR, Frank CW, Ta CN. Bioactive Interpenetrating Polymer Network Hydrogels that Support Corneal Epithelial Wound Healing. *J Biomed Mater Res* 90A. 2009 70-81.
- 20 Myung D, Farooqui N, Waters D, Schaber S, Koh W, Carrasco M, Noolandi J, Frank CW, Ta CN. Glucose-Permeable Interpenetrating Polymer Network Hydrogels for Corneal Implant Applications: a Pilot Study. *Current Eye Research.* 2008;33:29-43.
- 21 McLaughlin CR, Fagerholm P, Muzakare L, Lagali N, Forrester JV, Kuffova L, Rafat MA, Liu Y, Shinozaki N, Vascotto SG, et al. Regeneration of Corneal Cells and Nerves in an Implanted Collagen Corneal Substitute. *Cornea.* 2008;27:580-589.
- 22 González-Andrades M, Garzón I, Gascón MI, Muñoz-Avila JI, Sánchez-Quevedo MC, Campos A, Alaminos M. Sequential Development of Intercellular Junctions in Bioengineered Human Corneas. *Journal of Tissue Engineering and Regenerative Medicine.* 2009;3:442-449.
- 23 Hacker MC, Mikos AG. Synthetic Polymers. In: *Principles of Regenerative Medicine.* 2nd ed. 2011. p. 587-622.
- 24 Lutolf MP, Hubbell JA. Synthetic Biomaterials as Instructive Extracellular Microenvironments for Morphogenesis in Tissue Engineering. *Nat Biotechnol.* 2005;23:47-55.

- 25 Yang F, Williams CG, Wang DA, Lee H, Manson PN, Elisseeff J. The effect of incorporating RGD adhesive peptide in polyethylene glycol diacrylate hydrogel on osteogenesis of bone marrow stromal cells. *Biomaterials*. 2005;26:5991–5998.
- 26 Gabler S, Stampfl J, Koch T, Seidler S, Schuller G, Redl H, Juras V, Trattinig S, Weidisch R. Determination of the viscoelastic properties of hydrogels based on polyethylene glycol diacrylate (PEG-DA) and human articular cartilage. *International Journal of Materials Engineering Innovation*. 2009;1:3-20.
- 27 Hwang NS. Cartilage Tissue Engineering Directed Differentiation of Embryonic Stem Cells in Three-Dimensional Hydrogel Culture. In: Vemuri MC, editor. *Molecular Biology: Stem Cell Assays*. Vol 407. Totowa (NJ): Humana Press; 2007. p. 351-373.
- 28 Kadakia A, Keskar V, Titushkin I, Djalilian A, Gemeinhart RA, Cho M. Hybrid Superporous Scaffolds: An Application for Cornea Tissue Engineering. *Crit Rev Biomed Eng*. 2008;36:441-471.
- 29 Myung D, Duhamel PE, Cochran JR, Noolandi J, Ta CN, Frank CW. Development of Hydrogel-Based Keratoprosthesis: A Materials Perspective. *Biotechnology Progress*. 2008;24:735-741.
- 30 Keskar V, Marion NW, Mao JJ, Gemeinhart RA. In Vitro Evaluation of Macroporous Hydrogels to Facilitate Stem Cell Infiltration, Growth and Mineralization. *Tissue Eng Part A*. 2009;15:1695-1707.
- 31 Safranski DL, Weiss D, Clark JB, Caspersen BS, Taylor WR, Gall K. Effect of Poly(ethylene glycol) Diacrylate Concentration on Network Properties and In Vivo Response of Poly(b-amino ester) Networks. *J Biomed Mater Res A*. 2011;96A:320-329.
- 32 Lee W, Lee TG, Koh WG. Grafting of Poly(acrylic acid) on the Poly(ethylene glycol) Hydrogel Using Surface-initiated Photopolymerization for Covalent Immobilization of Collagen. *Journal of Industrial and Engineering Chemistry*. 2007;13:1195-1200.
- 33 Lin S, Sangaj N, Razafiarison T, Zhang C, Varghese S. Influence of Physical Properties of Biomaterials on Cellular Behavior. *Pharm Res*. 2011;28:1422–1430.
- 34 Mazzoccoli JP, Fekete DL, Baskaran H, Pintauro PN. Mechanical and Cell Viability Properties of Crosslinked Low- and High-molecular Weight Poly(ethylene glycol) Diacrylate Blends. *J Biomed Mater Res A*. 2010;93:558-566.
- 35 Lynn AD, Kyriakides TR, Bryant SJ. Characterization of the in Vitro Macrophage Response and In Vivo Host Response to Poly(ethylene glycol)-Based Hydrogels. *J Biomed Mater Res A*. 2010;93A:941–953.

- 36 Myung D, Koh W, Ko J, Hu Y, Carrasco M, Noolandi J, Ta CN, Frank CW. Biomimetic Strain Hardening in Interpenetrating Polymer Network Hydrogels. *Polymer*. 2007;48:5376-5387.
- 37 Sannino A, Netti PA, Madaghiele M, Coccoli V, Luciani A, Maffezzoli A, Nicolais L. Synthesis and Characterization of Macroporous Poly(ethylene glycol)-Based Hydrogels for Tissue Engineering Application. *J Biomed Mater Res*. 2006;79A:229-236.
- 38 Beamish JA, Zhu J, Kottke-Marchant K, Marchant RE. The Effects of Monoacrylated Poly(ethylene glycol) on the Properties of Poly(ethylene glycol) Diacrylate Hydrogels used for Tissue Engineering. *J Biomed Mater Res A*. 2010;92A:441-450.
- 39 Pfister PM, Wendlandt M, Neuenschwander P, Suter UW. Surface-Textured PEG-based Hydrogels with Adjustable Elasticity: Synthesis and Characterization. *Biomaterials*. 2007;28:567-575.
- 40 Hern DL, Hubbel JA. Incorporation of Adhesion Peptides into Nonadhesive Hydrogels Useful for Tissue Engineering. *J Biomed Mater Res*. 1998 266-276.
- 41 Franz S, Rammelt S, Scharnweber D, Simon JC. Immune Responses to Implants - a Review of the Implications for the Design of Immunomodulatory Biomaterials. *Biomaterials*. 2011;32:6692-6709.
- 42 Keskar V, Gandhi M, Gemeinhart EJ, Gemeinhart RA. Initial Evaluation of Vascular Ingrowth into Superporous Hydrogels. *J Tissue Eng Regen Med*. 2009;3:486-490.
- 43 Nishida T, Ueda A, Fukuda M, Mishima H, Yasumoto K, Otori T. Interactions of Extracellular Collagen and Corneal Fibroblasts: Morphologic and Biochemical Changes of Rabbit Corneal Cells Cultured in a Collagen Matrix. *In Vitro Cell Dev Biol*. 1988;24:1009-1014.
- 44 Duncan TJ, Tanaka Y, Shi D, Kubota A, Quantock AJ, Nishida K. Flow-Manipulated, Crosslinked Collagen Gels for Use as Corneal Equivalents. *Biomaterials*. 2010;31:8996-9005.
- 45 Phu D, Orwin EJ. Characterizing the Effects of Aligned Collagen Fibers and Ascorbic Acid Derivatives on Behavior of Rabbit Corneal Fibroblasts. In: 31st Annual International Conference of the IEEE EMBS; 2009; Minneapolis. p. 4242-4245.
- 46 Zhu J, Beamish JA, Tang C, Kottke-Marchant K, Marchant RE. Extracellular Matrix-like Cell-Adhesive Hydrogels from RGD-Containing Poly(ethylene glycol) Diacrylate. *Macromolecules*. 2006;39:1305-1307.
- 47 LaNasa SM. Presence of pores and hydrogel composition influence tensile properties of scaffolds fabricated from well-defined sphere templates. *J Biomed Mater Res Part B*:

- Appl Biomater. 2011;96B:294–302.
- 48 Guldberg RE, Gemmiti CS, Kolambkar Y, Porter B. Physical Stress as a Factor in Tissue Growth and Remodeling. In: Principles of Regenerative Medicine. Academic Press; 2008. p. 512-535.
 - 49 Engler AJ, Sen S, Sweeney HL, Discher DE. Matrix Elasticity Directs Stem Cell Lineage Specification. Cell. 2006;126:677-689.
 - 50 Ghosh K, Pan Z, Guan E, Ge S, Liu Y, Nakamura T, Ren XD, Rafailovich M, Clark RA. Cell Adaptation to a Physiologically Relevant ECM Mimic with Different Viscoelastic Properties. Biomaterials. 2007 ;28:671-679.
 - 51 Dunn MG. Orthopedic Biology and Medicine: Tissue Engineering Strategies for the Regeneration of the Anterior Cruciate Ligament. In: Walsh WR, editor. Repair and Regeneration of Ligaments, Tendons, and Joint Capsule. Totowa: Humana Press; 2006. p. 279-296.
 - 52 Baker MV, Brown DH, Casadio YS, Chirila TV. The Preparation of Poly(2-Hydroxyethyl Methacrylate) and Poly
 - 53 Jung YP, Kim J, Lee DS, Kim YH. Preparation and Properties of Modified PHEMA Hydrogel with Sulfonated PEG Graft. J Appl Polym Sci. 2007;104:2484–2489.
 - 54 Yan T, Sun R, Li C, Tan B, Mao X, Ao N. Immobilization of Type-I Collagen and Basic Fibroblast Growth Factor (bFGF) onto Poly (HEMA-co-MMA) Hydrogel Surface and its Cytotoxicity Study. J Mater Sci Mater Med. 2010;21:2425–2433.
 - 55 Son YK, Jung YP, Kim JH, Chung DJ. Preparation and Properties of PEG-Modified PHEMA Hydrogel and the Morphological Effect. Macromolecular Research. 2006;14:394-399.
 - 56 Curtis MW, Russell B. Micromechanical Regulation in Cardiac Myocytes and Fibroblasts: Implications for Tissue Remodeling. Pflugers Arch - Eur J Physiol. 2011;462:105-117.
 - 57 Lawrence BD, Pan Z, Liu A, D.L. K, Rosenblatt MI. Human Corneal Limbal Epithelial Cell Response to Varying Silk Film Geometric Topography in Vitro. Acta Biomaterialia. 2012;8:3732-3743.
 - 58 Patel AA, Thakar RG, Chown M, Ayala P, Desai TA, Kumar S. Biophysical Mechanisms of Single-Cell Interactions with Microtopographical Cues. Biomed Microdevices. 2010;12:287–296.
 - 59 Reynolds PM, Pedersen RH, Riehle MO, Gadegaard N. A Dual Gradient Assay for the

- Parametric Analysis of Cell-Surface Interactions. *Small*. 2012;8:2541-2547.
- 60 Zink C, Hall H, Brunette DM, Spencer ND. Orthogonal Nanometer-Micrometer Roughness Gradients Probe Morphological Influences on Cell Behavior. *Biomaterials*. 2012;33:8055-8061.
- 61 Ventre M, Causa F, Netti PA. Determinants of Cell–Material Crosstalk at the Interface: Towards Engineering of Cell Instructive Materials. *J R Soc Interface*. 2012;9:2017–2032.
- 62 Rapier R, Huq J, Vishnubhotla R, Bulic M, Perrault CM, Metlushko V, Cho M, Tay RT, Glover SC. The Extracellular Matrix Microtopography Drives Critical Changes in Cellular Motility and Rho A Activity in Colon Cancer Cells. *Cancer Cell Int*. 2010;10(24).
- 63 Anseth KS, Bowman CN, Brannon-Peppas L. Mechanical Properties of Hydrogels and their Experimental Determination. *Biomaterials*. 1996 1647-1657.
- 64 Cowie JMG, Arrighi V. *Polymers: Chemistry and Physics of Modern Materials*. 3rd ed. Boca Raton: CRC Press Taylor and Francis Group; 2008.
- 65 Litvinov VM, Dias AA. Analysis of Network Structure of UV-Cured Acrylates by ¹H NMR Relaxation, ¹³C NMR Spectroscopy, and Dynamic Mechanical Experiments. *Macromolecules*. 2001;34:4051-4060.
- 66 Nishiyama N, Suzuki K, Komatsu K, Yasuda S, Nemoto K. A ¹³C NMR Study on the Adsorption Characteristics of HEMA to Dentinal Collagen. *J Dent Res*. 2002 ;81:469-471.
- 67 Jacobsen NE. *NMR Spectroscopy Explained: Simplified Theory, Applications and Examples for Organic Chemistry and Structural Biology*. John Wiley & Sons, Inc.; 2007.
- 68 UC Davis ChemWiki. [Internet]. [cited 2013 June]. Available from: http://chemwiki.ucdavis.edu/Organic_Chemistry/Organic_Chemistry_With_a_Biological_Emphasis/Tables/Typical_values_for_13C-NMR_chemical_shifts.
- 69 Junien C, Weil D, Myers JC, Van Cong N, Chu ML, Foubert C, Gross MS, Prockop DJ, Kaplan JC, Ramirez F. Assignment of the Human Pro Alpha 2(I) Collagen Structural Gene (COL1A2) to Chromosome 7 by Molecular Hybridization. *Am J Hum Genet*. 1982;34:381–387.
- 70 Dziubla TD, Lowman AM. Vascularization of PEG-Grafted Macroporous Hydrogel Sponges: A Three-Dimensional in Vitro Angiogenesis Model Using Human Microvascular Endothelial Cells. *J Biomed Mater Res*. 2004;68A:603-614.
- 71 Horák D, Kroupova J, Sloufa M, Dvorak P. Poly(2-Hydroxyethyl Methacrylate)-Based Slabs as a Mouse Embryonic Stem Cell Support. *Biomaterials*. 2004;25:5249–5260.

- 72 Gemeinhart RA, Park H, Kinam P. Pore Structure of Superporous Hydrogels. *Polym Adv Technol.* 2000;11:617-625.
- 73 Gulsen D, Chauhan A. Effect of Water Content on Transparency, Swelling, Lidocaine Diffusion in p-HEMA Gels. *Journal of Membrane Science.* 2006;269:35-48.
- 74 Church RL, SundarRaj N, Rohrbach DH. Gene Mapping of Human Ocular Connective Tissue Proteins. *Invest Ophthalmol Vis Sci.* 1981;21:73-79.
- 75 Svoboda K, Gong H, Trinkaus-Randall V. Collagen Expression and Orientation in Ocular Tissues. *Prog Polym Sci.* 1998;23:329-374.
- 76 Panjwani N. Chapter 2: Cornea and Sclera. In: Harding JJ, editor. *Biochemistry of the Eye.* London: Chapman and Hall Medical; 1997. p. 16-51.
- 77 Edelhauser HF, Ubels JL. The Cornea and the Sclera. In: Kaufman PL, Alm A. *Adler's Physiology of the Eye Clinical Application.* 10th ed. Philadelphia: Mosby; 2003. p. 47-114.
- 78 Fini ME. Keratocyte and Fibroblast Phenotypes in the Repairing Cornea. *Prog Retin Eye Res.* 1999;18:529-551.
- 79 Yamane S, Iwasaki N, Kasahara Y, Harada K, Majima T, Monde K, Nishimura S, Minami A. Effect of Pore Size on in Vitro Cartilage Formation Using Chitosan-Based Hyaluronic Acid Hybrid Polymer Fibers. *J Biomed Mater Res.* 2007;81A:586-593.
- 80 Zeltinger J, Sherwood JK, Graham DA, Müller R, Griffith LG. Effect of Pore Size and Void Fraction on Cellular Adhesion, Proliferation, and Matrix Deposition. *Tissue Engineering.* 2001;7:557-572.
- 81 Kubinová S, Horák D, Kozubenko N, Vanecek V, Proks V, Price J, Cocks G, Syková E. The use of superporous Ac-CGGASIKVAVS-OH-modified PHEMA Scaffolds to Promote Cell Adhesion and the Differentiation of Human Fetal Neural Precursors. *Biomaterials.* 2010;31:5966-5975.
- 82 Park S, Nam SH, Koh W. Preparation of Collagen-Immobilized Poly(ethylene glycol)/Poly(2-hydroxyethyl methacrylate) Interpenetrating Network Hydrogels for Potential Application of Artificial Cornea. *J Appl Polym Sci.* 2012;123: 637–645.
- 83 Logan ME, Zaim MT. Histologic Stains in Dermatopathology. *J Am Acad Dermatol.* 1990;22:820-830.
- 84 Klement JF, Matsuzaki Y, Jiang QJ, Terlizzi J, Choi HY, Fujimoto N, Li K, Pulkkinen L, Birk DE, Sundberg JP, et al. Targeted Ablation of the Abcc6 Gene Results in Ectopic Mineralization of Connective Tissues. *Molecular and Cellular Biology.* 2005;25:8299–

8310.

- 85 Anderson HC, Harmey D, Camacho NP, Garimella R, Sipe JB, Tague S, Bi X, Johnson K, Terkeltaub R, Millan JL. Sustained Osteomalacia of Long Bones Despite Major Improvement in Other Hypophosphatasia-Related Mineral Deficits in Tissue Nonspecific Alkaline Phosphatase/Nucleotide Pyrophosphatase Phosphodiesterase 1 Double-Deficient Mice. *Am J Pathol.* 2005;166:1711–1720.
- 86 Caira FC, Stock SR, Gleason TG, McGee EC, Huang J, Bonow RO, Spelsberg TC, McCarthy PM, Rahimtoola SH, Rajamannan NM. Human Degenerative Valve Disease is Associated with Up-Regulation of Low-Density Lipoprotein Receptor-Related Protein 5 Receptor-Mediated Bone Formation. *J Am Coll Cardiol.* 2006;47:1707-1712.
- 87 Imai Y, Masuhara E. Long-Term in Vivo Studies of Poly(2-Hydroxyethyl Methacrylate). *J Biomed Mater Res.* 1982;16:609-617.
- 88 Buchen SY, Cunanan CM, Gwon A, Weinschenk JI, Gruber L, Knight PM. Assessing Intraocular Lens Calcification in an Animal Model. *J Cataract Refract Surg.* 2001;27:1473–1484.
- 89 Vijayasekaran S, Chirila TV, Robertson TA, Lou X, Fitton JH, Hicks CR, Constable IJ. Calcification of Poly(2-Hydroxyethyl Methacrylate) Hydrogel Sponges Implanted in the Rabbit Cornea: a 3-Month Study. *J Biomater Sci Polym Ed.* 2000;11:599-615.
- 90 Chirila TV. An Overview of the Development of Artificial Corneas with Porous Skirts and the Use of PHEMA for Such an Application. *Biomaterials.* 2001;22:3311-3317.
- 91 Dalton PD, Flynn L, Shoichet MS. Manufacture of Poly(2-Hydroxyethyl Methacrylate-co-Methyl Methacrylate) Hydrogel Tubes for Use as Nerve Guidance Channels. *Biomaterials.* 2002;23:3843–3851.
- 92 Yukna RA, Castellon P, Saenz-Nasr AM, Owens K, Simmons J, Thunthy KH, Mayer ET. Evaluation of Hard Tissue Replacement Composite Graft Material as a Ridge Preservation/Augmentation Material in Conjunction with Immediate Hydroxyapatite-Coated Dental Implants. *J Periodontol.* 2003;74:679-686.
- 93 Schild G, Schauersberger J, Amon M, Abela-Formanek C, Kruger A. Lens Epithelial Cell Ougrowth: Comparison of 6 Types of Hydrophilic Intraocular Lens Models. *J Cataract Refract Surg.* 2005;31:2375-2378.
- 94 Müllner-Eidenböck A, Amon M, Schauersberger J, Kruger A, Abela C, Petternel V, Zidek T. Cellular Reaction on the Anterior Surface of 4 Types of Intraocular Lenses. *J Cataract Refract Surg.* 2001;27:734-740.

- 95 Lloyd AW, Faragher RG, Denyer SP. Ocular Biomaterials and Implants. *Biomaterials*. 2001;22:769-785.
- 96 Espana EM, Acosta AC, Stoiber J, Fernandez V, Lamar PD, Villain FL, Lacombe E, Alfonso E, Parel JM. Long-Term Follow-up of a Supradescemetic Keratoprosthesis in Rabbits: an Immunofluorescence Study. *Graefes Arch Clin Exp Ophthalmol*. 2011;249:253-260.
- 97 Mimura K, Hiramatsu K, Moriya M, Sakamoto W, Kawado S, Uesu Y, Yogo T. Optical Properties of Transparent Barium Titanate Nanoparticle/Polymer Hybrid Synthesized from Metal Alkoxides. *J Nanopart Res*. 2010;12:1933–1943.
- 98 Temenoff JS, Mikos AG. *Biomaterials the Intersection of Biology and Materials Science*. Upper Saddle River: Pearson Prentice Hall; 2008.
- 99 De Clerck N, Postnov A. Chapter 2: High Resolution Microtomography: Applications in Biomedical Research. In: Ntziachristos V, Leroy-Willig A, Tavitian B, editors. *Textbook of In Vivo Imaging in Vertebrates*. John Wiley & Sons, Ltd. ; 2007.
- 100 Torris AT, Columbus KC, Saaj US, Nair MB, Krishnan KV. Evaluation of Biomaterials Using Micro-Computerized Tomography. In: Munshi P, editor. *Tomography Confluence: An International Conference on the Applications of Computerized Tomography*; 2008. p. 68-78.
- 101 Peyrin F, Mastrogiacomo M, Cancedda R, Martinetti R. SEM and 3D Synchrotron Radiation Micro-Tomography in the Study of Bioceramic Scaffolds for Tissue-Engineering Applications. *Biotechnol Bioeng*. 2007;97:638-648.
- 102 Wisniewski S, Kim SW. Permeation of Water-Soluble Solutes through Poly(2-Hydroxyethyl Methacrylate) and Poly(2-Hydroxyethyl Methacrylate) Crosslinked with Ethylene Glycol Dimethacrylate. *J Memb Sci*. 1980;6:299-308.
- 103 He W, Benson R. *Applied Plastics Engineering Handbook*. Elsevier ; 2011. p. 159-175.
- 104 Lou X, Dalton PD, Chirila TV. Hydrophilic Sponges Based on 2-Hydroxyethyl Methacrylate Part VII: Modulation of Sponge Characteristics by Changes in Reactivity and Hydrophilicity of Crosslinking Agents. *Journal of Materials Science: Materials in Medicine*. 2000;11:319-325.
- 105 Wang J, Chauhan A. Disruption of Tear Film and Blink Dynamics. In: *Ocular Disease Mechanisms and Management*. Elsevier; 2010. p. 123-130.
- 106 Rolando M, Zierhut M. The Ocular Surface and Tear Film and their Dysfunction in Dry Eye Disease. *Surv Ophthalmol*. 2001;45 Suppl 2:S203-S210.

- 107 Shiose Y. Intraocular Pressure: New Perspectives. *Surv Ophthalmol*. 1990;34:413-435.
- 108 Bhan A, Browning AC, Shah S, Hamilton R, Dave D, Dua HS. Effect of Corneal Thickness on Intraocular Pressure Measurements with the Pneumotonometer, Goldmann Applanation Tonometer, and Tono-Pen. *Invest Ophthalmol Vis Sci*. 2002;43:1389-1392.
- 109 Rafat M, Li F, Fagerholm P, Lagali NS, Watsky MA, Munger R, Matsuura T, Griffith M. PEG-Stabilized Carbodiimide Crosslinked Collagen-Chitosan Hydrogels for Corneal Tissue Engineering. *Biomaterials*. 2008;29:3960-3972.
- 110 Andreassen TT, Simonsen AH, Oxlund H. Biomechanical Properties of Keratoconus and Normal Corneas. *Exp Eye Res*. 1980;31:435-441.
- 111 Jue B, Maurice DM. The Mechanical Properties of the Rabbit and Human Cornea. *J Biomech*. 1986;19:847-853.
- 112 Renard G, Cetinel B, Legeais JM, Savoldelli M, Durand J, Pouliquen Y. Incorporation of a Fluorocarbon Polymer Implanted at the Posterior Surface of the Rabbit Cornea. *J Biomed Mater Res*. 1996;31:193-199.
- 113 Walsh JE, Bergmanson JP, Koehler LV, Doughty MJ, Fleming DP, Harmey JH. Fibre Optic Spectrophotometry for the in Vitro Evaluation of Ultraviolet Radiation (UVR) Spectral Transmittance of Rabbit Corneas. *Physiol Meas*. 2008;29:375-388.
- 114 Douth J, Quantock AJ, Smith VA, Meek KM. Light Transmission in the Human Cornea as a Function of Position Across the Ocular Surface: Theoretical and Experimental Aspects. *Biophys J*. 2008;95:5092-5099.
- 115 Campillo-Fernández AJ, Pastor S, Abad-Collado M, Bataille L, Gomez-Ribelles JL, Meseguer-Dueñas JM, Monleon-Padas M, Artola A, Alio JL, Ruiz-Moreno JM. Future Design of a New Keratoprosthesis. Physical and Biological Analysis of Polymeric Substrates for Epithelial Cell Growth. *Biomacromolecules*. 2007;8:2429-2436.
- 116 Campillo-Fernández AJ, Unger RE, Peters K, Halstenberg S, Santos M, Salmerón Sánchez M, Meseguer Dueñas JM, Monleón Pradas M, Gómez Ribelles JL, Kirkpatrick CJ. Analysis of the Biological Response of Endothelial and Fibroblast Cells Cultured on Synthetic Scaffolds with Various Hydrophilic/Hydrophobic Ratios: Influence of Fibronectin Adsorption and Conformation. *Tissue Eng Part A*. 2009;15:1331-1341.
- 117 Lou X, Vijayasekaran S, Sugiharti R, Robertson T. Morphological and Topographic Effects on Calcification Tendency of pHEMA Hydrogels. *Biomaterials*. 2005;26:5808–5817.
- 118 Pethrick RA, Zaikov GE, Horák D. *Polymers and Composites: Synthesis, Properties and*

Applications. New York: Nova Publishers; 2007.

- 119 Zainuddin, Hill DJT, Whittaker AK, Chirila TV. In-Vitro Study of the Spontaneous Calcification of PHEMA Based Hydrogels in Simulated Body Fluid. *J Mater Sci: Mater Med.* 2006;17:1245–1254.
- 120 Abdel-Mawgoud AM, Lépine F, Déziel E. Rhamnolipids: Diversity of Structures, Microbial Origins and Roles. *Appl Microbiol Biotechnol.* 2010;86:1323-1336.
- 121 Darouiche RO. Treatment of Infections Associated with Surgical Implants. *N Engl J Med.* 2004;350:1422-1429.
- 122 Garcia-Saenz MC, Arias-Puente A, Fresnadillo-Martinez MJ, Paredes-Garcia B. Adherence of Two Strains of Staphylococcus Epidermidis to Contact Lenses. *Cornea.* 2002;21:511-515.
- 123 Szczotka-Flynn LB, Imamura Y, Chandra J, Yu C, Mukherjee PK, Pearlman E, Ghannoum MA. Increased Resistance of Contact Lens-Related Bacterial Biofilms to Antimicrobial Activity of Soft Contact Lens Care Solutions. *Cornea.* 2009;28:918-926.
- 124 Behlau I, Mukherjee K, Todani A, Tisdale AS, Cade F, Wang L, Leonard EM, Zakka FR, Gilmore MS, Jakobiec FA, et al. Biocompatibility and Biofilm Inhibition of N,N-Hexyl,Methyl-Polyethylenimine Bonded to Boston Keratoprosthesis Materials. *Biomaterials.* 2011;32:8783-8796.
- 125 Nishikawa M, Yamamoto T, Kojima N, Kikuo K, Fujii T, Sakai Y. Stable Immobilization of Rat Hepatocytes as Hemispheroids onto Collagen-Conjugated Poly-Dimethylsiloxane (PDMS) Surfaces: Importance of Direct Oxygenation through PDMS for both Formation and Function. *Biotechnol Bioeng.* 2008;99:1472-1481.
- 126 Hersel U, Dahmen C, Kessler H. RGD Modified Polymers: Biomaterials for Stimulated Cell Adhesion and Beyond. *Biomaterials.* 2003;24:4385-4415.
- 127 Aucoin L. Interactions of corneal epithelial cells and surfaces modified with cell adhesion combinations. *J. Biomater. Sci. Polym. Ed.* 2002;13:447-462.
- 128 Li B, Chen J, Wang JH. RGD Peptide-Conjugated Poly(dimethylsiloxane) Promotes Adhesion, Proliferation, and Collagen Secretion of Human Fibroblasts. *J Biomed Mater Res A.* 2006;79:989-998.
- 129 Jacob JT, Rochefort JR, Bi J, Gebhardt BM. Corneal Epithelial Cell Growth over Tethered-Protein/Peptide Surface-Modified Hydrogels. *J Biomed Mater Res B Appl Biomater.* 2005;72:198-205.

- 130 Ponce Márquez S, Martínez VS, McIntosh Ambrose W, Wang J, Gantxegui NG, Schein O, Elisseeff J. Decellularization of Bovine Corneas for Tissue Engineering Applications. *Acta Biomater.* 2009;5:1839-1847.
- 131 Oelker AM, Grinstaff MW. Synthesis, Characterization, and in Vitro Evaluation of a Hydrogel-Based Corneal Onlay. *IEEE Trans Nanobioscience.* 2012;11:37-45.
- 132 Minami Y, Sugihara H, Oono S. Reconstruction of Cornea in Three-Dimensional Collagen Gel Matrix Culture. *Invest Ophthalmol Vis Sci.* 1993;34(7):2316-2324.
- 133 Stepp MA. Corneal Integrins and their Functions. *Exp Eye Res.* 2006;83:3-15.
- 134 Chirila TV, Constable IJ, Crawford GJ, Russo AV, inventors. Method of Producing a Keratoprosthesis. 1995 October 17. 5458819.
- 135 Falcinelli G, Falsini B, Taloni M, Colliardo P, Falcinelli G. Modified Osteo-Odonto-Keratoprosthesis for Treatment of Corneal Blindness: Long-Term Anatomical and Functional Outcomes in 181 Cases. *Arch Ophthalmol.* 2005;123:1319-1329.

Curriculum Vitae

EDUCATION

University of Illinois Chicago, Chicago, IL

Doctor of Philosophy in Bioengineering, August 2009 – May 2013

Graduation Date: August 2013

Thesis Advisor: Michael Cho, PhD

Dissertation: "Designing Novel Biomaterials for Cornea Replacement"

- Designed, fabricated, and tested polymers for a medical device application
- Developed materials for tissue engineering research

Johns Hopkins University, Baltimore, MD

Master of Science in Biotechnology, September 2005 - May 2009

University of Pennsylvania, Philadelphia, PA

Bachelor of Applied Science in Biomedical Science, September 1999 - May 2003

Major: Bioengineering Applied Science Minor: Mathematics

PROFESSIONAL EXPERIENCE

Technology Analyst, University of Illinois Chicago, Office of Technology Management

April 2010 – April 2011

- Evaluated the commercialization potential and novelty of university generated science and engineering related technologies; most technologies had medical applications
- Technology evaluations were used to secure patents and/or issue commercial licenses
- Attracted potential biotechnology industry investors via a direct marketing campaign for biological technologies; connected interested investors with supervisors/management team so that they could negotiate licensing terms

Intern, DePuy Mitek, Raynham, MA

April 2009 – August 2009

- Conducted experiments to support the development of osteoarthritis treatments in the Concept Development Department
- Evaluated the relationship between selected biomarkers and osteoarthritis progression for a specific therapeutic product that is currently commercially available

Research Assistant, CVPPath Institute, Gaithersburg, MD

March 2008 – March 2009

- Analyzed cardiovascular research tissues and medical devices per GLP standards and organizational SOPs; research materials included heart stents, vascular grafts, and stem cell treated heart tissue
- Data submitted to biotechnology industry, government, and academic clients was often used to solicit FDA approval

TECHNICAL SKILLS

Laboratory Instrumentation: Cell Culture, ELISA, Confocal Microscopy, Immunostaining, Light Microscopy, Mechanical Testing, Polymer Gel Preparation, and RT-PCR.

Computer: Matlab, Metamorph, Microsoft Office, SigmaStat

PUBLICATIONS

Zellander A, Gemeinhart R, Djalilian A, Makhsous M, Sun S, and Cho M. "Designing a Gas Foamed Scaffold for Keratoprosthesis." *Materials Science and Engineering C*. 2013; 33: 3396-3403.

Zellander A, Kadakia-Bhasin A, Makhsous M, and Cho M. "Mechanical Diversity of 3D Porous Poly (Ethylene Glycol) Diacrylate Scaffold." *Advances in Biomedical Engineering Research*. 2013; 1: 9-16.

Zellander A, Wardlow M, Djalilian A, Zhao C, Abiade J, Makhsous M, and Cho M. "Engineering Copolymeric Artificial Cornea by Salt Porogen." *Journal of Biomedical Materials Research Part A*. Accepted Manuscript, June 2013.

Zellander A, Zhao C, Kotecha M, Low K, Gemeinhart R, Abiade J, and Cho M. "Modifying Pore Structure in Poly(2-Hydroxyethyl Methacrylate) - Poly(Ethylene Glycol) Diacrylate (PHEMA-PEGDA)." *European Polymer Journal*. Manuscript in Preparation.

PRESENTATIONS

Zellander A, Gemeinhart R, Milani B, Djalilian A, Makhsous M, and Cho M. "Designing a Novel Porous Keratoprosthesis to Promote Cornea Cell Ingrowth." Association for Research in Vision and Ophthalmology Annual Meeting (Seattle, WA 2013). Poster presentation.

Zellander A, Makhsous M, Zhao C, Abiade J, and Cho M. "Potential Efficacy of Two Artificial Cornea Devices." BMES Midwest Engineering Career Conference (Chicago, IL 2013). Poster presentation.

Zellander A, Makhsous M, Zhao C, Abiade J, and Cho M. "Synthetic Sutable Keratoprosthesis." ASME International Mechanical Engineering Congress and Exposition (Houston, TX 2012). Poster presentation.

Zellander A, Makhsous M, Milani B, Djalilian A, and Cho M. "Cornea Engineering using Porous Poly (2-hydroxyethyl methacrylate) (PHEMA) – Poly (methyl methacrylate) (PMMA)." Biomedical Engineering Society Annual Meeting (Atlanta, GA 2012). Oral presentation.

Zellander A, Makhsous M, and Cho M. "Poly (ethylene glycol diacrylate) – Poly (2-hydroxyethyl methacrylate) (PEGDA-PHEMA) Based Keratoprosthesis." Association for Research in Vision and Ophthalmology Annual Meeting (Fort Lauderdale, FL 2012). Poster presentation.

Zellander A, Makhsous M, and Cho M. "Mechanical Optimization of a PEGDA-based Keratoprosthesis." Biomedical Engineering Society Annual Meeting (Hartford, CT 2011). Poster presentation.

TEACHING AND MENTORING EXPERIENCE

Research Assistant, University of Illinois Chicago, Department of Bioengineering
August 2009 – May 2013

- Designed experiments to solve biomedical and engineering problems
- Collaborated with other universities and departments to achieve project objectives
- Provided solutions to meet dissertation and business objectives
- Trained graduate and undergraduate students to conduct experiments and use equipment

Teaching Assistant, University of Illinois Chicago, Department of Bioengineering
August 2011 – May 2013

- Course assignments included Cell and Tissue Engineering and Modern Imaging Techniques for Tissue Engineering

Graduate Assistant, University of Illinois Chicago, Minority Engineering Recruitment and Retention Program

January 2012 – May 2013

- Mentored minority engineering students and hosted engineering recruitment events

AWARDS

- Scientist Mentoring and Diversity Program Scholar, 2013
- University of Illinois Chicago Abraham Lincoln Fellowship, 2010 – 2011
- The National Consortium for Graduate Degrees for Minorities in Engineering and Science, Inc. Fellowship, 2009 – 2013
- United States Navy ROTC Scholarship for Undergraduate Studies, 2000 – 2003
- National Defense Industrial Association ROTC Award in 2003

MILITARY SERVICE

United States Navy, Meteorologist and Oceanographer

December 2004 – December 2007

- Produced weather warnings and forecasts for US Navy ships and other Department of Defense assets in the Pacific and Indian Oceans
- Created and revised approximately 50 standard operating procedures
- Fitness Program Director for about 80 sailors

United States Navy, Surface Warfare Officer

June 2003 - December 2004

- Directed at-sea operations
- Supervised maintenance and upkeep of guns and related equipment
- Supervised maintenance and upkeep cryptology related equipment